Spitzer Space Telescope

Observer's Manual - Version 12.2

Warm Mission

Release Date: 9 Nov 2018

ii

Issue Dates

Version 12.2 Release: 9 Nov 2018
Version 12.1 Release: 19 July 2013
Version 12.0 Release: 1 May2013
Version 11.1 Release: 10 August 2012
Version 11.0 Release: 1May 2012
Version 10.2 Release: 23 November 2010
Version 10.1 Release: 15 October 2010
Version 10.0 Release: 27 January 2010
Version 9.0 Release: 7 July 2008
Version 8.0 Release: 15 Aug 2007
Version 7.1 Release: 8 Dec 2006
Version 7.0 Release: 1 Nov 2006
Version 6.0 Release: 1 Nov 2005
Version 5.0 Release: 1 Nov 2004
Version 4.6 Release: 6 Aug 2004
Version 4.5 Release: 28 Jun 2004
Version 4.0 Release: 19 Dec 2003
Version 3.0 Release: 8 Nov 2002
Version 2.2 Release: 15 Apr 2002
Version 2.1 Release: 1 Aug 2000
Version 2.0 Release: 30 Jun 2000
Version 1.0 Release: 28 Apr 2000

Acknowledgements

Version 12.2 Summary of Changes

This is a summary of the changes in version 12.2 based upon version 12.1.

Chapter 1 – No changes.
Chapter 2 – No changes.
Chapter 3 – No changes
Chapter 4 – No changes.
Chapter 5 – No changes.
Chapter 6 – Added text in Section 6.2.4.1.8 (High Precision Relative Photometric Monitoring).
Chapter 7 – No changes.
Chapter 8 – No changes.

Table of Contents: Major Sections

List of Tables

Table of Contents: All Sections

x

1 Philosophy and Scope of the Spitzer Space Telescope Observer's Manual

The Spitzer Space Telescope is the fourth element in NASA's family of Great Observatories and represents an important scientific and technical component in NASA's Astronomical Search for Origins program. The spacecraft carries an 85-centimeter telescope and, during the warm mission, one operational ambient temperature science instrument, capable of performing imaging from 3 to 5 μm. Spitzer was launched on a Delta 7920H from Cape Canaveral, Florida into an Earth-trailing heliocentric orbit on 25 August 2003. The warm mission began after the depletion of cryogen on 15 May 2009. After the in-orbit-checkout phase for the spacecraft and the one functioning science instrument — IRAC – warm mission science observations began in late July 2009.

1.1 Intended Audience

This document, the Spitzer Space Telescope Observer's Manual-Warm Mission ("Warm SOM," hereafter), is the essential technical reference manual for Spitzer observers. The Warm SOM provides information about the design, performance and operational constraints of Spitzer. It includes information on planning, editing and submitting Spitzer observations. Spitzer investigators using data from the cryogenic mission science instruments (i.e., archival investigators) should use Version 8.0 of the SOM as a reference to the cryogenic science instruments performance and data acquisition, calibration, and processing.

Many documents, including the SOM, are available on the public Spitzer Science Center (SSC) website at http://ssc.spitzer.caltech.edu/. We have updated this document with the latest information known as of April 2013.

For readers interested in data analysis, considerable additional documentation is available on the SSC website including instrument handbooks for each of the instruments, data analysis tools documentation, and data analysis cookbooks.

1.2 Document Organization

The Warm SOM is divided into four major parts: the Introduction (Chapters 1 and 2), the observatory chapters (Chapters 3 to 5), and the instrument-specific chapter (Chapter 6). The observatory section includes a technical description of Spitzer, its operational capabilities and constraints, and information about how Spitzer observations are planned and specified.

The IRAC science instrument has its own chapter, prepared by the instrument team and SSC IRAC instrument support team. It includes a technical description of the instrument, an overview of the instrument's performance and capabilities, a description of its observing modes, advice on how to best use them, and a discussion of the data reduction pipeline and the characteristics of the data. More extensive discussion of the data is presented in the IRAC Instrument Handbook which is available on the SSC website.

1.3 Document Update Plans

This manual is maintained by the SSC and is intended to support the current Call for Proposals (CP). Proposers should note that we have updated this document with the latest information known as of April 2013; in a very few cases, references are made here to information that is posted on the SSC website. In addition to maintaining the Warm SOM, the SSC maintains instrument web pages at: http://ssc.spitzer.caltech.edu/.

1.4 Other Relevant Documents

Current versions of the documents listed below are available on the SSC website:

Spitzer Space Telescope Observer's Manual – Warm Mission
Spitzer Space Telescope Call for Proposals
Spitzer Space Telescope Warm Mission Observing Rules
Spot User's Guide
Leopard User's Guide
Spitzer Space Telescope Observation Planning Cookbook
IRAC Instrument Handbook

Many other helpful documents can be found on the SSC website at
http://ssc.spitzer.caltech.edu/.

Previous years also mentioned the Spitzer Space Telescope Reserved Observations Catalog. It is easier (and recommended) at this point in the mission to use Leopard to search the set of objects observed or planned to be observed with Spitzer. (Leopard is packaged with Spot, and also has batch search capability.) However, we anticipate producing the plain ASCII ROC, obtainable from the SSC website, for each issued Call for Proposals.

2 Introduction to Observing with Spitzer

This chapter includes an overview of the Spitzer mission, a summary of the observatory's technical capabilities, and a description of the Science User Support services that are offered by the SSC. The relevant details of the mission and telescope design appear in Chapters 3-5.

A brief, high-level summary of the mission for astronomers appears in the ApJS Spitzer Special Issue, specifically the paper by Werner et al. (2004, ApJS, 154, 1) entitled "The Spitzer Space Telescope Mission." A copy of this paper is available on the SSC website.

2.1 Categories of Observing Programs

All observing time on Spitzer is now General Observer (GO). Up to ten percent of the total observing time is allocated by the SSC Director as Director's Discretionary Time (DDT), and is intended to facilitate proposals that address emerging scientific topics.

2.2 Mission Overview

Spitzer was launched from Cape Canaveral, Florida into an Earth-trailing heliocentric orbit on 25 August 2003. The observatory was launched with the telescope at ambient temperature; only the focal plane instruments were cooled to cryogenic temperatures. The telescope gradually cooled to ~6 K over a period of ~45 days.

Following launch, Spitzer entered a 63-day In-Orbit Checkout (IOC) phase, followed by a 35-day Science Verification (SV) phase, during which time the planned capabilities of the telescope were verified, the detailed performance characterized, and the three science instruments and their operational modes commissioned. Following completion of IOC + SV, Spitzer was commissioned for routine science operations on 1 Dec 2003.

The prime science mission continued until the exhaustion of the onboard cryogen used to cool the telescope and science instruments. The Spitzer cryogenic lifetime requirement was 2.5 years of normal operations, which was passed on 26 April 2006. The cryogen was finally depleted on 15 May 2009. After the end of cryogen the Warm Spitzer Mission began with an in-orbit-checkout/science verification of the spacecraft and single operating science instrument, IRAC, and then warm mission science observations began in late July 2009.

2.3 High Level Observatory Description: What Can Spitzer Do?

Spitzer is a 3-axis stabilized pointing and scanning observatory. The top-level observatory characteristics are summarized in Table 2.1. The observatory as a whole is presented in more detail in Chapter 3, the telescope optics in Chapter 4 and the science instrument, IRAC, in Chapter 6.

Spitzer's functional science payload consists of the InfraRed Array Camera (IRAC), which offers observational capabilities in the near-infrared.

The InfraRed Array Camera (IRAC) – Giovanni G. Fazio, Smithsonian Astrophysical Observatory/Harvard-Smithsonian Center for Astrophysics, PI
 IRAC provides images at 3.6, 4.5, 5.8 and 8.0 μm, with two adjacent 5.2′ × 5.2′ fields of view. One field of view images simultaneously at 3.6 and 5.8 μm and the other at 4.5 and 8.0 μm via dichroic beamsplitters. All four detector arrays are 256 × 256 with 1.2″ square pixels. IRAC is described in detail in Chapter 6. Only the two short wavelength arrays (3.6 and 4.5 μm) operate during the warm mission.

Table 2.1: Summary of Spitzer Characteristics

Aperture (diameter)	85 cm
Orbit	Solar (Earth-trailing)
Cryogenic Lifetime	5.5 years (approx)
Wavelength Coverage, cryogenic mission (passband centers)	3.6 - 160 μm (imaging) 5.3 - 40 μm (spectroscopy) 55 - 95 μm (spectral energy distribution)
Diffraction Limit	5.5 μm
Image Size	1.5″ at 6.5 μm
Pointing Stability (1σ, 200s, when using star tracker)	<0.1″
As commanded pointing accuracy (1σ radial)	<0.5″
Pointing reconstruction (required)	<1.0″
Field of View (of imaging arrays)	~ 5′×5′ (each band)
Telescope Minimum Temperature	5.6 K (cryo), 27.5 K (post-cryo)
Maximum Tracking Rate	1.0″/ sec
Time to slew over ~90º	~8 minutes

2.4 Spitzer Science Operations Overview

The Spitzer Science Center (SSC) conducts the science operations for Spitzer, and is charged with 1) acting as an interface and advocate for users, 2) capturing and conducting the science program efficiently, 3) producing and securing the Spitzer science legacy, and 4) conducting public and scientific outreach for the Spitzer program. The SSC is located on the campus of the California Institute of Technology in Pasadena, California, USA.

In carrying out its charter, the SSC issues annual Calls for Proposals, organizes science and technical reviews, selects approved programs based on a Time Allocation Committee review, and administers data analysis awards. The SSC

provides tools for detailed planning of Spitzer observations and proposal submission, and offers Science User Support services. In addition, the SSC schedules observations on the telescope, provides basic (pipeline) science data processing and data quality assessment, and creates a data archive that has been publicly accessible since May 2004.

2.4.1 Science Instrument Operations

After the end of cryogen the Infrared Spectrograph (IRS) and Multiband Imaging Photometer for Spitzer (MIPS) will not be able to produce unsaturated data. These two science instruments are therefore not available in the Warm Mission. The two shortest wavelength arrays within IRAC (3.6 and 4.5 μm) are the only operational science instrument and arrays for which new Spitzer observations can be proposed. Figure 2.1 shows that the two apertures for IRAC point toward different portions of the sky at the same time, so that switching apertures and staying on the same target involves re-pointing the telescope.

A central concept in Spitzer science operations is that of the Astronomical Observation Template (AOT). The IRAC instrument offers the observer a selected number of choices in configuring and operating the instrument. The AOT concept and the IRAC Post-Cryo Mapping AOT in particular are described in Chapter 5, and in greater detail in Chapter 6.

The SSC plans and executes calibration activities to maintain the instrument calibration. In general, observers should not need to supplement the instrument calibration, but may do so by incorporating observations for that purpose into their (proposed) observing program. The calibration for IRAC is discussed in Chapter 6.

Nominal Field-of-View Locations
Projected onto the Sky

Note: This is not an engineering diagram.
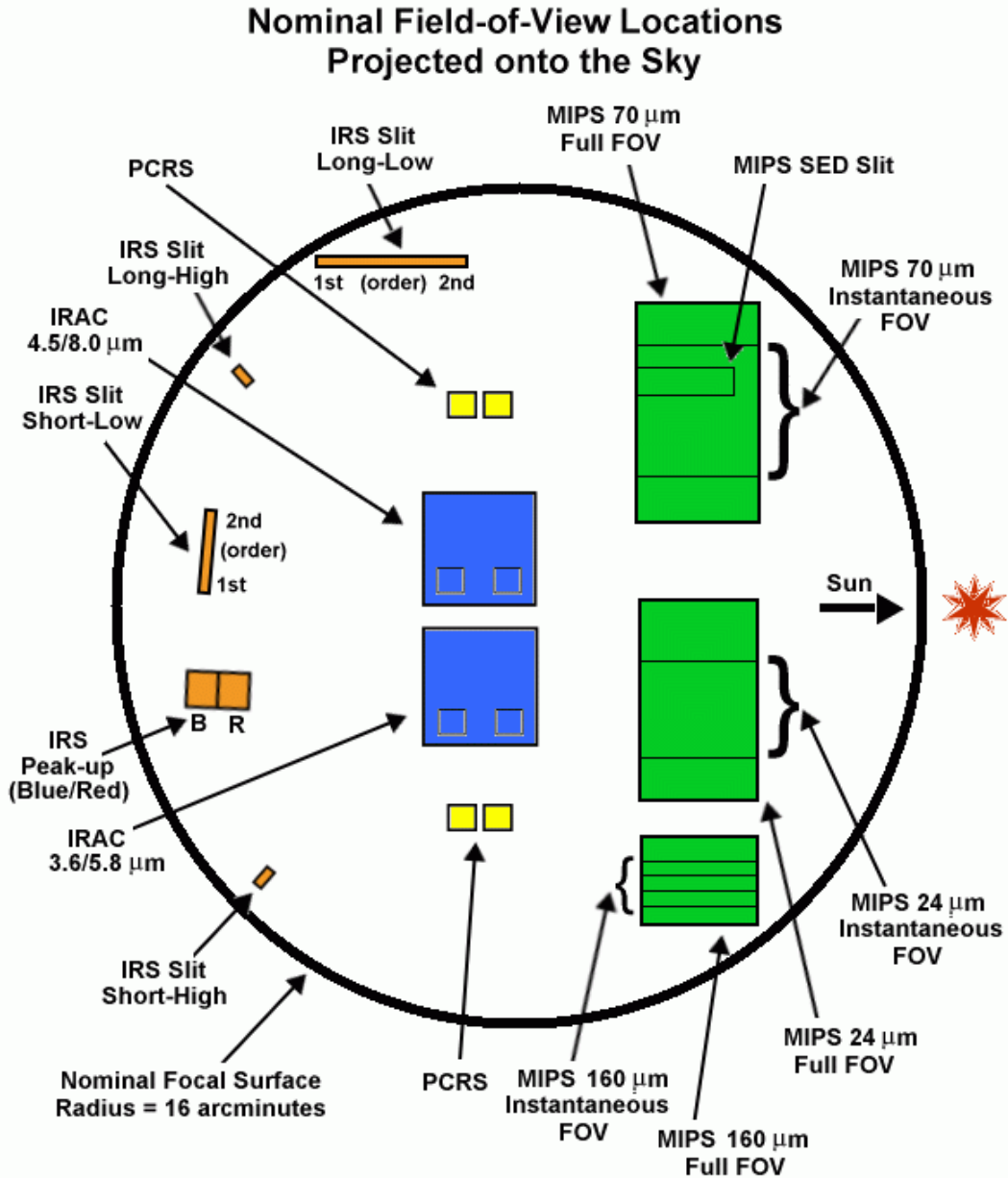
Figure 2.1: Science instrument apertures projected onto the sky. Because of the optical inversion in this projection, the section of sky closest to the projected Sun is on the MIPS side of the focal plane, e.g. to the right in this view. Because the spacecraft does not rotate about the line of sight, this vector is fixed relative to the focal plane on the sky. The IRAC sub-array fields are shown by the small boxes in the lower corners of both IRAC arrays. (The 4.5 and 3.6 *µ*m sub-arrays are on the left.) While this diagram depicts the apertures of the IRS and MIPS, those instruments will not function in the warm mission.

2.4.2 The Life Cycle of a Spitzer Observation
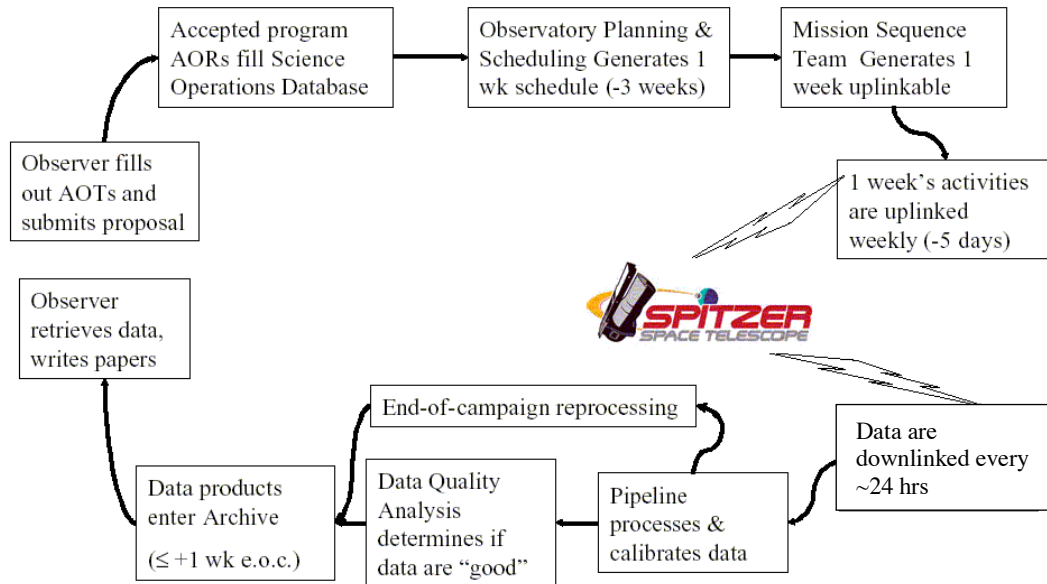
Figure 2.2: The life cycle of a Spitzer observation. The detailed definition of observations will occur at the time of each annual proposal solicitation. In the warm mission there is no longer a Data Quality Analysis check prior to archiving the data.

Figure 2.2 shows the basic stages through which a Spitzer observation passes. These processes are described in more detail in Chapter 5. An SSC-supplied software tool called Spot (section 5.2.1) is used to enter all the parameters (e.g., integration time, choice of modules, etc.) needed to fully specify the observation. This process is called "filling out the AOT front-end." Spot also provides wall-clock time estimates for the total duration of observations. Spot does not allow observers to create impossible observations (however, observer-supplied constraints can render an observation unschedulable; see section 5.4.3)

An observation that has been fully defined by supplying parameter values for an AOT is known as an Astronomical Observation Request (AOR), and is the basic scheduling unit for Spitzer. After the Time Allocation process has been completed, the AORs submitted for all of the approved Spitzer observations are loaded into a database known as the Science Operations Database (SODB), and are stored there in the form of a set of specific parameters and values. These parameters are used by the software AOR/IER Resource Estimator (AIRE) to expand the set of parameters into a set of instrument and spacecraft commands which execute the observation on board Spitzer, as well as to provide extremely high fidelity estimates of execution time for the scheduling process. Observers also access AIRE through Spot for their time estimates. The Spitzer planning and scheduling process produces observing schedules based on these resource estimates. After the content of the schedules has been approved and finalized, AIRE takes the AOR parameters and produces command product files which are

then processed by the JPL Mission Sequence Team and finally uplinked and executed by Spitzer. *It is important to realize that the process of creating commands to carry out an observation based on the AOR parameters is done by software, not by support astronomers at the SSC*.

After an observation has been scheduled and carried out, the resulting data are pipeline-processed and are placed in the Spitzer science archive and made available to the observer. In the warm mission the SSC will no longer perform a quality assessment of the data prior to it being made available to the observer.

2.5 SSC Science User Support Services

The Spitzer Science Center acts as the interface between the astronomical community and the observatory. The SSC offers support at all stages of Spitzer use, including proposal preparation, detailed observation design, and data analysis. The SSC provides this support primarily through supplying documentation, providing science user tools, and operating an online Helpdesk.

2.5.1 Documentation

The primary form of science user support is through the dissemination of information, including this Warm SOM. In addition to the Warm SOM, the SSC offers a comprehensive set of web pages, which includes further technical documentation, software downloads, Spitzer Frequently Asked Questions (FAQ) pages, observation scheduling status, frequently updated news, instrument status, performance reports plus tools, and information to assist with proposal preparation.

2.5.2 Helpdesk

The SSC Helpdesk service (help@spitzer.caltech.edu) is the primary interface to the Spitzer Science Center for the community. The Helpdesk provides answers to technical or policy questions, and is available to address concerns about any facet of Spitzer observing. The Helpdesk also provides support for special needs such as requesting modifications to Spitzer observations and the activation of Target of Opportunity (ToO) observations.

Once a Helpdesk question has been received, it is directed to an appropriate expert. An observer can expect a reply within two business days. Particularly complex requests may take up to 5 days for a response. On the other hand, easy questions can result in a nearly instantaneous response. (There is no auto-reply on our system.) Note that as the proposal deadline approaches, the turnaround times for an SSC response (particularly for definitive answers to complex technical questions) will likely increase. It is the responsibility of proposers to take this reality into consideration when submitting queries shortly before the proposal submission deadline.

2.5.3 Proposal Kit

The online Proposal Kit provides all of the information necessary for the prospective General Observer (GO) investigator. It can be found on the SSC website at http://ssc.spitzer.caltech.edu/warmmission/propkit/.

The Proposal Kit also includes instructions for downloading and installing the Spot software on the user's machine. Spot, discussed more in section 5.2.1 below, is used to plan and prepare Spitzer observations, and to submit GO proposals electronically to the SSC. *Prospective GO investigators are recommended to download Spot and to start planning their Spitzer observing programs well before the proposal submission deadline*.

In addition, the Proposal Kit includes many kinds of documentation, including this manual, the current Call for Proposals, Spitzer Warm Mission Observing Rules, an Observation Planning Cookbook, Proposal Submission Guidelines, and the proposal template files, guidelines pertinent to the calculation of the special overhead burdens applied to Targets of Opportunity, targets with late ephemeris changes, etc.

The online Proposal Kit also contains information specifically designed for Spitzer Solar System researchers. It includes asteroid count estimates, a summary of ephemeris management at the SSC, and tips for using the Horizon database supported by the Solar System Dynamics Group at the Jet Propulsion Laboratory.

2.5.4 Data Products

Once data are collected, the SSC creates and delivers pipeline-processed, calibrated data products to the observer and to the Spitzer science archive. Three levels of processed data are created: Raw data, Basic Calibrated Data (BCD) and Ensemble data (also known as "post-BCD data"). Raw data are unprocessed data, which have been packaged into FITS format. BCDs are single-frame FITS format data products, which have been processed to remove instrumental signatures, and which are calibrated in scientifically useful units. Ensemble data are higher-level products, and may include mosaicking or co-addition. The data products are described in more detail in the IRAC chapter and in the corresponding IRAC Instrument Handbook, available on the SSC website.

In general, the final calibration for an instrument campaign, which is typically about two weeks in duration, is based upon calibration observations taken at the beginning and periodically throughout the campaign, so pipeline data products are typically available two weeks after the end of the campaign. The SSC continues to use defined instrument campaigns in the warm mission even though the campaigns are always IRAC. Defined campaigns allow us to process, archive, and release to the commuity blocks of calibrations and science observations in a timely manner.

The SSC validates the pipeline processing for each observing mode prior to the release of data. In the warm mission basic quality assessment is no longer performed on Spitzer data before they are delivered to the observer. Observers should contact the Helpdesk (help@spitzer.caltech.edu) if they notice unusual features in Spitzer data. The SSC will investigate and, if needed, update the quality assessment information in the database for future archival use.

In November 2010 data access via Leopard was deactivated. Observers should use the Spitzer Heritage Archive (SHA) to access data (http://sha.ipac.caltech.edu/applications/Spitzer/SHA/). Leopard may still be used to search the Reserved Observations Catalog. The Leopard User's Guide is also available on the SSC website.

After obtaining data, investigators may be interested in the IRAC Instrument Handbook available on the SSC website off the IRAC instrument webpage.

3 Observatory Description and Constraints

This section addresses the Spitzer Space Telescope design and the observational constraints that arise from that design. The Spitzer Space Telescope consists of five basic elements: the cryogenic telescope assembly (CTA), the spacecraft, and the IRAC instrument. In this section the spacecraft and CTA design (not including the telescope design, see Chapter 4) are discussed. The design and performance of the pointing and control system (PCS) are also discussed.

3.1 Observatory Design and Operations Concept

A basic external view of Spitzer is shown in Figure 3.1. The spacecraft provides structural support, pointing control and telecommunications and command/data handling for the entire observatory. The spacecraft, including the spacecraft bus, the solar panel and PCS (including the Pointing Control Reference Sensors, or PCRSs, which are located in the focal plane) were provided by Lockheed Martin Space Systems Company.

The CTA, shown in Figure 3.2, consists of the telescope, the superfluid helium cryostat, the outer shell group and the Multi-Instrument Chamber (MIC), which hosts portions of the IRAC camera and the PCRS. The telescope assembly, including the primary and secondary mirrors, metering tower, mounting bulkhead (all made of beryllium) and the focus mechanism, is mounted and thermally connected to the cryostat vacuum shell. The barrel baffle of the telescope assembly is separately attached to the vacuum shell at its flange. The MIC, an aluminum enclosure containing the instrument cold assemblies, is mounted on top of the depleted helium tank. The CTA was provided by Ball Aerospace and Technologies Corporation.

The spacecraft and CTA (and science instruments) together comprise the observatory, which is ~4 m tall, ~2 m in diameter, and has a mass of ~900 kg.
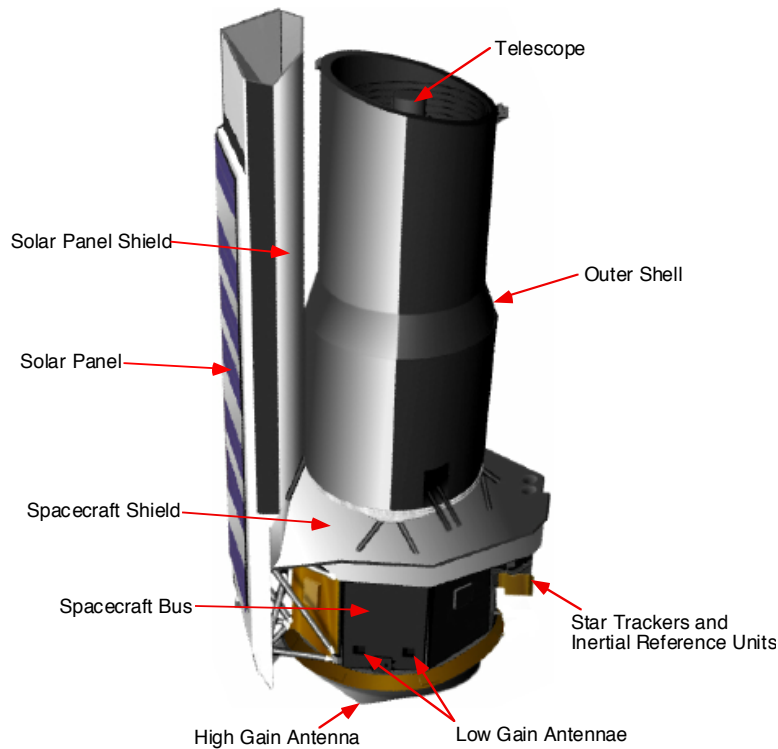
Figure 3.1: Basic external view of Spitzer.

The observatory coordinate system XYZ (shown in Figure 3.3) is an orthogonal right-hand body-fixed frame of reference. The X axis passes through the geometric center of the top surface of the spacecraft, is parallel to the CTA optical axis (which passes through the primary and secondary mirror vertices), and is positive looking out of the telescope. The Z-axis intersects the line forming the apex of the two surfaces of the solar panel. The Y-axis completes the right hand orthogonal frame. The X-axis origin is defined such that the on-axis point between the CTA support truss and the spacecraft bus mounting surface is located at X = +200 cm, in order to maintain positive X values throughout the observatory. The Sun always lies within 2° of the XY plane (i.e., the roll angle is constrained to ±2°).

Spitzer is operated autonomously for moderately long periods of time (24 – 48 hours) interspersed with periods (~170 minutes) of ground contact. In extreme circumstances, Spitzer is designed to survive for up to a week with no ground contact at all.

During routine science operations, Spitzer typically executes a pre-planned week-long schedule of science observations, calibrations and routine engineering activities, which has been uploaded in advance and stored on board. This "master sequence" might typically have 7 different 24-hour Periods of Autonomous Operation (PAOs), containing observations and calibration activities, each followed by a ~170 minute period spent re-orienting the spacecraft for downlink and transmitting the data to the ground. After the downlink, Spitzer returns to the

pre-planned sequence of observations and calibrations. Because efficient communication with the ground requires use of the high-gain antenna mounted on the bottom of the spacecraft (Figure 3.1), executing a downlink of the collected data requires slewing the spacecraft to orient the high gain antenna toward one of the Deep Space Network (DSN) stations on Earth. Any of the three DSN sites (Canberra, Madrid and Goldstone) can be used when visible. During the time that data are being transmitted to the ground, no science data can be collected.
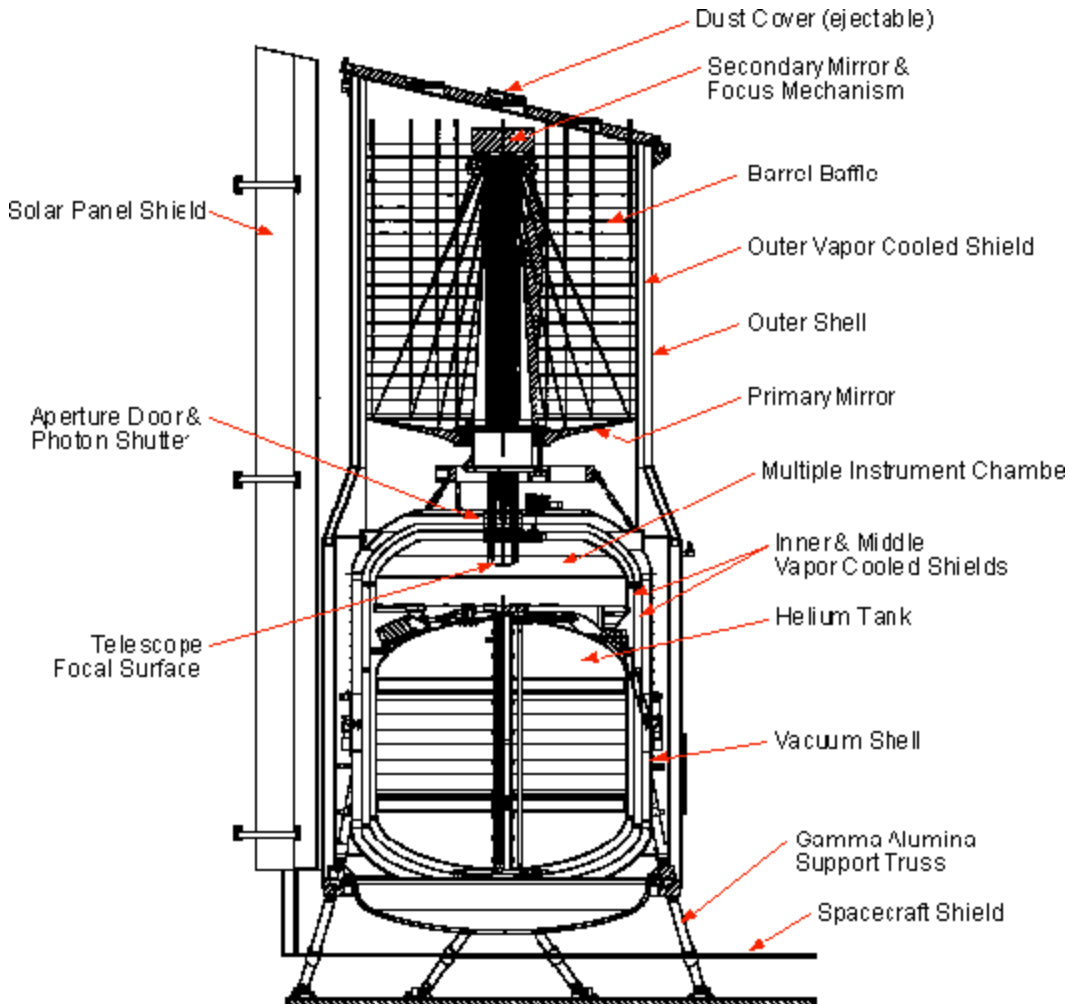
Figure 3.2: Cryogenic Telescope Assembly.

S/C-to-CTA interface plane at station $X = 200$ cm
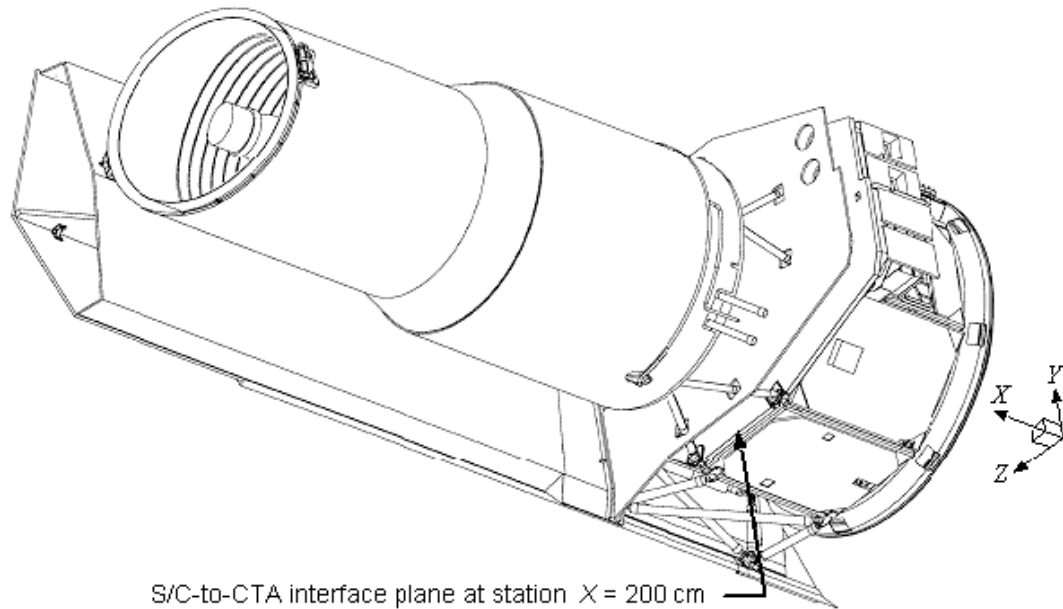
Figure 3.3: Observatory Coordinate System.

If a downlink opportunity is missed (e.g., due to a failure at the ground station), Spitzer preserves the collected science data, continues collecting new science data as scheduled, and attempts to downlink it at the next scheduled opportunity. Once a missed downlink opportunity has occurred, the spacecraft sequence is modified to provide additional downlink time within the next few opportunities if necessary. No data are lost or overwritten, unless the risk of overfilling the entire mass memory (16 Gbits) exists. (See also section 3.1.1 below.)

3.1.1 Data Storage

The Spitzer spacecraft includes the command and data handling subsystem (C&DH) which shares the flight computer (a RAD 6000) with the pointing control subsystem (PCS). The C&DH validates and executes either previously stored or real time commands, receives and compresses data, and writes the compressed data into the mass memory. The C&DH also provides a stable clock to correlate data and events.

During normal Spitzer science operations, the observatory collects, compresses, and stores ~24 hours' worth of science data prior to downlinking it. Spitzer has 8 Gbits of solid state memory available for each of two redundant flight computers, for a total of 16 Gbits of storage (for both science and engineering data). During each ~24-hour PAO, up to 6 Gbits of the memory are filled. Enough additional storage capacity is left unused during that ~24-hour PAO to permit missing a downlink opportunity (e.g., due to a problem at the ground station) and continuing to observe without overwriting previously collected science data. Since the full mass memory (16 Gbits) is available to both redundant computers, in general multiple passes would have to be missed before the risk of losing science data that had not been transmitted to the ground becomes significant.

3.1.2 Data Transmission

Spitzer has two antenna systems for data uplink and downlink. The high gain antenna (HGA) supported a maximum downlink rate of 2.2 Mbit/s for the first 2.6 years of the Spitzer mission. Since Spitzer drifts away from the Earth at about 0.12 AU per year, the data transmission rates on the HGA have had to decrease as a function of time, and late in the mission, we may have to change our downlink strategy to accommodate this. The two low gain antennae (LGA) give wide-angle coverage, but only support downlink at 44 kbit/s at the beginning of routine observing, decreasing to 40 kbit/s after 3 years. The LGA are used in safe mode, but are not normally used to transmit science data during routine science operations.

Because of the location of the HGA, it is necessary to stop observing and point the telescope in the anti-Earth direction to downlink the science data. Depending upon the details of the observations that are scheduled, Spitzer produces ~1 to 6 Gbits of (compressed) science data during 24 hours of observing. Initially, Spitzer collects data for about 24 hours and then spends ~170 minutes downlinking the data. The scheduling system predicts the compressed data volume that is generated during each downlink and schedules the downlink contact time accordingly. The downlink periods are also used for some spacecraft maintenance activities (such as dumping angular momentum) and for uplinking commands. If low volumes of data are being generated, longer periods of time between downlinks may be used.

At each downlink opportunity, Spitzer attempts to transmit all the data in the mass memory. Any data that the ground has not confirmed as received will be retransmitted at the next downlink pass. It is anticipated that some data could be missed at any pass, and it may take several passes before the ground receives all the science data for a given observation.

Whenever the HGA is used for downlink, it is also possible to uplink commands and files to Spitzer. Normally, up to ~5 communication periods per week are used to send up all the sequences and information needed to support the next upcoming week of observations. No communications with Spitzer are planned outside the scheduled downlink sessions.

3.1.2.1 Impact on Observers

The downlink strategy has little impact on observation planning with Spitzer. It is one component in determining the maximum length of an AOR[1]. A 24-hour interval between downlinks does imply that it can be a day or longer before science data are available on the ground after an observation is complete.

---

[1] Currently, the maximum planned length of an AOR is 24 hours for IRAC. Please note that this is the maximum length for an isolated AOR. In general, there would not be several contiguous periods of this length available.

The uplink strategy also does not directly affect observation planning, but it drives the time scale on which changes to the stored science schedule and its contents can be made (e.g., for a ToO).

3.2 Sky Visibility

3.2.1 Solar Orbit

An important innovation enabling Spitzer to accomplish ambitious scientific goals at a modest cost is its Earth-trailing heliocentric orbit (shown in Figure 3.4), in which the observatory drifts away from Earth at the rate of ~ 0.12 AU/year. This substantially helped prolong the coolant lifetime by supporting an operating regime in which most of the cryogen was used to take up the power dissipated by the detector arrays, rather than lost to parasitic heat loads. In addition, this orbit has less-constrained visibility, compared to what would have been the case in a near-Earth orbit, allowing all parts of the sky to be visible for at least two extended periods each year and some zones to be visible continuously.

3.2.2 Pointing Constraints

Spitzer's view of the sky is limited by two hard pointing constraints, illustrated in Figure 3.5 and (in a different fashion) in Figure 3.6:

> The angle between the boresight and the direction of the Sun may never be less than 82.5°. (NB: this was updated in early 2004.)
> The angle between the boresight and the direction of the Sun may never exceed 120°.

The area defined by these hard constraints is called the Operational Pointing Zone (OPZ). In addition, some bright objects (such as the Earth) are normally avoided, because they would degrade the quality of the observation, due to direct exposure or stray light, but this is not a strict constraint (see section 3.2.6 and Appendix 7.3). Note that the definition of the OPZ precludes observing Mercury or Venus with Spitzer. A second-order effect on the OPZ is provided by the limited roll angle of Spitzer around the Y-axis (see Figure 3.3), which is just ±2°.

Figure 3.6 shows the actual pointings of the observatory for one day in the life of Spitzer. Note the locations of the OPZ and how it constrains where we actually pointed on that day.
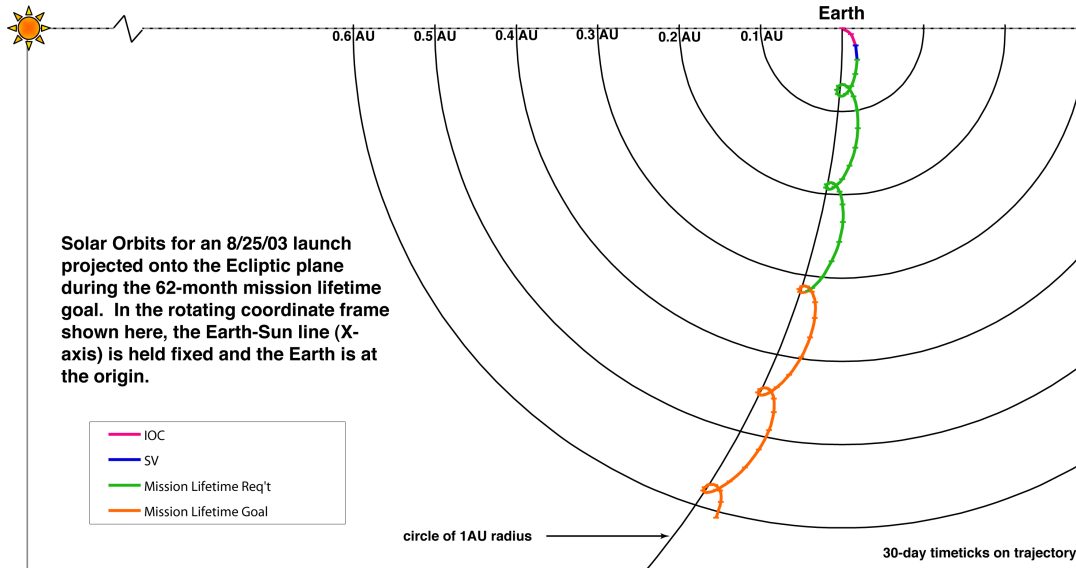
Figure 3.4: Spitzer's solar orbit projected onto the ecliptic plane and viewed from ecliptic North. In the rotating frame, the Earth is at the origin and the Earth-Sun line is defined as the X-axis. "Loops" and "kinks" in the trajectory occur at approximately 1-year intervals when Spitzer is at perihelion. Spitzer's orbit is also slightly inclined with respect to the ecliptic.

3.2.3 Viewing Periods

The amount of time during the year any particular target is visible depends primarily on the absolute value of its ecliptic latitude (Figure 3.7). As seen in Figure 3.5, Spitzer's instantaneous window of visibility on the celestial sky forms an annulus (the OPZ), perpendicular to the ecliptic plane, of ~40º width and symmetrical with respect to the Sun. This annulus rotates with the Sun over the period of a year; the edges of the OPZ move along the ecliptic at about 1º/day as Spitzer orbits the Sun. For an object near the ecliptic plane, the length of the visibility period is ~40 days twice a year (modulo periods when undesired bright moving objects are also present and bright object avoidance has been selected; see section 3.2.6). The visibility periods increase to ~60 days twice/yr at an ecliptic latitude of ~45º, ~100 days twice/yr at latitudes ~ 60º, then becoming a single long window ~250 days long for latitudes near 60-70º, finally reaching constant viewing near the ecliptic poles. About a third of the sky is visible to Spitzer at any time. Figure 3.8 illustrates how the total number of days of visibility varies over the sky in three coordinate systems.
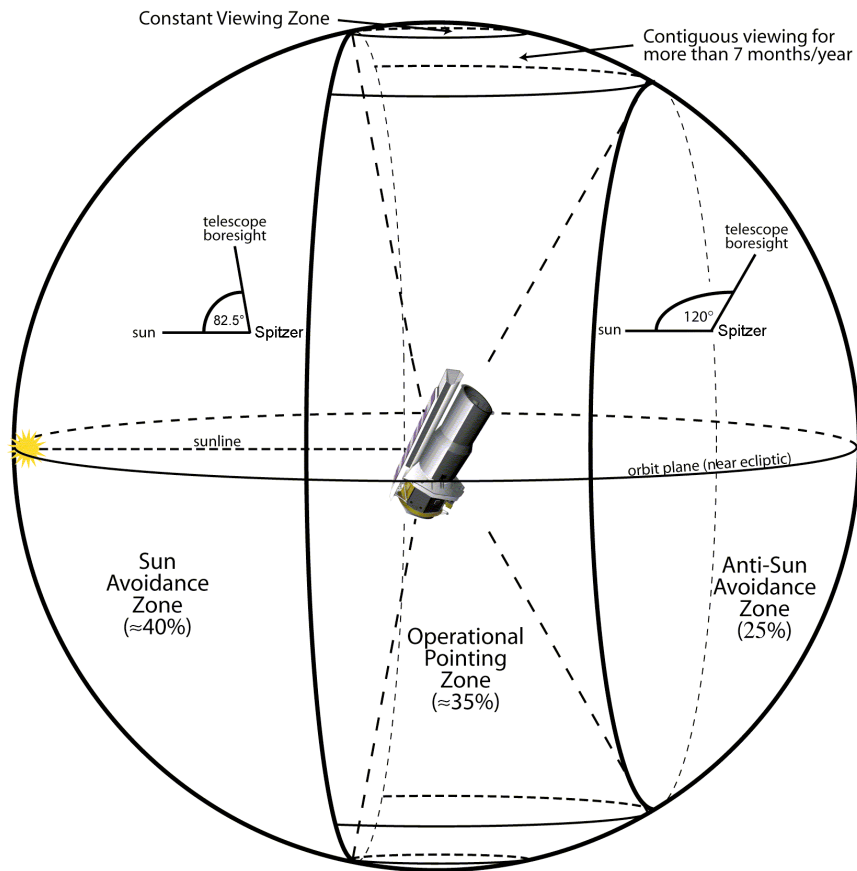
Figure 3.5: The main geometric observing constraints form an area called the Operational Pointing Zone (OPZ).
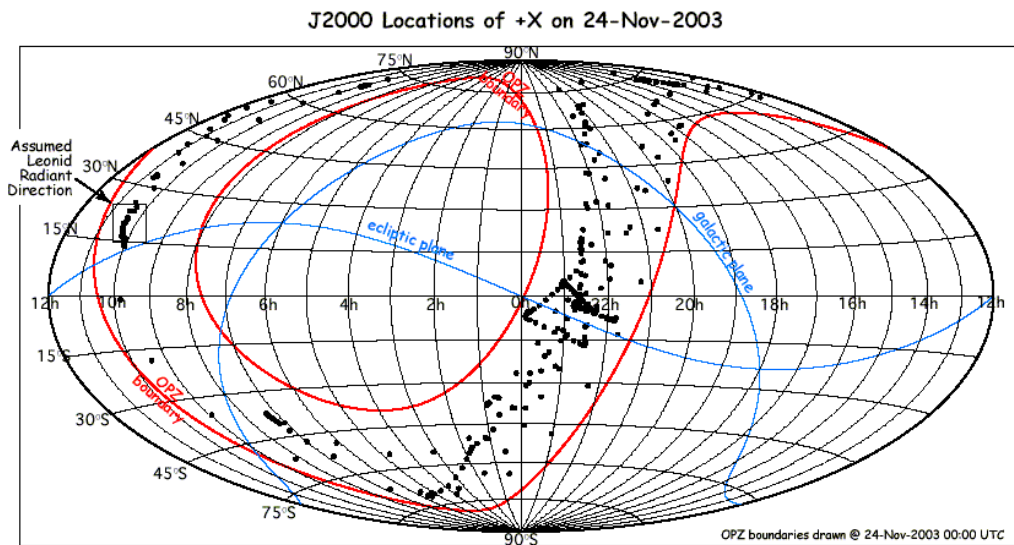
Figure 3.6: OPZ boundaries for 24 Nov 03 (0h UTC), with dots representing the actual locations of the telescope boresight for the subsequent 24 hours.
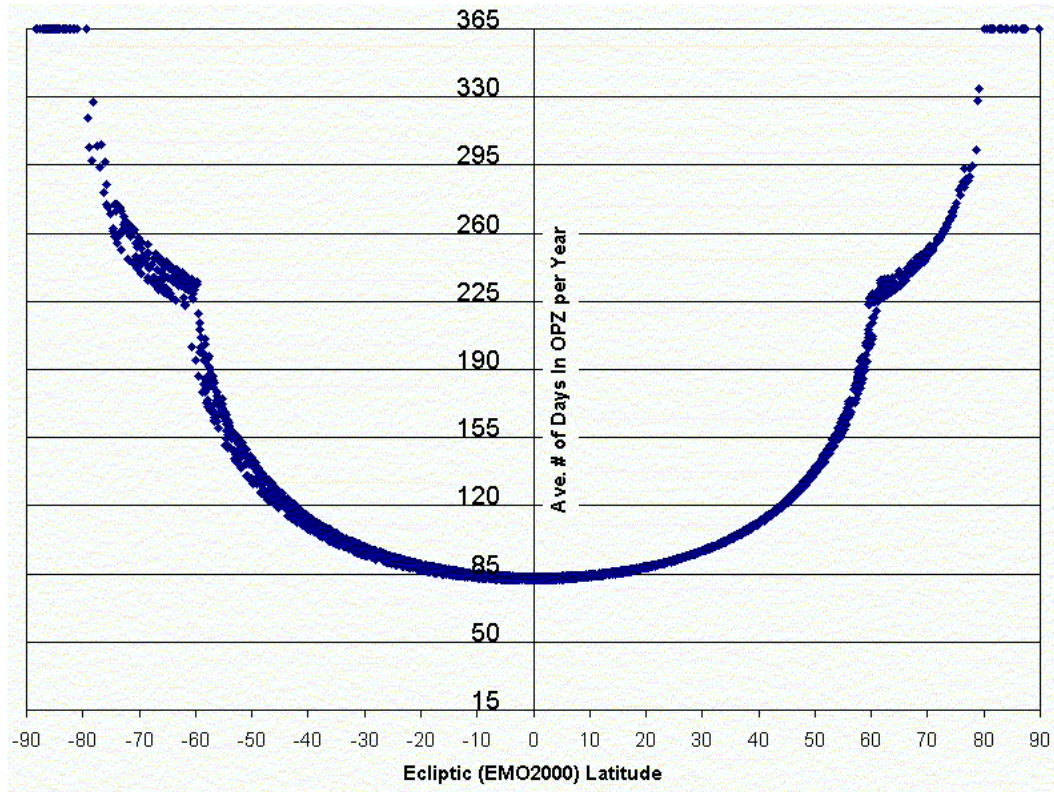
Figure 3.7: Variation of length of visibility period as a function of ecliptic latitude for all of the targets in the April 2003 ROC. (This figure is provided as indicative of the general concepts, despite the fact that the ROC has changed substantially since April 2003.)
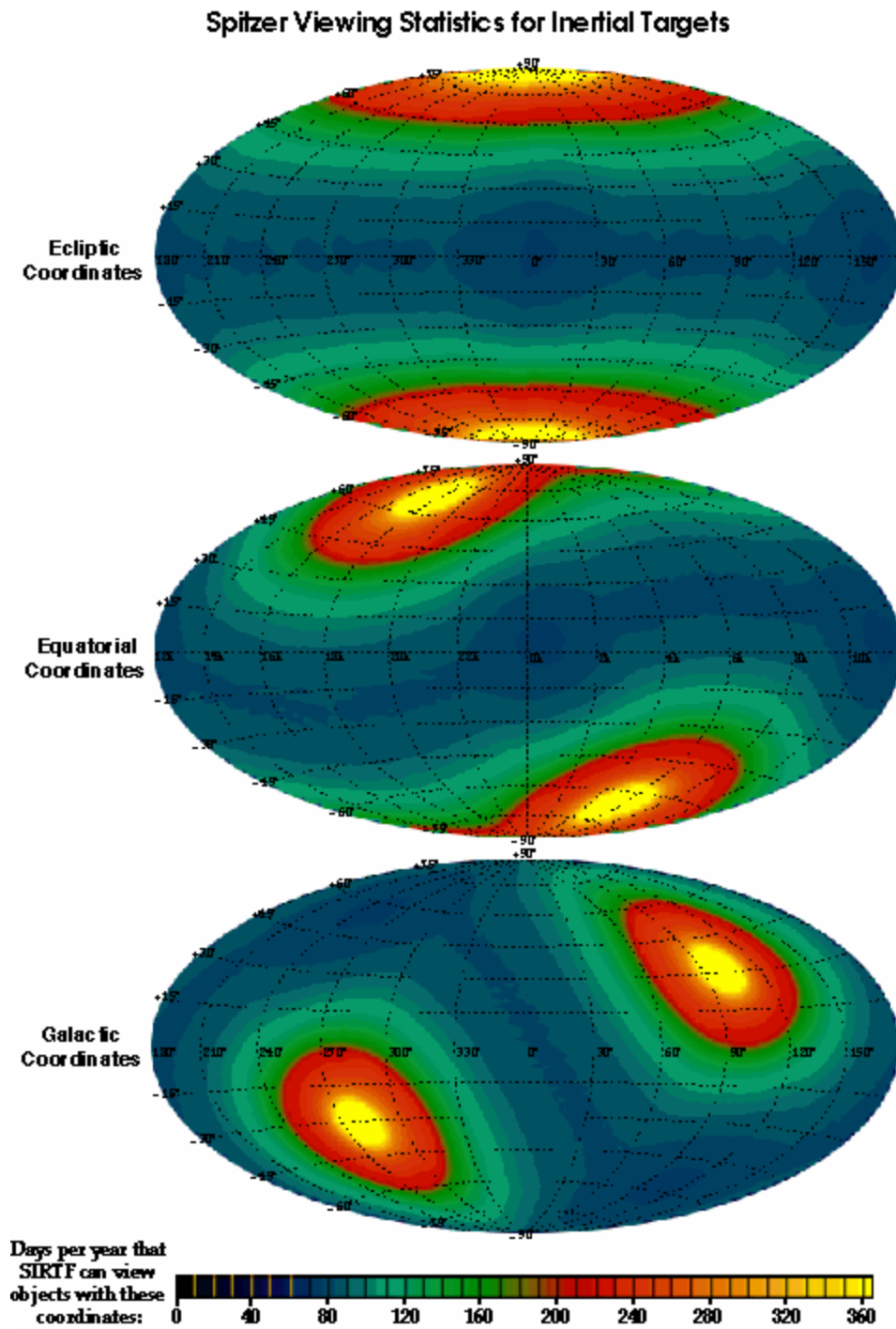
Figure 3.8: Total days of visibility per year in equatorial, ecliptic and galactic projections.

3.2.4 How Visibility Evolves with Time

Figure 3.9 illustrates the zone of visibility in equatorial coordinates for four specific dates during the first year of operations. Note how the sky passes into and out of visibility as the calendar date advances. Each set of contours shows the available and forbidden zones on a particular date (in this plot, 1 Sep 2003, 1 Dec 2003, 1 Mar 2004, and 1 Jun 2004). On each date, there is a forbidden zone in the anti-Sun direction, as well as a second, more extended-looking forbidden region on the side of the spacecraft towards the Sun; the Sun-ward forbidden region is in the center of the plot on 1 Sep and on the edges for the 1 Mar plot. Note that even targets at high declinations may fall in the forbidden zones part of the time, although objects at extreme declinations are generally visible for most of the year.

Although these plots are accurate, observers should always use Spot to determine visibility of a target on a particular day (see Chapter 5).
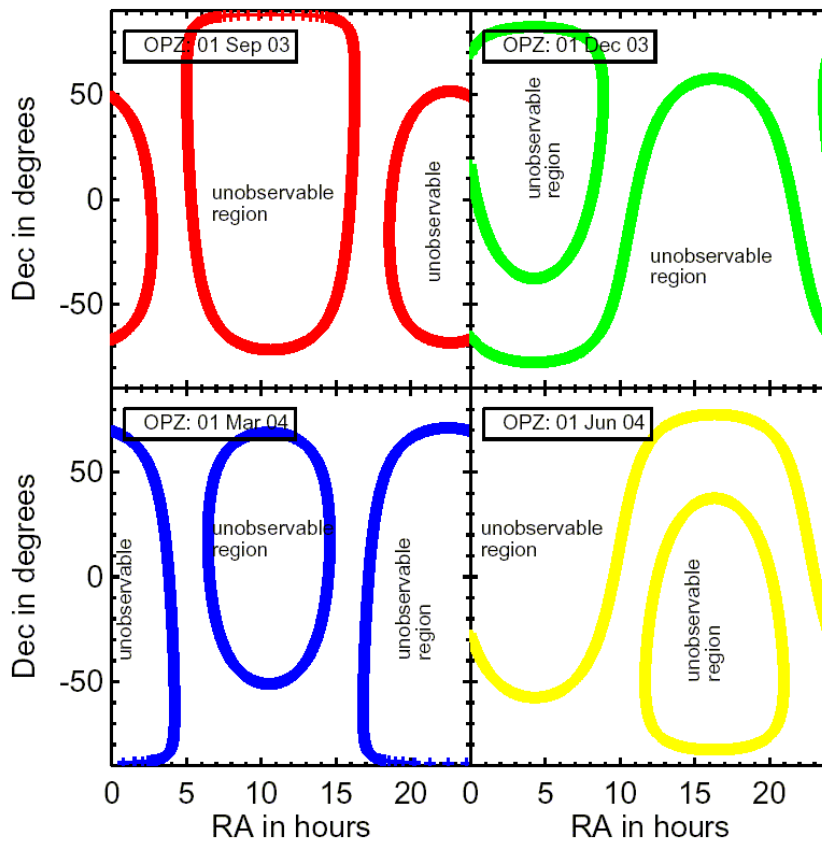
Figure 3.9: Example of time evolution of visibility zones over a year; see text.

3.2.5 Orientation of Focal Plane on the Sky

Spitzer has very limited ability to rotate the focal plane of the telescope. At any given time, the center of the sunshade (X-Z plane; see Figure 3.3) is always kept within ±2º of the Sun. This limited freedom in the "roll" angle is used to maintain a consistent orientation for long observations (AORs) and is not selectable by the observer. For each target, the orientation of the focal plane on the sky is a function of the position of the spacecraft along its solar orbit (i.e., the date of observation) and of the ecliptic latitude of the target. Targets in the ecliptic plane have only two possible focal plane orientation angles which are at 180º with respect to each other. Elsewhere in the sky, the focal plane has two ranges of orientation angles.

Science instrument aperture orientation within the focal plane is physically fixed, which affects mapping with IRAC.

3.2.5.1 Impact on Observers

Spitzer observations must be designed with this lack of roll control in mind. Observers who require a certain array orientation angle relative to the target must check to determine when, if ever, the needed orientation is achieved, and must request a suitable range of observation date(s). It is possible that a particular target might not be observable at the same time of the year that an array has the desired orientation. The focal plane/array orientation on any date can be calculated and projected on the sky using the Spitzer observation planning tools (see Chapter 5).

Because constraining the orientation tightly also constrains the scheduling time tightly, it increases the risk that an observation may be subject to schedule conflicts. In addition, the presence of many highly constrained observations tends to reduce the observatory's efficiency. Therefore, observers should design observations that are as robust as possible to the maximum range of focal plane orientations, even if this makes the observations somewhat less efficient. The use of a timing constraint to obtain a specific orientation requires a *very* strong scientific justification when the observations are proposed. See the Call for Proposals for more information.

3.2.6 Bright Object Avoidance

No object outside the solar constraint zone poses a threat to instrument safety. However, an observer may wish to avoid observing the Earth and other bright moving objects to avoid compromising observations of faint targets. Therefore, the visibility windows calculated by Spot avoid certain bright moving targets by default, although the observer can choose to override the default.

With bright object avoidance turned on (the default), the visibility windows calculated for both inertial and moving targets will exclude regions of time when the positions of (a) the Earth and Moon, and (b) a fixed list of bright moving objects (e.g., Jupiter, Saturn, bright asteroids) coincide with the target position.

The visibility windows will be trimmed to delete any time periods when the Spitzer target is within 7º of the Earth or Moon and when the target is within 30′ of the other bright objects. The complete list of the bright moving objects is in Appendix 7.3.

The observer may choose to override the default (a) Earth/Moon or (b) other bright object avoidance. For example, to observe Jovian satellites, one would turn off (b) and leave (a) in effect.

The latest version of Spot includes the option to overlay all known moving objects on an image for a particular date. Observers concerned about bright moving objects not included in the list above may wish to use this option.

It should be noted that it is the observer's responsibility to check for any bright *inertial* targets in the field of view that might compromise the observation. There are some that will heavily saturate the instruments and therefore compromise not only that observation, but also possibly subsequent science observations as well. A list of some of the inertial objects known to saturate IRAC is available on the SSC website. You can also visualize bright objects near your AOR in Spot. Spot does *not* exclude observations of these objects. **The SSC reserves the right to exclude some targets and AORs as a result of impacts that bright objects would have on subsequent observations.**

3.3 Pointing Capabilities

3.3.1 Pointing Control System

The PCS includes the hardware and flight software necessary for precision telescope pointing, stabilization, slewing, tracking, and safe mode functions. The PCS performed the initial attitude acquisition of the spacecraft following launch vehicle separation. It provides periodic boresight calibration for the telescope. The PCS provides the capability for both rapid large angle slews and small maneuvers to place and reposition science targets within the science instrument apertures; it maintains the solar array orientation toward the Sun; and, it points the high gain antenna toward Earth for downlink. The PCS also contains Wide Angle Sun Sensors (WASSs) that act as a second check on the spacecraft orientation to ensure that the hard pointing constraints (see section 3.1) are not violated. High-level fault protection will place the telescope in a safe mode if a violation is detected. The performance numbers presented in this and the following sections are based on our present understanding and measurements of the on-orbit PCS performance.

The PCS is a celestial-inertial, three-axis stabilized control system. A high performance star tracker/inertial reference unit (ST/IRU) package provides attitude determination and reconstruction capabilities. On-board pointing commands and variables use the J2000 coordinate system. Reference to the J2000 celestial sphere is implemented within the ST through autonomous identification

of stars carried in an on-board catalog of 87,000 Tycho stars down to 9th visual magnitude[2].

The ST is used to point an instrument boresight to a desired location on the sky with an initial accuracy of at least 0.5″ (1σ radial). The ST field of view is 5°×5°, which ensures that Spitzer can point to any part of the sky and have the ST meet its pointing requirements. Typically 40 stars are used simultaneously. The IRUs (gyros) provide pointing stability when not using the ST as a pointing reference; however the IRUs exhibit drift. The pointing drift derived from the gyros is <3 mas/sec over 8 hours. The drift rate when using the IRU-only mode should generally be better than 1 mas/sec over 200 sec.

All telescope pointing is defined and calibrated relative to redundant PCRSs located in the focal plane. During the course of the mission, the PCRS is periodically (about every 12 hours) used to calibrate the telescope-to-star tracker boresight alignment that may drift due to thermo-mechanical effects. Each PCRS detector is a Si PIN photodiode array divided into two 4×4 subarrays for redundancy. Each pixel is 250 μm square, with a plate scale of 10″ per pixel. The PCRS calibration measures the star position with an accuracy of 0.1″ (1σ per axis), and is sensitive down to 10th visual magnitude at a wavelength of 550 nm.

Spitzer also has WASSs, which measure the Sun's position with respect to the spacecraft. These sensors were used during initial attitude acquisition after launch, as well as for Sun avoidance, fault protection, and safe mode during the mission. Each WASS provides a field of view of 2π sr with an accuracy of ±0.1° at null. They are placed at the top and the bottom of the solar panels to maximize the coverage, with their boresights aligned to the spacecraft Z-axis.

Four reaction wheels provide the primary control actuation for all modes of operation. They are mounted in a pyramid orientation about the X-axis; each canted at 30° towards the X-axis. Over time, angular momentum accumulates in the reaction wheels, due primarily to the small offset between the center of mass and the center of (radiation) pressure. Unlike an observatory in low Earth orbit, which can dump this momentum magnetically, Spitzer has a "Reaction Control System" (RCS), which uses cold nitrogen gas thrusters to provide the reaction wheel momentum unloading capability; opportunities to dump momentum are scheduled during routine downlinks. The nitrogen supply was sized to accommodate a mission lifetime in excess of 5 years. Due to the random nature of observations with respect to the solar direction and the resulting torque on the spacecraft, fewer momentum dumps than expected have been required to remove angular momentum. Spitzer currently has enough nitrogen gas to run for an additional ten years or more with a similar balance of science programs.

---

[2] The on-board catalog actually uses the ICRS coordinate system, so, in fact, the on-board pointing system is really ICRS. However, the differences between ICRS and J2000 are so small (≤120 mas) that no conversions are made, and Spitzer is effectively considered to use the J2000 coordinate system.

On-orbit measurements show that the PCS is capable of slewing the telescope 180° in 900 sec, 1° in 60 sec, and 1′ in 6 sec, while maintaining its inertial pointing knowledge. These times include the acceleration and deceleration of the telescope, but do not include the time it takes for the PCS to stabilize after the slew has completed. The pointing system has several operating modes, and the AOTs are designed to use the pointing mode most appropriate for each observing mode. Settling time varies with operating mode and slew magnitude. For IRU-only slews, slews less than 30′ settle to within 0.2″ rms within 10 sec. (Settling may take longer in some cases.) The AOTs make use of on-board slew completion and stabilization indicators to proceed with the observation as soon after a slew as is possible. Note that the time required for small slews, dithers, offsets, settling, etc., within an AOR is considered part of the observation. Time estimates provided through Spot account for these transparently and accurately.

The best available pointing system models are incorporated into Spot. However, note that Spot estimates may change if, e.g., Spitzer's slew rate changes.

3.3.2 Pointing Accuracy and Stability

The blind pointing accuracy is the same as the on-board attitude knowledge, <0.5″ (1σ radial rms) with a stability of <0.1″ (1σ radial rms over 200 sec). In the incremental pointing mode, the PCS performs controlled repositioning of the boresight with an offset accuracy usually no worse than 0.55″ (1σ radial rms) across angular distances of up to 30′ and usually better than 0.4″.

3.3.3 Tracking Capabilities

Spitzer does not have a true tracking capability for Solar System Objects (SSOs). However, Spitzer simulates tracking by scanning in linear track segments at rates up to 1″/s. The linear track segments are linear in equatorial coordinate space; they are commanded as a vector rate in J2000 coordinates, passing through a specified RA and Dec at a specified time.

The SSO ephemerides are maintained on the ground, rather than on-board Spitzer, but an observer may specify flexible scheduling constraints, and the linear pseudo-track specification (start point, rate and direction, in equatorial J2000 coordinates) is calculated at the time of scheduling. The observation is executed at the scheduled time (within a window of +3, -0 s), and the PCS follows the track as specified, assuming the given start point corresponds to the time given in the track command. All other PCS movements can be superposed on a specified track, including dithers and scans.

PCS measurements indicate that the blind track acquisition accuracy is ≤ 0.5″, independent of the track rate, which is consistent with expected performance on fixed targets. The track stability is better than scan mode requirements: ~0.5″ in 1000s. The offset accuracy during tracking is better than ~0.55″, also consistent with the required performance on fixed targets.

Section 5.5 presents more detailed information on observing Solar System Objects, including ephemeris management.

3.3.4 Pointing Reconstruction

Pointing reconstruction refers to the post-facto determination of where the telescope was pointed with a greater accuracy than was known by the flight system. Spitzer has a requirement to perform pointing reconstruction to 1.4″. Based on in-orbit results, Spitzer meets this requirement. The nominal pointing is reported in the data products. Based on post-BCD processing and comparison of extracted sources with 2MASS sources, users will receive data with IRAC data pointing reconstruction generally <1″, with respect to the 2MASS coordinate system. Relative pointing (relative separation of two objects within an AOR) is good to <0.5″.

4 Telescope and Focal Plane

4.1 Optical Design

The telescope is a Ritchey-Chrétien design, known from on-orbit measurements to be diffraction-limited at 5.5 μm over the IRAC field of view, and expected to be diffraction-limited at 6.5 μm over the entire field of view. The 85-cm diameter primary mirror and the rest of the telescope structure are fabricated entirely of beryllium, utilizing advances in optical design, testing, and fabrication to produce a lightweight telescope that operates at cryogenic temperatures. The optical design parameters for the telescope are summarized in Table 4.1 below. The telescope configuration is shown in Figure 4.1.

Note that this chapter addresses the telescope itself; the point spread function (PSF) for IRAC is discussed in chapter 6.

Table 4.1: Telescope Configuration

Optimal Parameter Description	Value at 5.5 K
System Parameters:	
Focal Length	10,200 mm
Focal Ratio	f/12
Back focal length (PM vertex to focus)	437 mm
Field of View (diameter)	32.0 arcmin
Field curvature radius	140.5 mm
Wavelength coverage	3 μm–180 μm
Aperture Stop:	
Location	Edge of primary mirror
Diameter of OD obscuration	850.00 mm
Diameter of ID obscuration	320.00 mm
Linear obscuration ratio	0.3765
Primary Mirror (hyperbola)	
Radius (concave)	-2040.00 mm
Conic constant	-1.003546
Clear aperture	850.00 mm
Focal ratio	f/1.2
Secondary Mirror (hyperbola)	
Radius (convex)	-294.343
Conic constant	-1.531149
Clear aperture (OD)	120.00 mm
PM to SM spacing (vertex to vertex)	887.528 mm
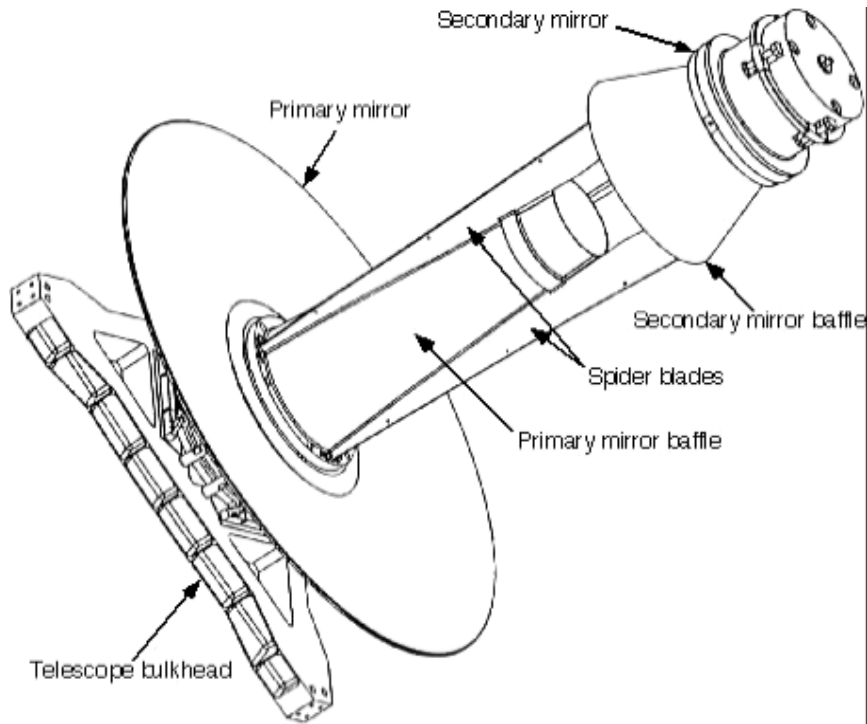
Figure 4.1: Spitzer Telescope Assembly.

The telescope employs a single arch primary mirror, which reduces mass. The primary mirror is supported on three bipod flexures relatively close to its axis. The spider blades, primary mirror baffle, and secondary mirror baffle are integrated into a one-piece, relatively small diameter metering tower extending through the central hole in the primary mirror.

4.2 Optical and Thermal Performance

4.2.1 Surface Accuracy

The Ritchey-Chrétien design minimizes spherical aberration and coma over large fields of view. Field curvature varies quadratically with field angle. Similarly, the rms wavefront error at best focus varies quadratically with field angle and equals 0.52 waves ($\lambda = 0.6328$ μm) at the edge of the field. Essentially all of this error is due to astigmatism.

The surface figure for the primary mirror was measured at cryogenic temperatures to be 0.067 μm rms over the entire clear aperture, meeting the specification of 0.075 μm rms (Figure 4.2).
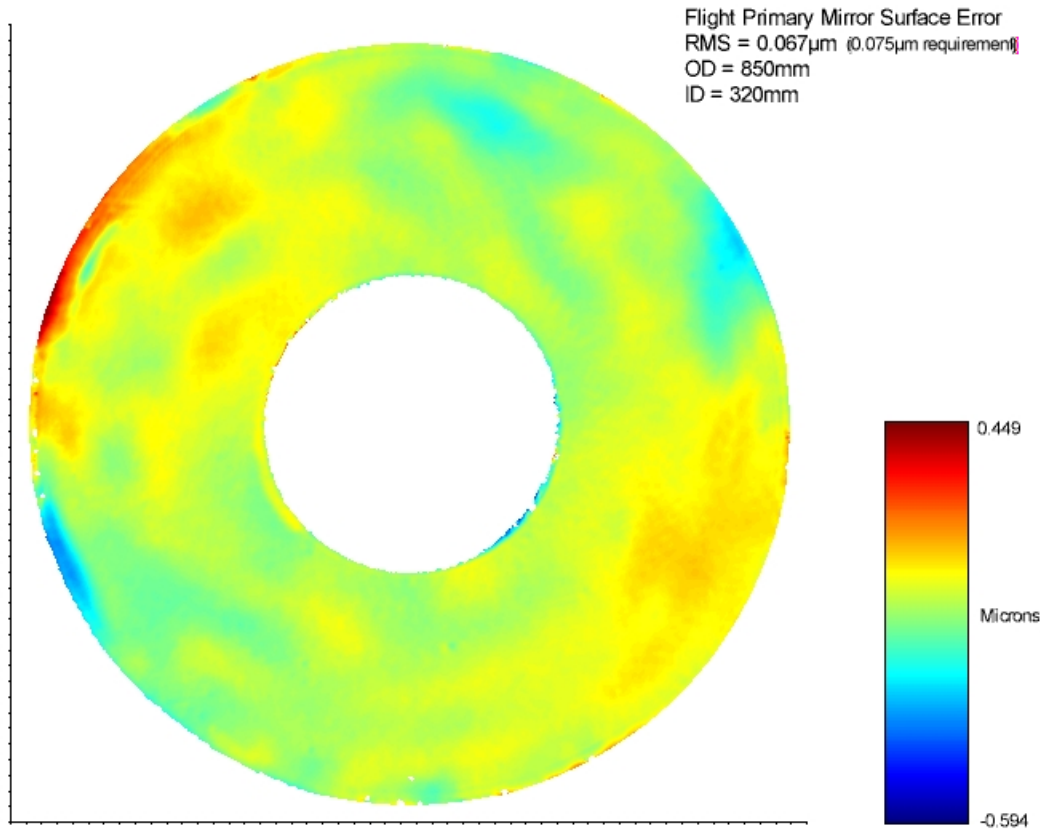
Figure 4.2: The deviations in the flight primary mirror surface. The RMS error was measured at cryogenic temperatures to be 0.067 μm rms over the entire clear aperture, meeting the specification of 0.075 μm rms.

4.2.2 Wave-front Errors

The telescope is required to provide a beam to the telescope focal surface that is diffraction limited (transmitted wave front error $< \lambda / 14$ rms) at 5.5 μm over the entire field at operating temperature. At a wavelength of 3.5 μm, the telescope produces a wave front error of less than 0.13λ rms over the IRAC field of view, and the image of a point source contains 45% of the encircled energy within a diameter of 2″. The actual performance of the telescope is slightly better than the requirements; see IRAC chapter (specifically, Table 6.1) for more information.

4.2.3 Throughput

The requirements for the telescope assembly are that it shall provide a minimum end-of-life throughput no less than that given in Table 4.2. Telescope throughput is defined as the ratio of energy from a point source reaching the telescope focal surface to the energy collected by an 85 cm diameter mirror. Factors that degrade telescope throughput are the central obscuration (including spiders), mirror reflectivity as a function of wavelength and losses due to contamination.

Table 4.2: Telescope Throughput

Wavelength (μm)	End of Life Throughput
0.55	> 0.18
3.5–6.5	> 0.70

4.2.4 Stray Light Rejection

The cryostat, telescope, multiple instrument chamber and science instruments are designed and baffled such that, at all wavelengths, celestial stray radiation and internal stray radiation:

> Do not, except for lines of sight near bright sources, increase by more than 10% the photon noise of the natural background in the direction of the line of sight of the telescope. This requirement implies that the combination of celestial stray radiation and internal stray radiation must be <21% of the natural background at the instrument detector arrays.
> Display no gradients or glints in the celestial stray light that will increase confusion noise over natural levels or produce false sources.
> Do not significantly decrease the contrast of the first dark ring of the diffraction-limited point spread function.

The conformance of the Spitzer design to its stray light requirements was verified by analysis using the APART stray light analysis program and an analytical test source designed to approximate the brightest celestial source expected in each of Spitzer's wavelength bands. The actual scattered light performance of the Spitzer telescope was characterized on-orbit during the early parts of the mission and will continue to be characterized during nominal operation of the telescope. In some cases, there are modifications or caveats to the requirements above. Discussion of stray light as it pertains to each instrument is covered in the instrument chapters later in this document.

A useful output from the stray light analysis is a set of predicted point source transmission curves. The point-source transmission function (PST) is the inverse of the ratio of the flux density (W/m²/Hz) of an off-axis source to the flux density at the telescope focal plane due to light scattered from that source. The separate PST curves in Figure 4.3 refer to different azimuthal locations of the celestial point source. An azimuth of 0° refers to the anti-Sun direction. The differences among the azimuths are mainly due to the changing illumination of struts supporting the secondary mirror. Figure 4.4 shows the variation as a function of wavelength.
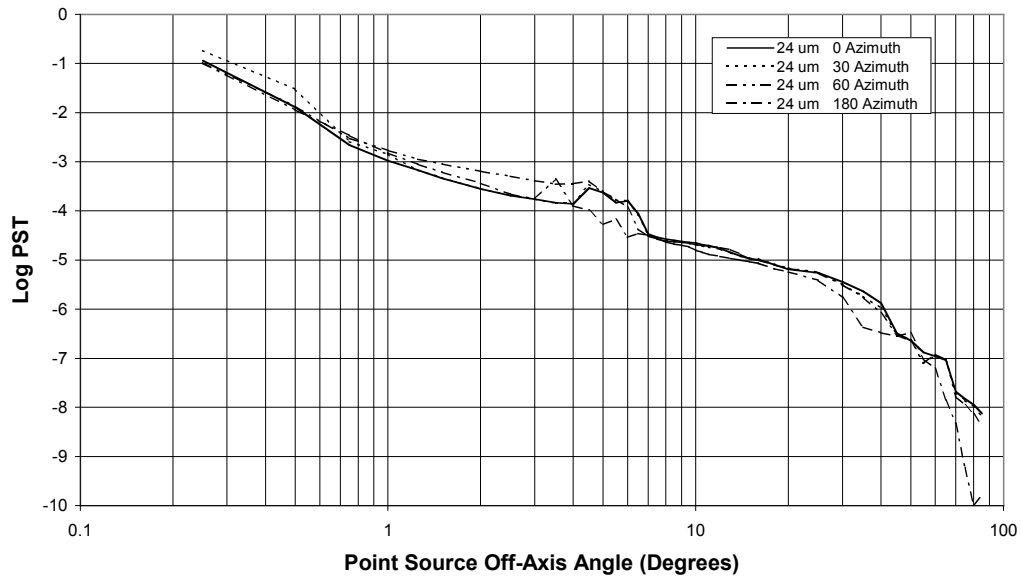
Figure 4.3: Theoretical PST off-axis as a function of azimuth for 24 μm.
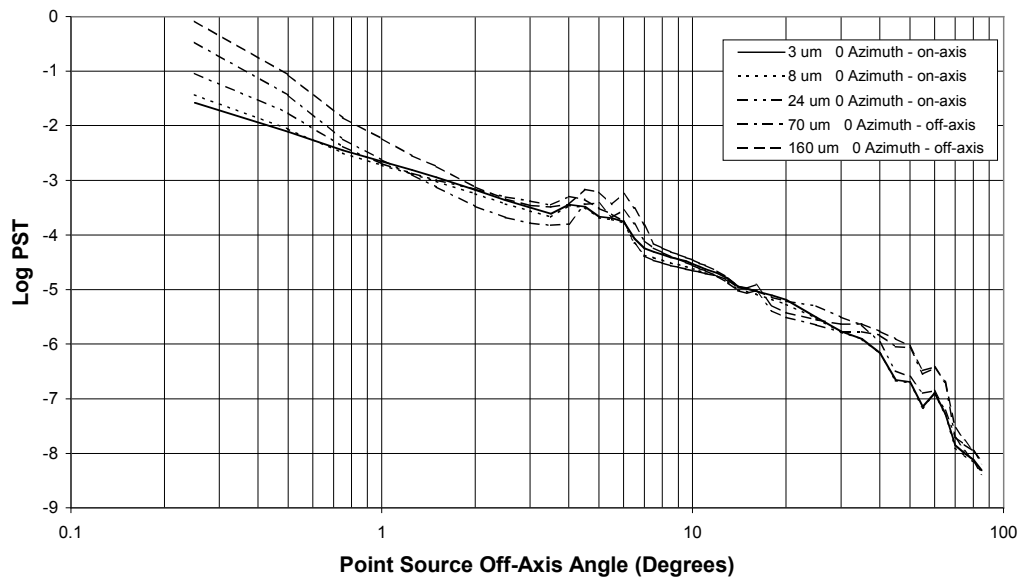
Figure 4.4: Theoretical PST as function of wavelength for fixed azimuth on-axis.

These plots can be used to estimate the stray light contribution from a given source. For example, at 8 μm, Vega has a flux density of ~62 Jy. From Figure 4.4, the 8 μm PST at 1° off axis is ~2×10³, so the predicted flux density in the Spitzer focal plane due to Vega at 1° off axis is 120 mJy[3].

4.2.5 Telescope Temperature/Thermal Background

The telescope and science instrument operate at ambient temperature. The telescope temperature is approximately 27.5 K during the warm mission.

4.2.6 Telescope Focus

Spitzer is equipped with a secondary mirror focus mechanism, which was operated both on the ground and on orbit. Prior to launch, the end-to-end image quality was measured on the ground and the mechanism was set to the position that was predicted to give optimal focus following in-orbit cool-down. During the cryogenic In-Orbit Checkout (IOC), it was found that the telescope focus point was about 1.85 mm above (toward the back of the primary mirror) the optimum focus position for the science instruments. Thirty-eight days after launch, when the telescope had become thermally stable, the secondary mirror was moved toward the primary mirror to bring the telescope into focus. A re-focus was not needed for the warm mission.

4.3 Focal Plane Layout

Figure 4.5 shows the actual location of the pick-off mirrors that feed the science instruments as viewed from above (looking down the boresight). The Y- and Z-axis directions are the same as the telescope coordinate system described in Chapter 3; the +X direction comes out of the page. Figure 2.1 shows the Spitzer entrance apertures as projected onto the sky and appears inverted compared to Figure 4.5, due to the combined effects of looking out from behind the focal plane and the projection of the sky onto the focal plane through the telescope optics. (To understand this inversion, recall the 3-D geometry and the fact that a Cassegrain telescope inverts its image.)

---

[3] The natural background at 8 μm near an ecliptic pole is 5.3 MJy/sr, which is imaged to a flux density of 5.3 MJy/sr × π /(4×12²) = 2.9x10⁴ Jy in the focal plane of the *f*/12 Spitzer telescope. The scattered light from Vega at 1° off-axis is far below the natural background. The first stray light trouble from Vega at 8 μm should come from the outer parts of its diffraction-limited PSF.

Nominal Aperture or Pick-Off Mirror Locations Viewed Down the Telescope
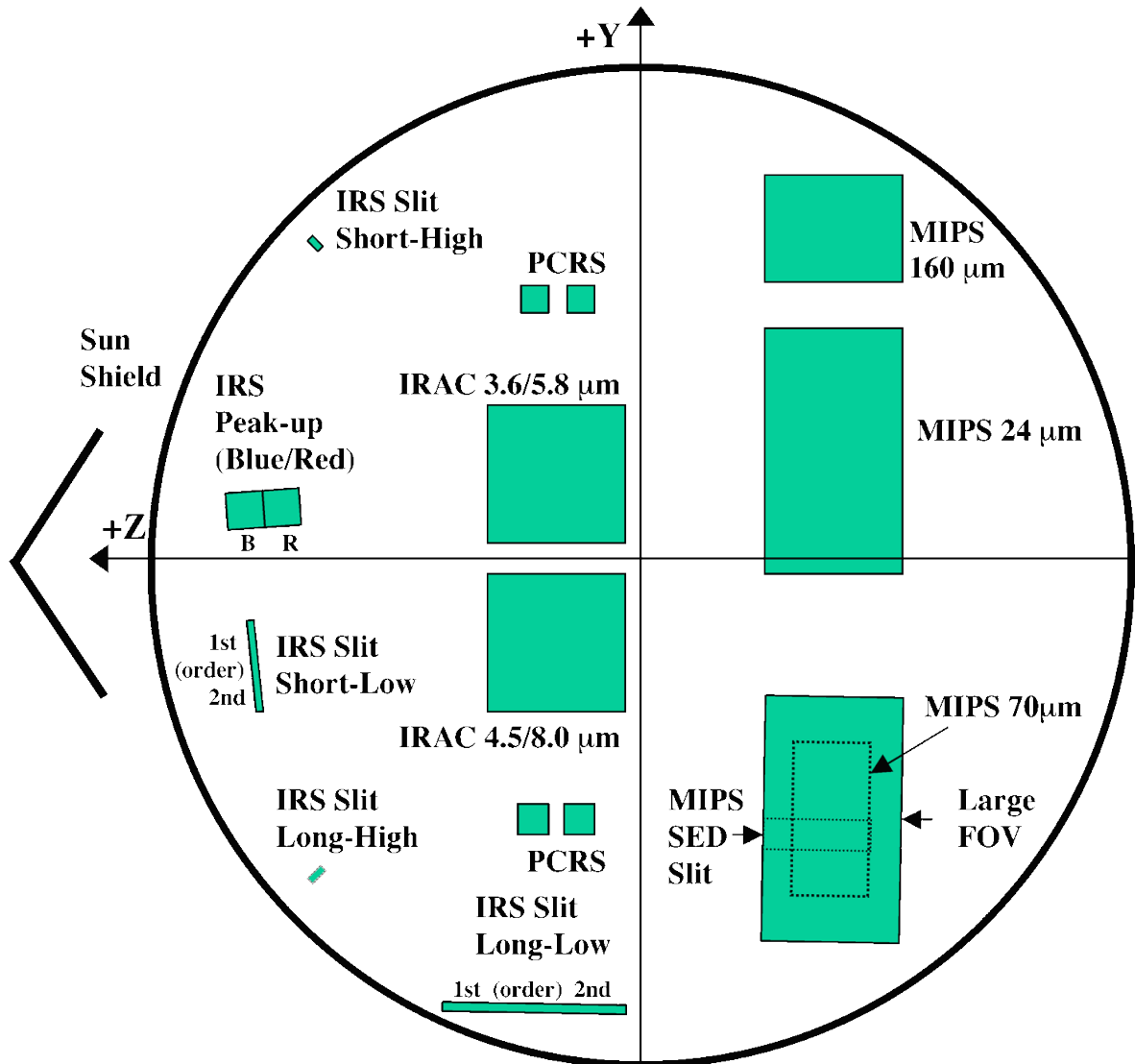
Nominal Field Radius = 16 arcminutes

Note: This is an approximate mechanical layout of the focal plane as viewed from above. It is not a projection onto the sky.

Figure 4.5: Schematic view of Spitzer focal plane from above, looking down the boresight. The solar panel is on the IRS side of the spacecraft. This figure shows the region of the focal surface where the pick-off mirrors for each instrument are located. This is in contrast to where the apertures project onto the sky. See Figure 2.1 for comparison.

Table 4.3: Spitzer focal plane layout: approximate offsets from boresight to aperture centers

Aperture	Z (')	Y (')
IRAC 3.6 μm	2.86	3.67
IRAC 3.6 μm subarray	4.97	5.88
IRAC 4.5 μm	2.72	-3.05
IRAC 4.5 μm subarray	4.80	-0.92

Table 4.3 gives the measured offsets from the center of the field of view to the centers of the main Spitzer science apertures. The values were determined post-launch based on the results from the focal plane mapping survey during IOC+SV.

Each of the fields of view that are used by Spitzer has a code that specifies the position in the focal plane. The uplink software uses the field-of-view index for commanding the target position, and the pipelines similarly use it to reconstruct where the telescope was pointing. These indices and field-of-view names appear in the headers of Spitzer data, and are listed in Table 4.4.

Table 4.4: Field-of-View Indices

FOV name	FOV index
Telescope Boresight	1
PCRS 1A	4
PCRS 1B	5
PCRS 2A	8
PCRS 2B	9
IRAC center of 3.6 array	67
IRAC center of 3.6 array	68
IRAC center of 3.6 subarray	70
IRAC center of 4.5 array	74
IRAC center of 4.5 array	75
IRAC center of 4.5 subarray	77
IRAC between arrays	81

5 Observing with Spitzer

The Spitzer observer's interface to the observatory is the AOT (Astronomical Observation Template). AOT is a central design concept in Spitzer's science operations. The use of relatively simple parameterized observing modes enhances the reliability of Spitzer observations and calibration, improves the archival value of Spitzer data, and reduces cost.

This chapter describes the IRAC Post-Cryo Mapping AOT, introduces the concept of an AOR (Astronomical Observation Request), introduces the SSC-provided tools for planning and creating observations, and describes some of the rules and procedures related to observing with Spitzer. Special types of observations, such as Solar System Objects (SSOs), ToOs, and Generic Target observations are also discussed.

The tool which Spitzer observers must use for planning observations and submitting proposals is Spot, which is described in section 5.2.

5.1 Astronomical Observation Request – AOR

When all the relevant parameters for the AOT are specified and linked to a description of the target, the resulting fully specified observation is called an AOR, which is the fundamental unit of Spitzer observing. AORs are created using Spot (see section 5.2). An AOR can be thought of as a list of parameters that, when properly interpreted, completely describe an observation. In fact, an AOR, as represented in the SODB, contains a series of keywords and values that are used to create the sequence of commands that are sent to the observatory to carry out the observation. This ASCII format is what Spot actually creates and stores in its output file. The parameters of the AOT are specified in Spot by filling out a form, sometimes called an "AOT Front End."

The AOR is the fundamental scheduling unit for Spitzer: An AOR cannot be subdivided, will not be interrupted for other activities (such as downlinks), and is handled as a unit by the observatory. Because of this non-interruptible nature and the need to perform certain activities periodically (e.g., detector anneals, pointing system calibrations, and downlinks) a maximum duration exists for an AOR. That maximum time is 24 hours for IRAC AORs. Longer observations can be specified using multiple AORs and relational constraints to identify these AORs as members of a related group (see section 5.4.3). When specifying such related groups, it should be taken into account that, in general, several AORs of the maximum length cannot be placed back-to-back. Even taking into account only that the spacecraft generally must downlink every ~24 – 48 hours (ignoring calibrations and maintenance of the science instruments), it can be seen that the observatory schedule may be broken up into irregular chunks of time. Observing programs that are composed of short, independent AORs that can be scheduled any time their targets are visible are easiest to schedule. Observing programs that require building related groups of constrained observations are more likely to fit into a schedule if the AORs themselves are short and the constraint is constructed to allow maximum flexibility (for details on constraints see section 5.4).

An AOR contains three categories of information:

Astronomical Target
> The target of an AOR can be a single pointing or a cluster of pointings within a 1º radius, at which the specified observation is repeated identically. The single pointing or cluster may be either of an inertial target or a moving target.

AOT-Specific Parameters
> These parameters include instrument configuration, exposure time and dedicated mapping parameters.

Timing and Relational Constraints
> These constraints represent scheduling directives for an AOR or for a related group of AORs. The details of the kind of constraints that are supported are in section 5.4.3. Timing constraints are used to specify a window when an AOR should be executed (e.g., to observe a comet at maximum solar elongation). Relational constraints are used to specify how AORs within a group are related to one another (e.g., a series of AORs that define a very deep map and must be executed consecutively).

5.2 Science User Tools

Science User Tools are software packages and other materials (such as tables and graphs) that are provided by SSC to help the astronomical community plan, prepare, submit, monitor, and interpret the results of their Spitzer observations. They are all available from the SSC website, specifically in the Proposal Kit area (http://ssc.spitzer.caltech.edu/). We highlight a few tools here for illustrative purposes. Note: there is also a perl-based tool, available from the Proposal Kit area, allows proposers to format the Observations Summary Table portion of the proposal template, using the AORs to be submitted.

5.2.1 Spot

Spot is a multi-platform JAVA-based client-server GUI-driven software tool intended to assist potential and approved Spitzer observers in planning and modifying their observations. Spot, along with the Spot User's Guide, can be downloaded from the Proposal Kit section of the SSC web pages (http://ssc.spitzer.caltech.edu/). It allows investigators to construct and edit detailed AORs by entering targets and selecting from a variety of preset instrument-specific functions (e.g., exposure times, instrument modes, dither patterns, and observing constraints). Spot also includes useful visualization tools to permit an investigator to see how proposed Spitzer observations and the Spitzer focal plane is laid out on the celestial sky. These capabilities allow observers to retrieve relevant images from other astronomical surveys (in any of a number of wavelengths) and archives. It calculates estimates of Spitzer observing time (including telescope overheads) for each AOR in a proposed program, along with target visibility information, focal plane position angle for a selected observation date, and estimates of the zodiacal and cosmic infrared background at the target. Spot allows investigators to view AORs from all previously approved programs;

it also supports "check-in" of active Spitzer programs for approved modifications by investigators (see section 5.3).

Spot allows prospective investigators to plan, develop and modify their proposal in an iterative manner. That is, a proposer can write a portion of their proposal and define their accompanying AORs, save the results locally, and then re-load those results at a later time for subsequent modification. The saved cover sheet, proposal text, and AORs can be modified repeatedly before the proposal submission deadline.

Prospective investigators are encouraged to download Spot and to start planning their Spitzer observing programs well before the proposal submission deadline.

Spot is currently supported on multiple Windows, Linux, Sun Solaris, and Macintosh platforms. For details, see the Spot User's Guide and Release Notes, available at the SSC website with the downloadable software. While running Spot, a network connection to the Spitzer Science Center is required to obtain observing time estimates, visibility, orientation, or background estimate information, and to submit and update proposals; a network connection is not necessary for selecting observation parameters.

5.2.2 Performance Estimation Tool (PET)

The most important web-based SSC tool is the Performance Estimation Tool (PET). The PET is actually a set of Javascript tools to aid in designing Spitzer observations. There are three PET components: The Sensitivity PET, the Extragalactic PET, and the Stellar PET. Users of the PET should pay close attention to the various notes and warnings on both the main PET pages and the help pages.

The Sensitivity PET (SENS-PET) is an imaging sensitivity estimator. It takes as input the IRAC imaging instrument configurations, and a background level. It produces as output the instrument sensitivities (both for point source and extended objects), and the total exposure depth per pixel.

The Extragalactic PET (EX-PET) makes predictions for imaging of extragalactic sources. As input, users may choose an SED model, background level, and IRAC instrument configurations. The output includes flux in the instrument passbands, instrument sensitivities, S/N, and total exposure depth per pixel.

Finally, the Stellar PET (STAR-PET) predicts fluxes for imaging of stars. For input, users select a stellar spectral type + MK class, K-band magnitude or K-band flux density. The tool calculates the expected flux density in the IRAC 3.6 and 4.5 μm passbands.

5.2.3 Flux Unit Converter

Although Spitzer predictions and products are in Janskys, some astronomers may be more familiar with magnitudes. Another Javascript tool available at the SSC website converts back and forth between the flux (density) units of magnitudes and Janskys, as well as a variety of other flux (density) units. See also the Appendix of this document for more information.

5.2.4 Leopard and the Spitzer Heritage Archive

Prior to November 2010 the observer's interface to the Spitzer archive was via Leopard. Leopard comes with the Spot software download on the Proposal Kit web pages. In November 2010 data access via Leopard was turned off. Observers should now use Leopard only as their primary source for checking the Reserved Observations Catalog.

Access to public and/or proprietary data is via the web-based Spitzer Heritage Archive (SHA) (http://sha.ipac.caltech.edu/applications/Spitzer/SHA/). Information on using the SHA can be found on the SHA web pages.

5.3 Modification of Observing Programs

The SSC envisions that it will execute most observations exactly as they are specified in response to the Call for Proposals. Therefore, the SSC *will expect observers to provide sufficient information at the time of proposal submission to implement the observations* (i.e., completed AORs); also, see the current Call for Proposals for more information.

In cases of conflicts or special needs, it will be possible for observers to request a modification of their (not yet scheduled) AORs via the Spitzer Helpdesk. *The request must be accompanied by a strong justification for the proposed changes*. Major modifications by observers are only allowed in exceptional circumstances and only outside of blackout periods. Minor modifications can be made at any time. See the SSC web pages for details on blackout periods and the definition of major vs. minor modifications. An observer can, at any time, request (again with strong justification) that a scheduling "hold" be placed on observations that need to be delayed. Only certain types of modifications are permitted, and the observer should check the Spitzer Observing Rules prior to requesting a modification of his or her observing program.

Upon completion of approved modifications, the observer will need to resubmit the revised AORs. Viewing, modification, and resubmission of AORs can all be done within Spot. Modification of programs requires the program username and password set at the time of proposal submission, once Science User Support has reactivated the password. The Science User Support Team at the SSC will review the changes and re-check for duplications prior to re-releasing the AORs for scheduling. Once a program has been resubmitted, the access for modifications will be disabled, and any further modification will require a new request for

access, accompanied by supporting justification. Check the Science User Support section of the SSC web pages for full details on program modification.

5.4 Scheduling Considerations

The technical issues of telecommunications and telescope performance that drive science instrument campaign planning and the basic scheduling timescales are addressed in Chapter 3. In this section, the planned scheduling process is addressed from the observer's point of view.

The use of scheduling constraints is also discussed in this section. Scheduling constraints restrict the ability of the planning and scheduling system to create efficient schedules and to ensure the feasibility of scheduling all AORs. Therefore, a scientific justification is required for the use of scheduling constraints and must be provided in the science proposal at the time of submission.

5.4.1 Scheduling Methodology

The Spitzer scheduling process constructs short-term observing schedules of one week in length. Each week's observing schedule is finalized about five weeks in advance of execution, to allow for processing of the command sequences by the Mission Operations team at JPL and review of the resulting command products. The one-week schedule loads are uplinked weekly, following final review and project approval. In general, Spitzer "weeks" run from Thursday to Wednesday. After a schedule has been finalized, changes are only made in unusual circumstances (e.g., activation of ToO programs). Due to the fact that Spitzer is in contact with the ground for only a brief period every 24-48 hours, it is not practical to make changes to the on-board schedule on very short time-scales; the fastest a ToO can be accommodated is about 48 hours from the time of SSC's receipt of the approved AORs.

Observations are grouped into campaigns which will be approximately 14 days duration. Rules regarding schedule changes on short notice are discussed in more detail in the Spitzer Observing Rules.

5.4.2 Notification That an AOR Has Been Scheduled

Approximately three weeks before a schedule has been uplinked to the spacecraft, the list of scheduled AORs and their nominal execution times will be published on the SSC website. Unless an absolute scheduling time has been specified at the time of scheduling, the actual execution time of an AOR may differ from the scheduled time by a small amount (possibly up to several minutes). This is due to the non-deterministic nature of the on-board indicators for slew completion and settle time.

The appearance of a particular AOR in the published schedule is not the only notification to observers that the AOR has been officially scheduled. An email is sent to the observer notifying him/her that his/her observation has been scheduled.

Once an AOR has been scheduled, only a significant anomaly (e.g., a missed downlink opportunity or a safing event) or a rapid-turnaround ToO could cause the schedule to change. Observers will generally not be notified if this happens. **Only under extreme circumstances can AORs be modified after they have been scheduled, but this is *highly* discouraged.**

In the case of AORs that are highly time-constrained for science reasons, if a specific sequence or dates have been provided to the observatory in advance, the Observatory Planning & Scheduling Team (OPST) will make every effort to schedule those AORs accordingly. This information should be provided at the time of proposal submission, and always **requires a very strong scientific justification**. A Spitzer observer may assume that any specific dates and times requested in an approved proposal will be accommodated, unless otherwise notified by the SSC (however, see note in section 5.4.3 below regarding constraint limitations). In the event of a serious conflict, the SSC will contact the affected observer(s) as soon as possible to resolve the problem. However, even for heavily constrained AORs, the only formal announcement of their place in the Spitzer schedule will be their appearance in the latest online weekly schedule and in the above-mentioned e-mail message. We will do our best to maximize the scientific return via scheduling, but specific requests for ordering of AORs in the schedule cannot generally be accommodated.

5.4.3 Requesting Scheduling Constraints for Science Reasons

The scheduling software is able to handle common types of constraints and logical linkages, such as those needed for periodic monitoring of a target. However, because scheduling constraints restrict the ability of the scheduling system to produce efficient schedules and may render scheduling some observations infeasible, **the usage of any type of timing or relational constraint requires a very strong scientific justification**. The justification must be provided at the time of proposal submission (or modification if the constraint has been subsequently added).

5.4.3.1 Recommendations for the Use of Scheduling Constraints

If a scheduling constraint is required, it is **strongly recommended that the minimum constraint necessary** to preserve the scientific goal of the observation(s) be applied. In general, larger timing windows and/or loose groupings are preferred to non-interruptible sequences of observations. For very long observations, strategies which permit independent scheduling of the component AORs are much preferred; this not only enhances scheduling efficiency, but also makes the observation as a whole much more robust against the failure of component AORs. As a general rule of thumb, groups of constrained AORs that occupy more than about half of the time period during which they can be scheduled will have a strong negative impact on efficiency and may not be feasible to schedule. In other words, any constraint that involves a

time range should be twice as long as the AORs you want scheduled within that time range. For example, 40 hours of observations that must be done within a 40-hour period cannot be scheduled, whereas the same 40 hours of AORs may be quite feasible if they can be scheduled anytime within the same one-week period. In addition, shorter AORs of 2-3 hours duration are easier to schedule than many 12 hour AORs.

When designing scheduling constraints, the observer must take into account the natural 24-hour time scale for PAOs and that PCS calibration and instrument and spacecraft maintenance activities can take 15% or more of the available time during a given PAO, but usually takes just a few percent of the available time within a given campaign.

5.4.3.2 Specification of Scheduling Constraints

Scheduling constraints should be submitted at the time the AORs are submitted, using the constraint-editing capabilities of Spot. Please see the Spot User's Guide for details on how to specify constraints, and the Spitzer Observation Planning Cookbook for an example of creating constrained observations. Note that constraints are requests that the SSC will work to accommodate. In the event of a serious conflict, the SSC will contact the affected observer(s) as soon as possible to resolve the problem. However, even for heavily constrained AORs, the only formal announcement of their place in the Spitzer schedule will be their appearance in the latest online weekly schedule, as described above. **Any scheduling constraint imposed on an AOR will increase the difficulty of scheduling the AOR.**

The following types of scheduling constraints are supported for both inertial and moving targets:

Timing Constraints
> Timing constraints consist of defining a window or series of windows for the start time of an AOR. Absolute-time observations that will be executed at a specific time, or no more than 3 seconds later, can only be supported for moving targets. To specify an absolute time observation in a *moving target* AOR, set the open and close times for the timing window to be identical. Spitzer's scheduling architecture generally operates on relative time, so for inertial targets, the (inertial target) AORs will simply run in order. Timing constraints for inertial target AORs should be macroscopic (days, weeks, months), not microscopic (seconds, minutes, hours).

Relational Constraints
> Relational constraints are ordering or grouping constraints that are applied to a group of AORs. There are four basic types of relational constraint supported by Spitzer:

Chain = Ordered Non-interruptible Group
> A chain can be thought of as a list of AORs that must be executed consecutively in the order specified and without any other kind of activity

intervening. Note that the total time for the entire ordered non-interruptible group cannot exceed the maximum time for an individual AOR; for longer observing sequences, an interruptible group must be used. This type of constraint might be used for an on/off source pair of observations.

Sequence = Ordered Interruptible Group

A sequence constraint is similar to, but less stringent than, a chain constraint. The AORs will be executed in the order specified and a duration in which they should be completed is specified. The sequence constraint should only be used when the science requires sequential ordering of the AORs. For AORs in which the order of observation is not important, a "group within" constraint (see below) should be used, instead of a sequence constraint.

Group-within

A group-within constraint specifies that a group of AORs will be executed within a specific length of time, but with no particular starting date/time constraint. Once the first AOR has been executed, the rest of the AORs in the group will begin within the specified time interval. They may be executed in any order within the time interval. This is similar to a sequence constraint, but the observations may be executed in any order.

Follow-on

This constraint forces a follow-on AOR to be scheduled within a given time after a precursor AOR. It can be thought of as a statement that Follow-On-AOR must be scheduled within Time-Window after the end of Precursor-AOR. The follow-on constraint can be used to prevent early execution of an observation when the success or content of the follow-on is dependent upon the successful execution of a precursor observation. This constraint could also be used for periodic observation of a target where the interval between observations is relatively short (hours to a small number of days). One AOR may serve as the precursor to more than one follow-on, but a follow-on may have only one precursor (e.g. one follow-on constraint can tie together only two AORs).

Shadow

The shadow constraint is a special case of the follow-on constraint, and is used to obtain background measurements for moving targets. The primary AOR is executed as specified. The shadow AOR will be executed to repeat the track of the primary observations. The selected AOR parameters must be identical in the two AORs. The shadow may be executed before or after the primary AOR. Note that the shadow does not re-observe the target at a later date, but rather the background of the primary observation. (As with all constraints, shadow observations must be strongly scientifically justified in the observing proposal.)

Timing and Relational Constraints can be combined. For example, a series of AORs used to obtain images of a comet over a long track which needed to be

broken up into segments due to curvature, might be constrained as a chain with an associated timing constraint related to the acceptable range of solar elongations.

Spot software checks for viability of relational constraints. Spot will warn the user if a timing constraint is set such that the target is not visible for some portion of time within the timing window, but Spot will still allow the constraint to be set. Observers should make sure that the timing windows they introduce overlap sufficiently with the visibility of the target(s), in order for the complete AOR, or set of relationally constrained AORs, to be completed. *Timing windows that barely overlap a visibility window for a given AOR will make scheduling of that AOR very difficult or perhaps impossible* (e.g., through small visibility window changes caused by a more accurate Spitzer orbit calculation).

5.5 Solar System Objects

Spitzer supports observations of SSOs, tracking in linear segments at rates up to 1″/s as described in Chapter 3. Updated information on Solar System specific observing issues can be found on the web in the "Solar System Observing with Spitzer" document in the Solar System subsection of the Proposal Kit section on the SSC website.

5.5.1 Tracking Performance

Spitzer's SSO tracking capability is similar to its scanning capability and the performance is described in section 3.3.3.

One significant consequence of this for the SSO observer involves sources whose tracks, on an equatorial map, have significant curvature during an AOR. Such AORs may need to be broken up into a series of short (linear) AORs. The spacecraft does not carry any target ephemerides on board, so the track is defined at the time of scheduling and formulated as a vector rate in an equatorial frame. A start time and equatorial J2000 start point and time are also provided for use by the PCS. Once the track command has been issued, the on-board system maintains knowledge of where the telescope should be at what time, and "catches up" with the specified track and maintains it.

Any further updates to SSO tracking performance will be posted in the Solar System subsection of the Proposal Kit area on the SSC website.

5.5.2 Ephemeris Management

Spitzer uses a database of ephemerides for known SSOs derived from the Horizons database maintained by the Solar System Dynamics group at the Jet Propulsion Laboratory. For proposal planning purposes, Spot can retrieve the ephemerides for a specified target, by resolving the NAIF ID (which, in most cases, corresponds to the Horizons SPK-ID). These ephemerides are used to calculate visibility windows and resource estimate calculations for SSOs through Spot.

If the object is newly discovered, is not released through the Minor Planet Center (MPC), and does not yet have a NAIF ID, the observer will still be able to send the orbital elements to the Spitzer Helpdesk (help@spitzer.caltech.edu) and request generation of an ephemeris for planning purposes. Requests received at the SSC for non-standard ephemerides during the last week of the Proposal Call will be supported on a best effort basis.

Note that observations which require ephemeris updates <5 weeks prior to execution significantly perturb the scheduling process and must be identified in the proposed AORs at the time of submission via the "special" button in the Spot AOT window. Late ephemeris updates are considered equivalent to medium- or high-impact ToOs, depending upon the amount of lead time given (see Spitzer Observing Rule #5), and will incur a special observing overhead (for more details see http://ssc.spitzer.caltech.edu/warmmission/propkit/sor/).

Late ephemeris updates, i.e. specification of the final ephemeris less than 5 weeks prior to scheduling, are no longer supported in GO proposals. Any observations requiring a late ephemeris update must be submitted via a DDT proposal.

5.5.3 Target Specification and Scheduling Considerations

SSO observations will normally be performed as tracked observations with both the position and the track rate/direction computed from the orbital elements derived as discussed in the previous section.

5.5.3.1 Shadow Observations

The infrared flux from background sources, and particularly small-scale structure in that background, frequently limits the sensitivity of Spitzer. To assist in background subtraction, Spitzer Solar System observers can specify "shadow" background observations. A shadow observation allows the track across the sky taken during observation of a moving target to be replayed or pre-played when the target is not there. Shadow observations allow the Solar System observer to remove background small-scale structure, thereby improving moving target sensitivity. Shadow observations will help to mitigate the effects of background sources, but not completely eliminate them. Therefore, if possible, it is best to avoid viewing faint objects while they traverse crowded fields, such as near the Galactic plane, and timing constraints should be selected accordingly. To reduce potential errors due to time-dependent changes in the zodiacal light, instrument characteristics, and calibration, a shadow observation is generally most effective when taken as close in time to the primary observation as is scientifically possible. In addition, the shorter the interval of time between primary and shadow, the larger the visibility window for the primary-shadow pair, and the higher the likelihood that the observation can be scheduled. Often a balance must be struck, then, between the brevity of the interval separating the primary and shadow observations and the object's motion in that interval, so that the motion is sufficient between the observations to image the background. The Spot

visualization tools and instrument sensitivity information can be used to determine whether a particular Solar System observation would benefit from a shadow observation.

As with all observing constraints, the need for a shadow constraint must be scientifically justified. Execution of the shadow observation *after* observation of the science target is the default, although there may be situations where this is not the optimal execution order. However, shadows specified to execute *before* the primary observation are much more difficult to schedule than shadows executed after the primary, and although allowed, require even more compelling scientific justification in the proposal than shadows executed after the primary.

5.5.3.2 Timing Constraints

SSO observations can be scheduled with timing constraints, as long as these constraints are scientifically justified. Observers are encouraged to specify observing windows that are as generous as possible, within the scientific constraints, to both enhance the efficiency of our scheduling system and to increase the probability that the observation can be scheduled. However, when precise timing is scientifically required, an absolute time can be specified for the SSO observation, and the flight computer will start the track and initiate the data taking at that time, or no more than 3 seconds later. Note that there are other required activities at the beginning of the moving target AOR which could vary in duration from target to target, such as slewing to the target from a previous target, or settling and waiting at the acquisition point before starting the track. However, these variable duration activities are executed *before* the absolute timing constraint is applied, to specify the beginning of the track.

The scheduling constraints that are supported for both inertial targets and SSOs are described in section 5.4.3.

5.5.4 Science Instrument Issues

The saturation of the IRAC instrument is discussed Chapter 6, and the scattered light characteristics of the telescope are discussed in Chapter 4, in addition to Chapter 6. IRAC observers interested in milli-magnitude photometry of bright sources should be particularly mindful of the stability issues discussed in these chapters.

5.5.5 Overheads

The time duration of each AOR an observer submits with a program includes a fixed slew overhead. For both inertial and moving targets, this is 180 seconds in duration. An additional 300 seconds overhead is now charged for moving targets. This extra overhead accounts for the target acquisition and tracking requirements for moving targets (see "Solar System Observing with Spitzer" in the Proposal Kit for details). Check the current Call for Proposals for any updates to these overheads.

5.5.6 Best Observing Practices for Solar System Objects

The following "best practices" for Solar System objects are provided *in addition to* the discussions of general best practices of IRAC observations in the IRAC chapter 6.2.4.1. There is also a moving target example in the Observation Planning Cookbook, found in the Proposal Kit on the SSC website.

5.5.6.1 Choosing your targets

Whereas fixed targets can have absolute time errors on the order of an hour (usually executing earlier than expected), moving targets can be executed with an absolute time error of only -0, +3 seconds. Please be aware of this if you are planning to observe a Solar System target as an absolute time-fixed target observation. Generally, it is better to request moving target observations (i.e., with tracking) for Solar System observations.

Remember to check for availability of positional error information for the ephemerides for your targets (instructions in the document entitled "Horizons tips for Solar System Observers," found on the SSC website). Some objects have extremely poor positional information (e.g., several 100s of arcseconds) and would have a very low probability of being acquired by Spitzer. There are 3 known ways of dealing with targets in this situation:

1. Select another target of comparable scientific interest, but with better ephemeris accuracy.

2. Use ground-based support facilities to acquire astrometric observations of your proposed target. Please send these data in MPC ingest format to the Helpdesk (help@spitzer.caltech.edu) and we will ensure that they are included in Horizons.

3. Request that SSC ask the JPL Solar System Dynamics team to provide observational support to improve the object's ephemeris. Note that this capability is limited.

Spot now queries the Horizons database at JPL for ephemerides of solar system moving targets if they are not already at the SSC. If this is the case Spot will usually take a few seconds longer to return visibility information because it has to query Horizons for the information, deposit the ephemeris file at the SSC and only then calculate the visibility. However once this is done for a target the ephemeris file is in place at the SSC and it can be immediately accessed for any subsequent visibility calculation request.

5.5.6.2 Late Ephemeris Updates

Late ephemeris updates are most useful if your object has a high probability of behaving unpredictably *during* the 5 weeks prior to the observation, as might be the case for an active comet near perihelion. Another good justification for a late ephemeris update is a target that, just prior to observation by Spitzer, has

relatively few observations and a correspondingly large positional error. However, if your target is known to have poor positional accuracy at the time you submit your proposal to a Spitzer GO call, a late ephemeris update may not be necessary. In this case, there is likely to be several months of time in which to improve the ephemeris, but you should be proactive about acquiring and transmitting the additional observations required to reduce the ephemeris error so that a late ephemeris update will not be needed.

Late ephemeris updates, i.e. specification of the final ephemeris less than 5 weeks prior to scheduling, are no longer supported in GO proposals. Any observations requiring a late ephemeris update must be submitted via a DDT proposal.

5.5.6.3 Timing Constraints

Make sure that any observer-imposed timing constraints are still within the Spitzer visibility period for your target (see section 3.2 above). Even though a given timing window may be optimal for the science goals, the object may not be visible to Spitzer in that timing window. It is important also to check that the object flux, positional uncertainty, and sky-plane motion remain within acceptable values during the constraint interval.

5.5.6.4 Visualization

It is EXTREMELY important to visualize your proposed AORs. This is especially true for moving target observations.

Spot will allow you to overlay the orbital track of your object on the infrared background, and will also overlay your AOR in the sequence in which it would be observed on a date that you enter. You can use this feature to check for structure in the infrared background around your object.

If you have a time-constrained observation, you can use the "Animate with Trail" feature in the visualization tool to see the time sequence and positions at which individual apertures will be observed. For cometary, satellite, or ring observations in particular, check this time sequence for potential unplanned slews across the cometary nucleus, major planet, or some other bright object, both in the instrument's field of view and in the potential zones of avoidance for scattered light (see the IRAC specifications in Chapter 6).

5.6 Targets of Opportunity

ToOs (see Observing Rule #5) are transient events whose timing is unpredictable. Predictable phenomena whose precise timing is not known a priori (e.g., novae, newly discovered comets, gamma-ray bursts) may be requested in a General Observer (GO) proposal. Observations of completely unanticipated phenomena can be requested through DDT procedures (see SSC website for details). A GO proposal must include an AOR for each predictable ToO observation, filled in with as much information as possible.

An example demonstrating proper construction of ToO AORs is included in the Observation Planning Cookbook.

5.6.1 Classification of ToOs

ToOs are classified based solely on their impact on the observatory scheduling process, which depends on the time elapsed between the activation of a ToO observing request and the desired date of execution of the corresponding observation; see Table 5.1 for ToO classification criteria.

Table 5.1: Classification of ToOs

High impact	<1 week (48 hour minimum turnaround)
Medium impact	1–8 weeks
Low impact	>8 weeks

Special overhead burdens will be assessed against high- and medium-impact observations. See this discussion in the Proposal Kit section of the SSC website.

Because of the reduction in SSC staffing to support science operations during the warm mission, high/medium-impact ToO requests can only be submitted as DDT proposals. See the current Call for Proposals for details.

5.6.2 Activation of AORs

A request for ToO activation must be sent to the SSC Director via the Helpdesk (help@spitzer.caltech.edu). If the ToO involves a previously accepted AOR, then the request is to activate this AOR. Modification (e.g., to position) of the AOR is possible, and a request for this should be included with the ToO activation request. Target of Opportunity activation requests will be supported during normal business hours.

5.7 Generic Targets

Generic targets denote observations that fail to qualify as Targets of Opportunity (i.e., they generally have more refined and predictive spatial and temporal information than ToOs), and can be scientifically described, but lack precise celestial coordinates or brightness estimates *at the time of Spitzer proposal submission*. A generic target can be selected from a complementary observing program with Spitzer, or with any other telescope, but one where the conditional observations (assumed to be under the control of or clearly available to the Spitzer Principal Investigator) are scheduled or will be scheduled with high likelihood, but not yet executed or analyzed prior to the Spitzer proposal deadline.

Prior to Cycle-8, generic targets were defined as targets that can be described scientifically, but lacked celestial coordinates known to better than 2 degrees and/or the brightness estimate is only known to within a factor of 1.5 *at the time of the proposal submission deadline*. Beginning with Cycle-8 the definition is modified to remove the requirement that the celestial coordinates be known to

within 2 degrees. This will allow follow-up of well-defined scientific targets from, for example, the WISE mission.

An investigator may propose observations of generic targets, describing them in as much detail as possible in a Spitzer observing proposal. After the complementary observations are obtained and analyzed, the Principal Investigator must modify the generic target AOR and include the precise celestial coordinates and integration time before the observations can be scheduled. The observations must be completed within the observing time allocation awarded when the proposal was approved. If your proposed targets are not known at the time of proposal submission you must provide a credible schedule for determining the targets and delivering the AORs.   Details will be worked with all successful teams. For nominal generic targets the AOR must be fully specified 8 weeks prior to execution.

6 Infrared Array Camera (IRAC)

The InfraRed Array Camera (IRAC) was built by the NASA Goddard Space Flight Center (GSFC) with management and scientific leadership by the Smithsonian Astrophysical Observatory (SAO) under principal investigator Giovanni Fazio. The information in this manual is based on the design requirements, on the characterization of the flight instrument in pre-flight ground tests and on in-flight performance at cryogenic temperatures, including the In-Orbit Checkout (IOC)/Science Verification (SV) period in August-November 2003, the limited testing of arrays similar to the flight arrays at 30K (see McMurtry et al. 2006, SPIE, 6265, 626508, for more information) and in-flight characterization at the start of the post-cryo mission.

This section describes the performance of IRAC from 18 September 2009 onward. On 18 September 2009, the final warm IRAC operating setpoints were asserted and are presumed to remain the same for the duration of the warm mission. Both the telescope and IRAC instrument are at stable operating temperatures. By passive cooling, the telescope is equilibrated at a final primary mirror temperature of 27.5 K. At this higher temperature, only the 3.6 and 4.5 μm arrays will usefully operate. The longer wavelength (Si:As) arrays have extremely high dark currents at this higher temperature and saturate in even the shortest frametime and will be dropped from the discussion in the remainder of this section. Both IRAC arrays are actively thermally controlled to 28.7K. The programmable voltages for each array have been optimized. In addition to the operating temperature, the primary difference in array operation is a lower applied bias of 500 mV for the 3.6 μm array compared to 750 mV of applied bias for the cryogenic mission. This change was necessary to reduce the number of noisy pixels present at the higher operating temperature. The temperatures quoted in this document are based on the IRAC Cernox temperature sensors which are estimated to be uncertain by ~0.5 K at these operating temperatures.

This section presents our current knowledge of the performance of IRAC during the warm mission and should be sufficient for planning science observations. Our understanding is derived whenever possible from data at the final operating setpoints. A brief calibration campaign was conducted immediately following the final setpoint assertion. From this campaign, the linearity, flux conversion and flat-field were derived. In addition, a much longer calibration campaign was conducted at a slightly higher operating temperature (31 K) and lower applied bias (400 mV) at the beginning of the warm mission. The optical properties and array photometric variations were measured at this time. As a result of this initial characterization, it was determined that the instrument could be operated at a lower temperature with a significant improvement in noise properties resulting in the final setpoint assertion. For quantities that cannot be measured on-orbit or have not yet been done on-orbit due to scheduling pressures, we rely on the limited 30 K testing of similar detectors conducted by the University of Rochester group and/or cryogenic measurements.

Our current understanding is that the arrays are slightly less sensitive overall and the optical properties have changed imperceptibly. The saturation limits are slightly lower while the necessary photometric corrections for high accuracy photometry have increased. Long-term residual images (e.g lasting days or weeks) are no longer an issue, but shorter-term residual images (latents) survive longer, in some cases for up to 12 hours. Our understanding will continue to improve as ongoing analysis is completed. The most up-to-date information on the performance of warm IRAC can be found on the SSC website (http://irsa.ipac.caltech.edu/data/SPITZER/docs/irac/warmfeatures/).

A brief, high-level summary of IRAC for astronomers appeared in the ApJS Spitzer Special Issue, specifically the paper by Fazio et al. (2004, ApJS, 154, 10) entitled "The Infrared Array Camera (IRAC) for the Spitzer Space Telescope" and in the paper by Hora et al. (2004, SPIE, 5487, 244) entitled "In-flight performance and calibration of the Infrared Array Camera (IRAC) for the Spitzer Space Telescope," *and the paper by Carey et al. (2010, SPIE, 7731,17) for specifics on warm mission calibration.* Copies of these papers are available on the SSC website.

In the remainder of this chapter, we will use "cryogenic" to refer to data and operations of Spitzer/IRAC before the exhaustion of cryogen. During this phase the IRAC short-wavelength arrays operated at a temperature of 15 K. "Warm" will refer to data and operations after cryogen depletion, when the telescope is at 27.5 K and the IRAC arrays are operated at 28.7 K.

6.1 Instrument Description

6.1.1 Overview

6.1.1.1 Instrument Description

IRAC is a four-channel camera that provided simultaneous $5.2' \times 5.2'$ images at 3.6, 4.5, 5.8, and 8 µm. After the depletion of cryogen, the two shortest wavelength channels at 3.6 and 4.5 µm remain operational. The two operational channels image two adjacent fields of view. Both detector arrays are 256×256 pixels in size, with a pixel size of $\sim 1.2'' \times 1.2''$. The two short wavelength channels use InSb detectors.

The IRAC instrument was originally designed to address the four major scientific objectives defining the Spitzer mission. These are (1) to study the early universe, (2) to search for and study brown dwarfs and superplanets, (3) to study ultraluminous galaxies and active galactic nuclei, and (4) to discover and study protoplanetary and planetary debris disks. The utility of IRAC is in no way limited to these objectives, which we only mention to explain the scientific drivers for the instrument design. IRAC remains a powerful survey instrument because of its high sensitivity, large field of view, and mapping capabilities.

6.1.1.2 Technical Overview

IRAC consists of the Cryogenic Assembly (CA) installed in the Multiple
Instrument Chamber (MIC) in the CTA (Cryogenic Telescope Assembly), and the
Warm Electronics Assembly (WEA) mounted in the spacecraft. Harnesses
connect the detectors and calibration subsystem in the CA to the WEA. The
WEA communicates with the spacecraft over three RS-422 serial lines that allow
receiving commands from, and sending acknowledgements and image data to, the
spacecraft Command & Data Handling (C&DH) computer.

The IRAC Cryogenic Assembly, depicted in Figure 6.1, consists of the following
major subassemblies: the Pickoff Mirrors; the Shutter; the Optics Housings,
which hold the doublet lenses, beamsplitters, filters, and cold stops; the Focal
Plane Assemblies (FPAs) that include the detector arrays and associated
components; the Transmission Calibrator with its Source and Integrating Spheres;
and the Housing Structure, consisting of the Main Housing Assembly and the
wedge-shaped MIC Adapter Plate.
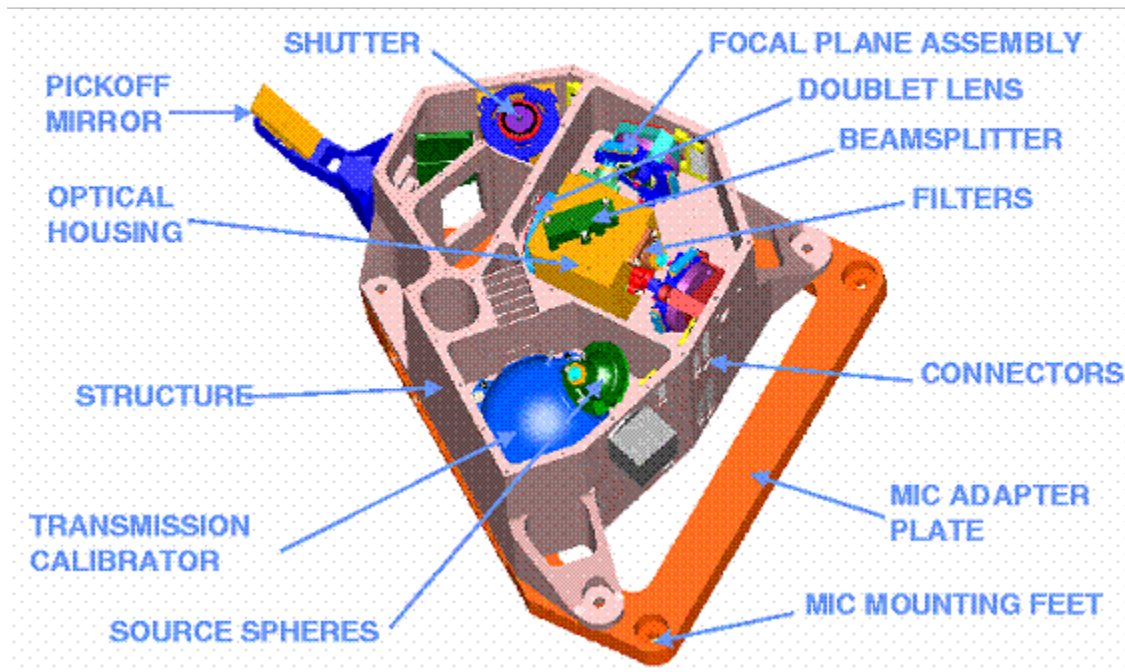
**Figure 6.1: IRAC Cryogenic Assembly model, with the top cover removed to show the inner
components.**

6.1.2 Optics

6.1.2.1 Optical Layout

The IRAC optical layout is shown in Figure 6.2 and Figure 6.3. Light from the
telescope is reflected into the IRAC structure by the pickoff mirrors for the two

fields of view (FOVs). Each working channel has a doublet lens which re-images the Spitzer focal plane onto the detectors. A beamsplitter reflects the short wavelength light to the InSb detectors (Channels 1 and 2). The edges of the two IRAC fields of view are separated by approximately 1.5′, with no overlap on the sky. The IRAC pixel scale is nearly the same in both channels (~1.2″ per pixel), providing a 5.2′×5.2′ FOV.
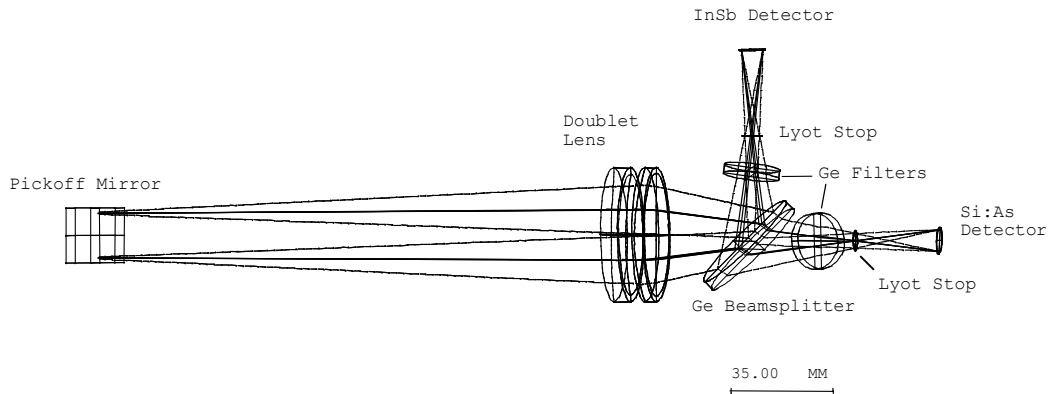
Figure 6.2: IRAC optical layout, top view. The light enters the doublet lens and the short wavelength light is reflected to the InSb detectors (Channels 1 and 2). Note that the long wavelength detectors (5.8 and 8.0 μm) are not operational during the Warm Mission.
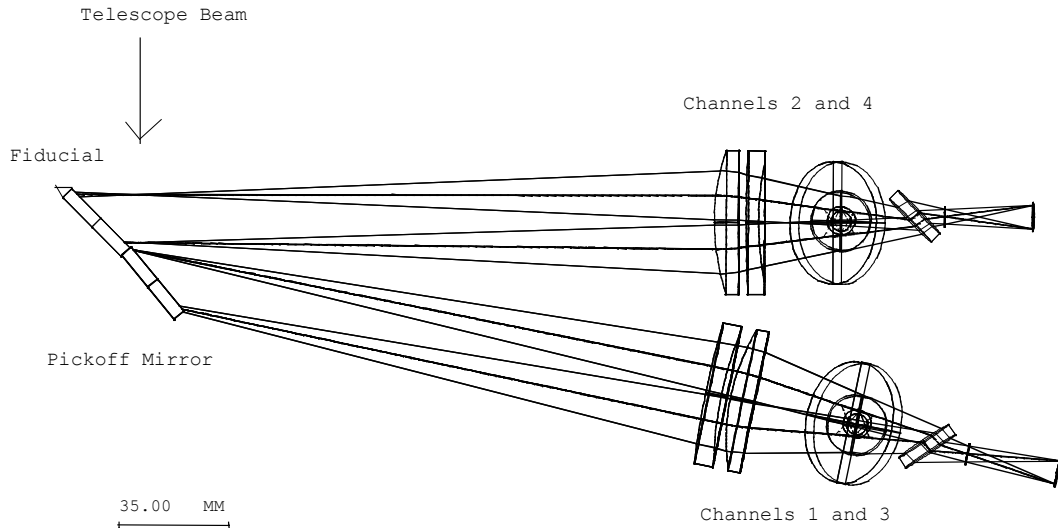
Figure 6.3: IRAC optics, side view.

6.1.2.2 Image Quality

The IRAC optics specifications limit the wavefront errors to $< \lambda /20$ in each channel. IRAC provides diffraction-limited imaging internally, and image quality is limited primarily by the Spitzer telescope. The majority of the IRAC wavefront error is a lateral chromatic aberration that is most severe at the corners of the IRAC field. The aberration is due to the difficulty of producing an achromatic

design with a doublet lens over the large bandpasses being used. The effect is small, with the total lateral chromatic dispersion less than a pixel in the worst case. The sky coordinates of each pixel have been accurately measured in flight using astrometric observations of an open cluster, resulting in distortion coefficients for each image. The main effect is that the PSF and distortion may be slightly color-dependent, which may be detectable for sources with extreme color variations across the IRAC bands.

At the current temperature of the IRAC optics, we observe no measurable difference from the cryogenic image quality. This is expected as the thermal expansion and variation in refractive index for the optical components is imperceptible from 15 K to 30 K.

A much larger variation in the flux of sources measured in different parts of the array is due in part to the tilt of the filters, which leads to a different spectral response in different parts of the field of view (Hora et al. 2008, PASP, 120, 1233; Quijada et al. 2004, Proc. SPIE, 5487, 244). The flat field calibration is done with the zodiacal light, which is relatively red; blue sources have a flux variation of up to 10% from one side of an array to the other (see the IRAC Instrument Handbook for more details).

Figure 6.4 shows the IRAC point response functions (PRF), reconstructed from images of a bright star obtained during IOC/SV. (Here we use the language common in the optics field; the point spread function [PSF] is before sampling by the detector array, and the point response function [PRF] is after sampling by the detector array). More information is available on the SSC website *including the technical report "25 Position Model Pixel Response Functions (PRF) Description and Quality" detailing the PRF construction. The PRFs were developed by adapting a set of synthetic stellar images sampled over the focal plane and phase relative to a pixel center by a convolution kernel that minimizes the differences between the noiseless model representation and images of a bright star as a function of position and phase.* The resulting PRFs are the "optical" point spread function projected onto the focal plane by the IRAC and telescope optics, convolved with the response function of a single detector pixel. The images were combined using a drizzle algorithm (Fruchter & Hook, 2002, PASP, 114, 144) to minimize smoothing of the PRF during the reconstruction process. The resulting PRF sampling was 1/5 the width of an IRAC pixel. Images of a bright star at the native IRAC pixel scale are also displayed for comparison. FITS images of IRAC PRFs are available on the SSC website. The appropriateness of a given PRF is dependent on the observation sampling and the photometric reduction package used (see IRAC Instrument Handbook). The best current PRFs are available at the SSC website (http://irsa.ipac.caltech.edu/data/SPITZER/docs/irac/calibrationfiles/psfprf/). *Note that warm PRFs are still in development and will differ in detail from the cryogenic ones.*
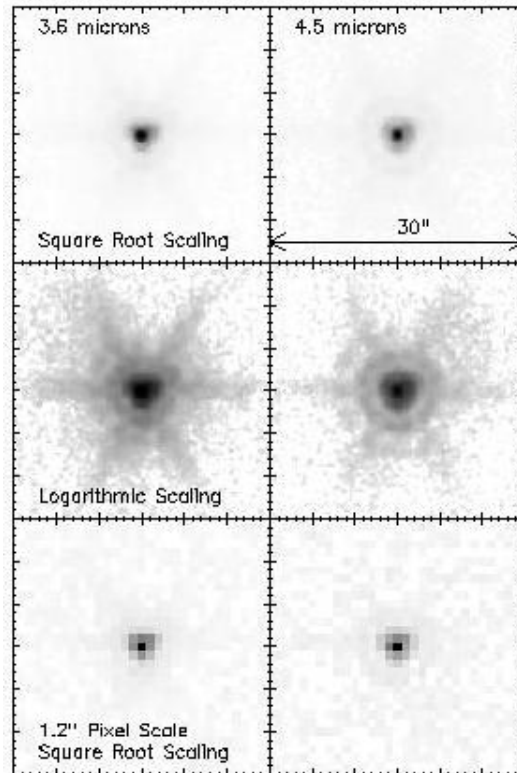
Figure 6.4: The in-flight IRAC point response functions (PRFs) at 3.6 and 4.5 μm. The PRFs were constructed using cryogenic observations. Warm versions of the PRFs are in development. The PRFs were reconstructed on to a grid of 0.24″ pixels, 1/5 the size of the IRAC pixel, using the drizzle algorithm. We display the PRF with both a square root and logarithmic scaling, to emphasize the structure in the core and wings of the PRF, respectively. The bottom panels display an instance of a point source as constructed from the PRF at the IRAC pixel scale of 1.2″. The reconstructed images clearly show the first and second Airy rings, with the first Airy ring blending with the core in the 3.6 and 4.5 μm data.

Table 6.1 lists some importatnt IRAC image quality properties. These numbers were derived from cryogenic measurements of bright stars. Analysis of warm measurements has shown that the optical properties of both IRAC and the telescope have not measurably changed. The "noise pixels" column in Table 6.1 gives the equivalent number of pixels whose noise contributes to a linear least-squares extraction of the flux of a point source from a

Table 6.1: IRAC image quality properties

Channel	Noise pixels (mean)	FWHM (mean;″)	FWHM of centered PRF (″)	Central pixel flux (peak; %)	Pixel size (″)	Maximum Distortional Displacement (pixels relative to square grid)
1	7.0	1.66	1.44	42	1.221	1.3
2	7.2	1.72	1.43	43	1.213	1.6

13×13 pixel portion of an unconfused image and assuming the PRF is perfectly known. In more detail, the quantity is derived as follows.

Let the PRF in pixel i be P_i and the intensity of an image in pixel i be I_i. If a point source with flux F is present in the image, then $I_i = FP_i$. If we do a least-squares fit to determine F, then we minimize $\chi^2 = \sum \frac{(I_i - FP_i)^2}{\sigma_i^2}$ where σ_i is the measurement uncertainty in pixel i. We will assume here that σ_i is independent of pixel and set $\sigma_i = \sigma$ (this condition is approximately true for background and/or read noise limited observations). Now we take the derivative of χ^2 with respect to the source flux and set it to zero to find the optimum value. We find $0 = \sum (I_i - FP_i)P_i$; solving for F, we find $F = \frac{\sum I_i P_i}{\sum P_i^2}$.

Now we derive the uncertainty in the flux. Using the well-known theorem for propagation of errors $\sigma_F^2 = \sum (dF/dI_i)^2 \sigma^2$, and applying it to the result above, we find that $\sigma_F^2 = \sum \left(\frac{P_i}{\sum P_i^2}\right)^2 \sigma^2 = \frac{\sum P_i^2 \sigma^2}{\left(\sum P_i^2\right)^2} = \frac{\sigma^2}{\sum P_i^2}$, or equivalently, $\sigma_F = \sigma \sqrt{N}$ where $N = \frac{1}{\Sigma P_i^2}$, which is the definition of noise pixels. The number of noise pixels is used for the sensitivity predictions in the following sections of this chapter.

There are two columns for the full width at half-maximum (FWHM) of the PRF. The mean FWHM is from observations of a star at 25 different locations on the array. The FWHM for "centered PRF" is for cases where the star was most closely centered in a pixel. The fifth column in Table 6.1 is the fraction of the flux in the central pixel for a source that is well centered in a pixel. It was determined from the images of the focus star (after the telescope was focused) that were the most symmetric and concentrated. These values for the flux in the central pixel were used in the saturation predictions in the following sections of this document. The flux in the central pixel for a random observation will be lower, depending on the centering of the source with respect to a pixel.
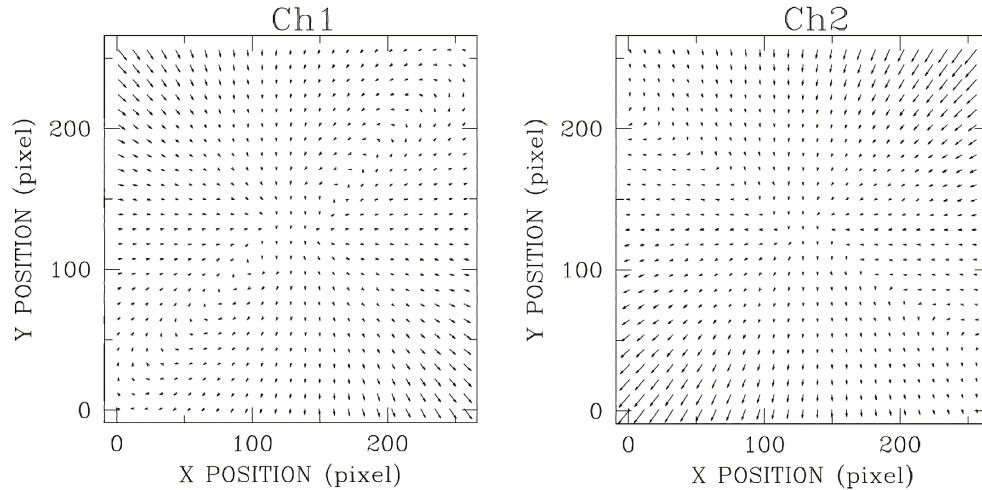
Figure 6.5: Optical image distortion in IRAC channels. The panels show the image distortions as calculated from a cubic polynomial model that has been fit to in-flight data. The magnitude of the distortion and the direction to which objects have moved from their ideal tangential plane projected positions are shown with arrows. The length of the arrows has been increased by a factor of ten for clarity. The maximum positional deviations across the arrays for this cubic distortion model are less than 1.3 and 1.6 pixels for channels 1 and 2. The derivation of the pixel scales that are listed in Table 6.1 fully accounts for the cubic distortion effects shown here.

The sixth and seventh columns in Table 6.1 were determined from astrometric measurements of star fields.

6.1.2.2.1　Distortion

Due to the off-axis placement of IRAC in the Spitzer focal plane, there is a small amount of distortion over the IRAC FOV. The maximum distortion in each IRAC channel is <2 pixels (compared to a perfectly regular grid) over the full FOV. Figure 6.5 shows the distortion across the two short IRAC channels, as determined from data taken during IOC/SV. The IRAC pipeline provides data with a full astrometric solution including the array distortion using the SIP convention (Shupe et al. 2005, ASPC, 347, 491). *Future versions of the pipeline will use a higher order distortion correction to improve the residual distortion error to ~20 milli-arcseconds.*

6.1.2.2.2　Location of Sources on the Arrays

For an observation specifying a target with no offsets or dithers, the source will be positioned at the pointing center of each field of view, modulo the blind pointing uncertainty of Spitzer (~0.5″ rms). In BCD coordinates, the source will appear as listed in Table 6.2. The x and y are the row and column positions, respectively, in the BCD, counting from the lower left-hand corner (1, 1), with integer values specifying the center of a pixel. Offsets in the positive column direction will move the source in the negative y-direction on the BCD. Offsets in the positive row direction will move the source in the positive x-direction on the BCD.

Table 6.2: Source location on the arrays

Array	x (pixel)	y (pixel)
3.6 μm	131.0	128.0
4.5 μm	128.0	129.0

The relative placement of the BCDs on the sky is shown in Figure 6.6. The figure also shows the subset of pixels used for subarray observations. The 3.6 μm subarray subtends the location (9, 217) to (40, 248) of the 3.6 μm full array BCD. The 4.5 μm subarray orientation with respect to the full array is the same as in the 3.6 μm array. The pointing centers of both arrays for both the full and subarray are free of hot or noisy pixels in a 10 pixel radius aperture.
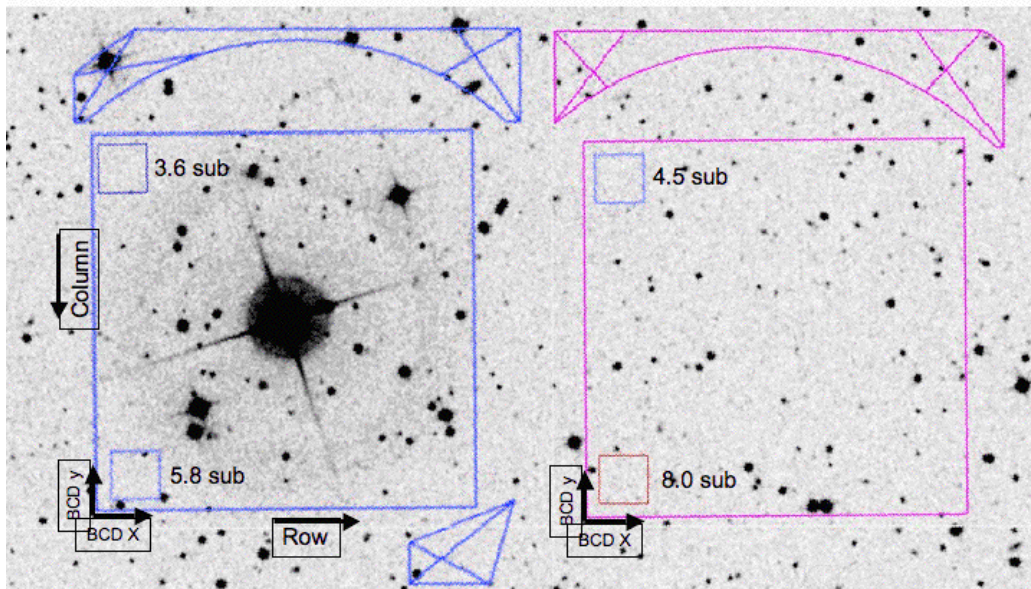
Figure 6.6: The orientation of the BCDs on the sky.

6.1.2.2.3   Scattered and Stray Light

Stray light from outside the IRAC fields of view is scattered into the active region of the IRAC detectors in both channels. Stray light has two implications for observers. First, patches of stray light can show up as spurious sources in the images. Second, background light, when scattered into the arrays, is manifest as additions to the flat fields when they are derived from observations of the sky.

Stars which fall into those regions which scatter light into the detectors produce distinctive patterns of scattered light on the array. We have identified scattered light avoidance zones in each channel where observers should avoid placing bright stars if their observations are sensitive to scattered light. The zones for channels 1 and 2 are shown in the Spot overlays (Figure 6.7). Zones 1A, 1B, 2A,

and 2B (which produce the strongest scattered light) typically scatter about 2% of the light from a star into a scattered light "splatter pattern" which has a peak of about 0.2% of the peak of the star (Figure 6.8). They arise due to scattering of light from the edges of the holes in the covers of the focal plane arrays. The A and B zones join up to form a continuous region of scattering which is widest at the upper left and right corners of the array, and narrows to a waist in the center. Zone 1C produces diffuse scattered light across the array, but the light is only noticeable if Zone 1C is illuminated by very bright stars. See the SSC website for more details.

Scattered light is well-rejected by the post-BCD pipeline if dithering and mapping offsets are large enough to ensure stars are moved out of the scattering zones, and the redundancy is high enough to allow for effective outlier rejection. The medium and large dither pattern scales with 4 or more dithers per position are adequate for this. Most cases of scattered light are identified and flagged as part of the pipeline processing. No secure model for the distribution of scattered light from point sources exists and scattered light from point sources cannot be reliably removed from images.
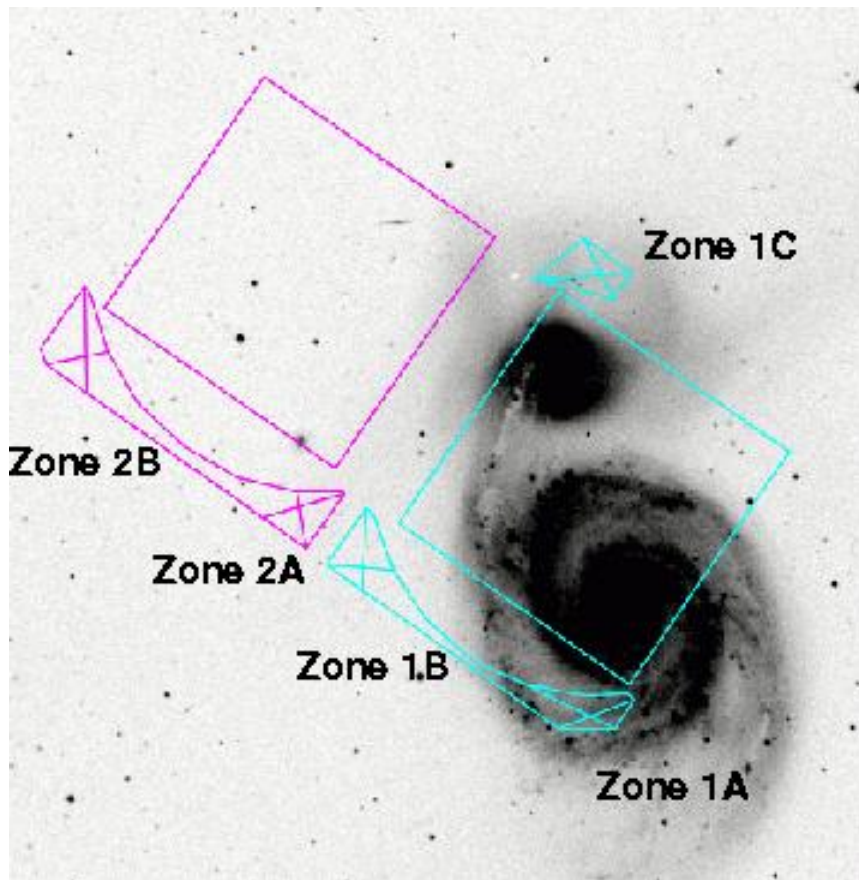
Figure 6.7: Locations of IRAC stray light avoidance zones as seen in Spot visualizations. See text and SSC website for more detail.

The SSC has implemented a correction in the pipeline to remove diffuse stray light from the BCDs, flats, and skydarks. This correction scales a template of the diffuse scattered light pattern by the expected zodiacal background level and subtracts it from the data. In channels 1 and 2, the pattern is in the form of a "butterfly wing" at the bottom of the array in raw data coordinates (i.e., at the top of the array in BCD coordinates). The scattered light avoidance zones 1A, 1B, 2A, and 2B are larger than the regions the scattered light falls into. This concentration results in the diffuse scattered light ("butterfly wings") having amplitudes ~5% of the background intensity, even though only about 2% of the light from a given point in the stray light zones is scattered into them.

Additional information and figures on this subject are available in the IRAC Instrument Handbook.
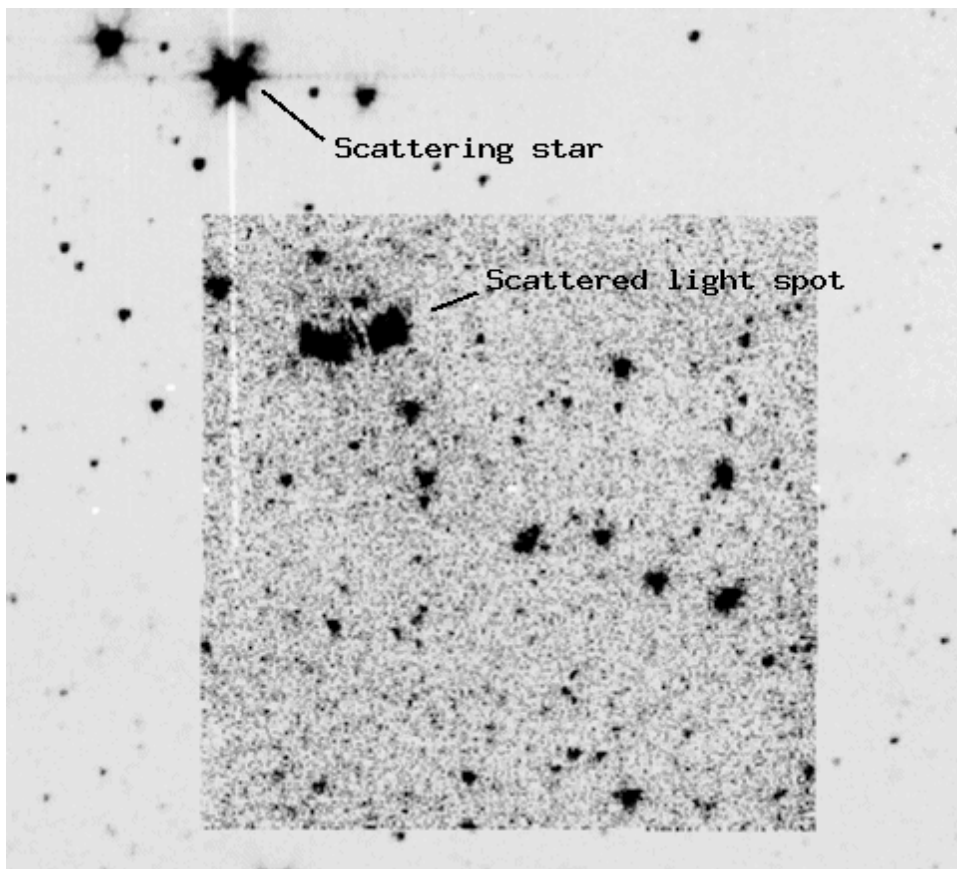
Figure 6.8: Stray light pattern in BCD data when a bright source falls in the stray-light avoidance zone 2A in channel 2. See text and IRAC Instrument Handbook for more detail.

6.1.2.2.4   Ghost Images

Ghost images are visible near very bright sources in channels 1 and 2. These ghost images are caused by internal reflections within the tilted filters. Because of the increase in the optical path length, ghost images are not in focus. The separation between the main image and its ghost is roughly proportional to the

distance of the main image from the Spitzer optical axis. In terms of pixel offsets in the BCDs, the ghost positions are $(\Delta x, \Delta y) = (A_x x + B_x, A_y y + B_y)$ where *(x,y)* are the pixel coordinates of the source in a BCD. The coefficients for channel 1 are A_x=0.049686, B_x=-14.6110, A_y=0.048301, and B_y= 0.54605. The coefficients for channel 2 are A_x=0.051957, B_x=1.20675, A_y=0.053381, and B_y=-0.45258. The peak intensity of the ghost is roughly 0.05% of the (unsaturated) peak intensity of the star. Examples of ghost images are available in the IRAC Instrument Handbook. The SSC pipeline flags filter ghosts. The filter ghosts are treated as part of the point spread function and are included in both the measured PRFs and the nominal flux calibration which is derived from photometry using 10 pixel radius source apertures.

6.1.2.2.5   Polarization

The tilted elements within IRAC produce a small amount of instrumental polarization that can lead to small photometric errors when viewing polarized sources. The filter transmission is shown as a function of wavelength in Figure 6.9; the expected polarizations are 0.794% and 0.282%, for channels 1 and 2, respectively.

Table 6.3: IRAC Channel characteristics

Chan	Effective λ (μm)	Bandwidth (μm)	Average transmission (η_i)	Minimum in-band trans- mission	Peak trans- mission
1	3.550	0.750 (21%)	0.676	0.563	0.748
2	4.493	1.015 (23%)	0.731	0.540	0.859

6.1.2.3 Chromatic Elements

The IRAC system throughput and optical performance is governed by a combination of the system components, including the lenses, beamsplitters, filters, mirrors, and detectors. The system parameters are summarized in Table 6.3. The system response is based on measurements of the final in-flight system, including the beamsplitter, filter, ZnS & ZnSe coating transmissions, mirror reflectance, BaF_2 and MgF_2 coating transmissions, and detector quantum efficiency.

The system out-of-band transmission (more than 2.5 times the central wavelength of the band) is less than 10^8 relative to the transmission at the center of the band. Tests during IOC/SV showed that the out-of-band leaks are less than the astronomical background at all locations for sources of any temperature detectable in the IRAC bands.

6.1.3 Detectors

6.1.3.1 Physical Characteristics

The IRAC detector arrays were developed by the Raytheon/Santa Barbara Research Center (SBRC) in Goleta, CA, under contract to SAO (Hoffman et al. 1998, Proc. SPIE, 3354, 24; Estrada et al. 1998, Proc. SPIE, 3354, 99). Channels 1 and 2 use InSb arrays operating at ~28.7 K. The arrays use the CRC744 CMOS readout circuit, and the same physical pixel size of 30 μm. The arrays are anti-reflection coated with SiO. The power dissipation for each array is <1 mW. Table 6.4 gives some of the detector properties. The "operability" is the percentage of the pixels in an array that are within usable specifications as measured from warm calibration data. The read noise is our best estimate based on actual flight performance and 30 K ground testing. Read noise is not directly measurable from in-orbit data and is particularly hard to measure for the longer frametimes. *The warm in-flight read noises have been updated to include 1/f noise. 1/f noise is particularly significant for the channel 1 array at the higher operating temperature.* The effective warm well depth is smaller than the value indicated in Table 6.4, as discussed in Section 6.1.3.2.1
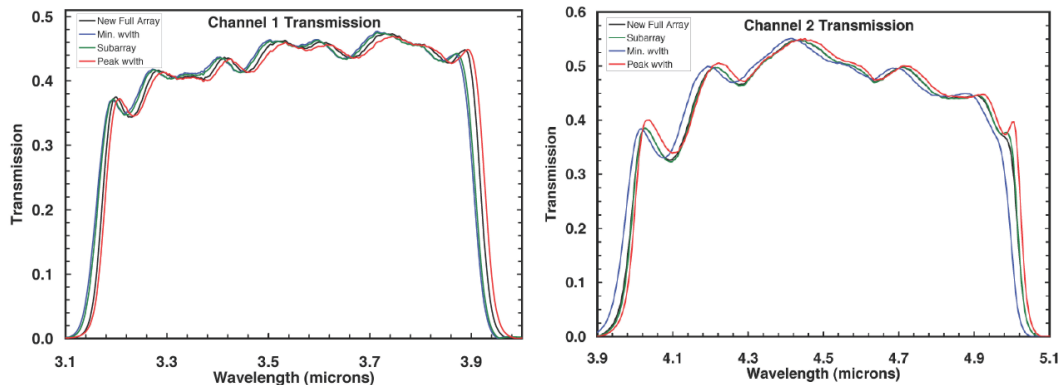
Figure 6.9: IRAC total system response for channel 1 (left) and channel 2 (right), including transmission of the optics and quantum efficiency of the detectors. Digitized versions of these curves are available on the SSC website.

6.1.3.2 Detector Calibration

The following subsections outline some of the more important data calibration steps and the nature of residual images. The IRAC pipeline provides a science caliber calibration for the detector non-linearity, bias and flat-field. The pipeline also flags inoperable pixels, residual images and radiation hits. Inter- and intra-pixel response variations and their impact on photometry are discussed in detail in the IRAC Instrument Handbook and in http://irsa.ipac.caltech.edu/data/SPITZER/docs/irac/warmfeatures/.

6.1.3.2.1 Photometric Linearity Calibration

InSb detectors have measurable nonlinearity. The InSb arrays are nearly linear until they reach saturation. Both arrays are linearized to better than 1% up to

approximately 90% of their full-well capacity (defined in electrons in Table 6.4, with the gain listed in Table 6.6, corresponding typically to ~30,000 DN). Note that the linearizable well depth for both arrays has decreased from ~45,000 DN in the cryogenic mission. As part of the warm calibration, the detector linearity has been determined by observations of a large number of point sources over a large dynamic range compared to comparable cryogenic observations of those sources. The warm linearity measurements are shown in Figure 6.10. The arrays were illuminated with a constant flux, and successively longer exposures were taken. For a perfectly linear system, the flux would be directly proportional to the exposure time, and the graph would show a straight line. In fact, the arrays were driven past their saturation levels, and the shape of the curve up to 90% of the saturation level was fitted with a polynomial for the linearization module in the pipeline.

Table 6.4: IRAC detector characteristics

	FPA designation	Effective read noise for frame with specified frame time (electrons)[a]					Quantum Efficiency (%)[b]	Well Depth (e-)[b,c]	Operability (%)
		0.4s	2s	12s	30s	100s			
1	48534/34 (UR)	*22.4*	*16.0*	*15.0*	*14.6*	*21.0*	87	*110,000*	99.01
2	48975/66 (GSFC)	23.7	*12.1*	*10.4*	*10.4*	*16.0*	86	*125,000*	99.97

[a] Effective read noise includes contribution due to 1/f noise. Actual read noise is predicted to be similar to cryogenic operations which it is at 4.5μm and higher at 3.6 μm.
[b] Values from pre-flight laboratory measurements. The QE and actual well depth are not uniquely measured in flight.
[c] Updated from the 145/140 K values from the cryogenic mission to match observed saturation limits.

6.1.3.2.2   Effects of Overexposures

After observing a bright source, a residual image will remain on the array in subsequent frames. In the cryogenic mission, very bright sources produced a very long term (tens of hours) residual image at 3.6 mm that had to be mitigated by thermal annealing and judicious scheduling of bright sources. For warm IRAC, there are no very long-term residual images. The arrays are not annealed as part of nominal operations and there are no strong constraints on observing very bright sources. The predicted saturation levels for point sources are given in Table 6.13.

Very bright sources will produce noticeable short term residuals as well as slew latents noticeable as streaks in images and produced in the course of moving from one observation to the next. While it is not always possible, steps should be taken to avoid generating persistent images, including keeping bright sources off the arrays and using multiple short exposures instead of longer ones. Also, observations should be planned so as not to be susceptible to persistent images generated by preceding observations. Well-dithered observations will yield mosaics with much-reduced persistent images and are strongly recommended; in

straight averages, the amplitude decreases as the number of dithers is increased, and the worst ones are eliminated from robust averages or medians.
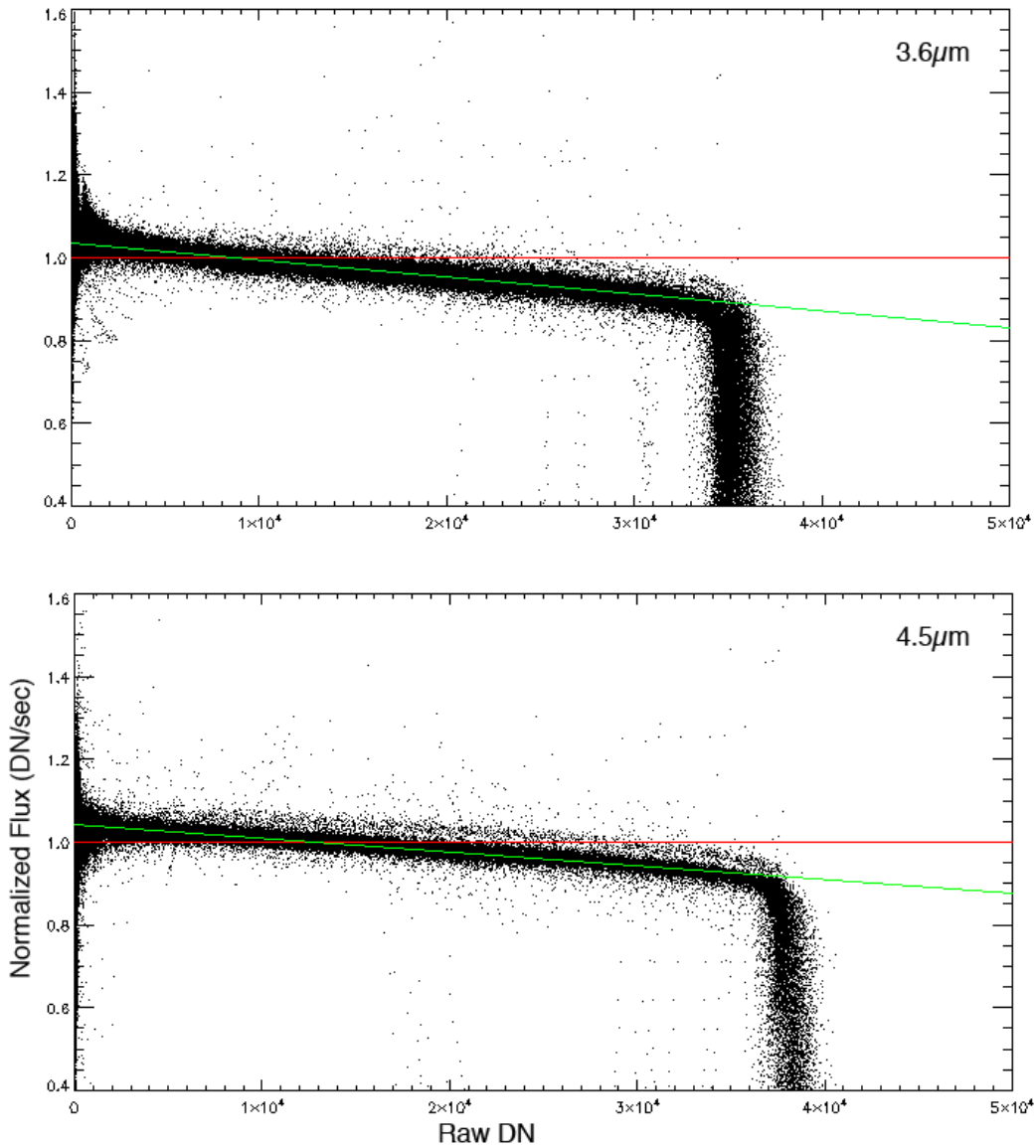
Figure 6.10: Non-linearity curves for the IRAC detectors. Measured source flux as a function of peak DN is plotted. The detector responses are fairly linear until saturation, where there is a steep drop-off in responsivity. The linearity solution is indicated by the green curve.

6.1.3.2.3   Short-Term Residual Images

Both IRAC channels have residual images of a source after it has been moved off a pixel. When a pixel is illuminated, a small fraction of the photoelectrons is trapped. The traps have characteristic decay rates, and can release a hole or electron that accumulates on the integrating node long after the illumination has ceased.   The warm mission short-term residual images are different in character

than the cryogenic residuals, as the behavior of the trap populations is a function of the impurity type and temperature. Typically for channel 1, warm residuals are <0.01% of the fluence of the source after 60 seconds. The residual image never exceeds 1% of the illuminating source for integrations beginning immediately after the illumination ends. Usually the residual will be orders of magnitude smaller, but the residual image of a star can persist as a false point source for up to several hours for the most saturating sources followed by low background deep observations. Channel 2 residual images decay much more rapidly than those in channel 1, lasting at most 10 minutes for the brightest sources.

For reference, Figure 6.11 shows the residual decay for a strongly saturating first magnitude source observed in a 12 second integration time in channel 1. The data residuals are measured using aperture photometry of subsequent frames and the residuals are averaged over time. In this extreme example, the residual persists above the noise in the background for more than five hours after the residual is produced.
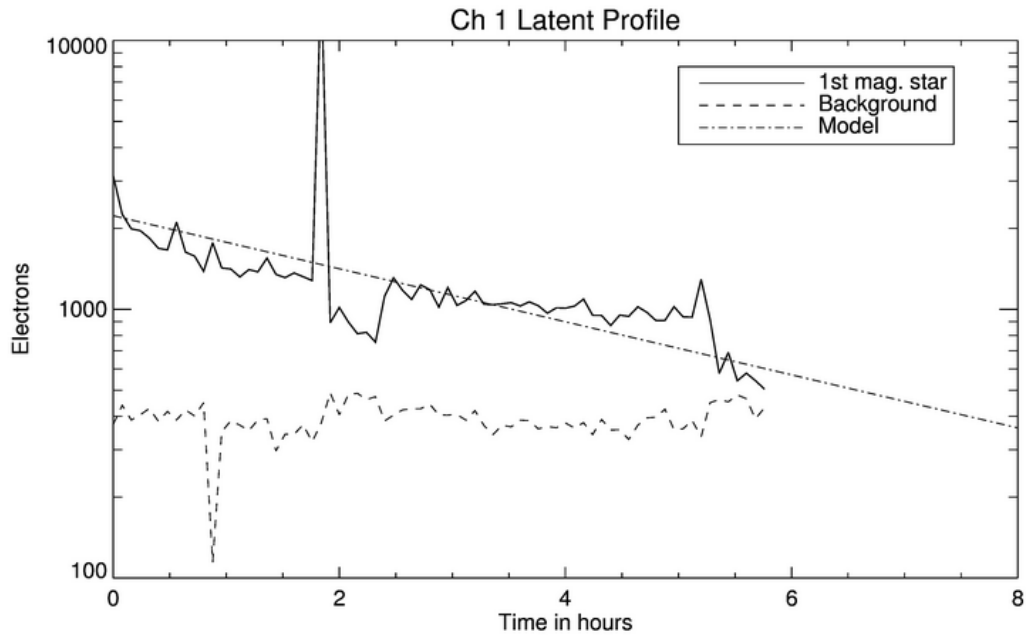
Figure 6.11: Residual image brightness decay as a function of time interval since exposure to a bright source at 3.6 μm. The residual is compared to 3 times the noise in the sky background as measured in an equivalent aperture. The fitted exponential decay function is plotted as the dot-dashed line. These curves have been smoothed to mitigate flux jumps due to sources at the position of the original source in subsequent images.

An example of the residual images for channel 1 is displayed in Figure 6.12 which displays the residuals produced by 3rd and 4th magnitude stars observed in a 12 second integration. In addition to the compact residuals, there are streaks that can be produced when bright sources cross the array during slews between AORs.
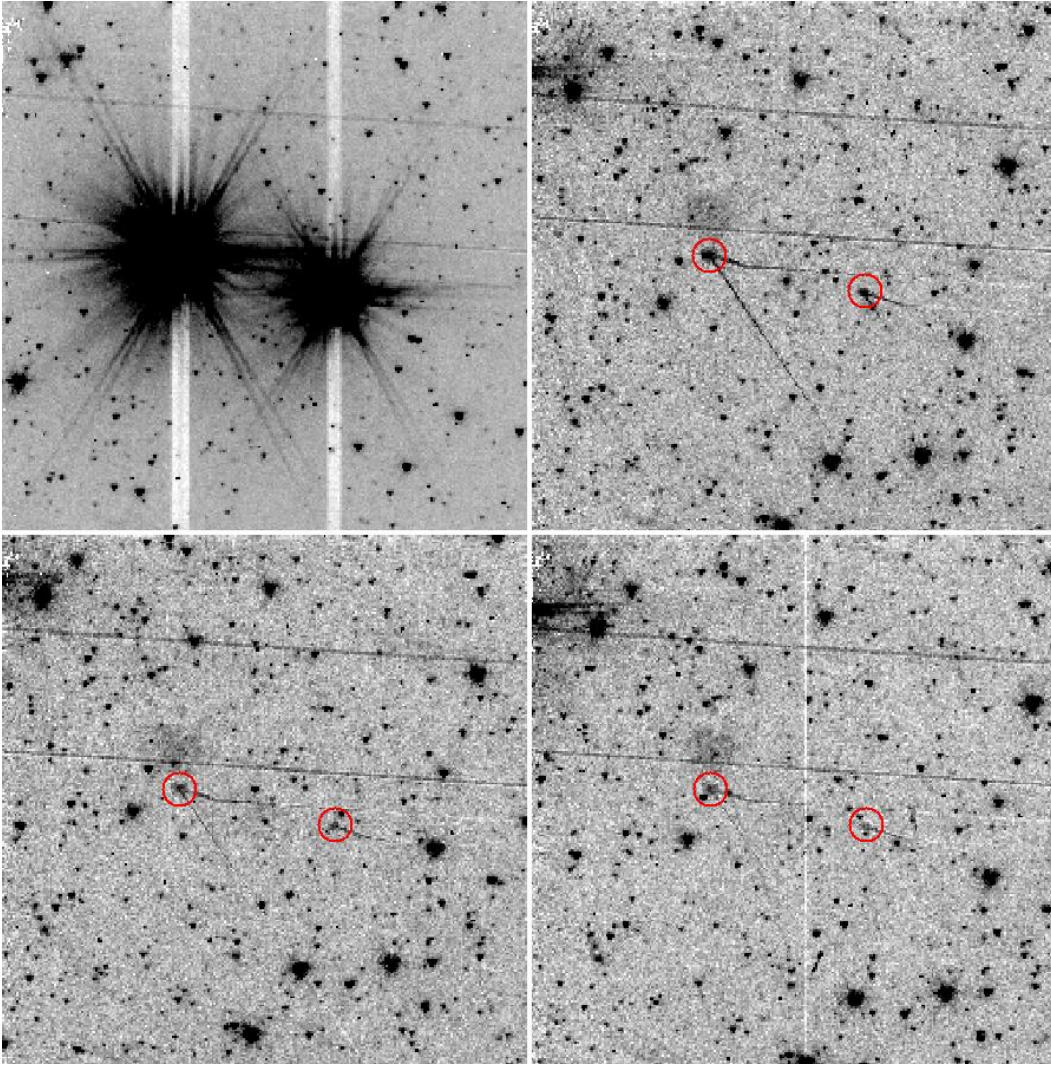
Figure 6.12: Illustration of residual images in warm data for channel 1. 3ʳᵈ and 4ᵗʰ K-magnitude stars were observed in a single 12 second frame (upper left panel). The upper right, lower left and lower right panels show the decay in the residual in 12 second frames taken 60, 120 and 180 seconds after the bright sources were observed. The positions of the bright sources on the array are identified by red annuli in subsequent frames. The linear features connecting to the bright residuals are from slews, produced as those bright sources move on and off the array. The dark patch above the 3ʳᵈ K-magnitude star residual (leftmost residual) is a diffuse residual from a previous observation and the linear features crossing the entire array are slew residuals from bright sources crossing the array during earlier observations.

6.1.3.2.4 *Pixel-to-Pixel Sensitivity Variations*

The gain varies from pixel to pixel on the array, due to intrinsic gain differences in the pixels themselves and in the output electronics gain, and due to variations in the light over the FOV transmitted by the telescope and camera optics. The gain variation for each array is mapped as described in Section 6.1.3.2.8. However, the gain maps do not strictly apply for point sources with stellar-like spectral slopes due to the variation in filter effective wavelength across the array.

A location-dependent photometric correction for point sources is provided for each array on the IRAC web pages. The peak-to-peak variation in photometry is 6% at 3.6 μm and 8% at 4.5 μm. Images of the photometric correction are shown for each IRAC InSb detector in Figure 6.13. More information on the pixel-to-pixel sensitivity variations can be found in http://irsa.ipac.caltech.edu/data/SPITZER/docs/irac/warmfeatures/.
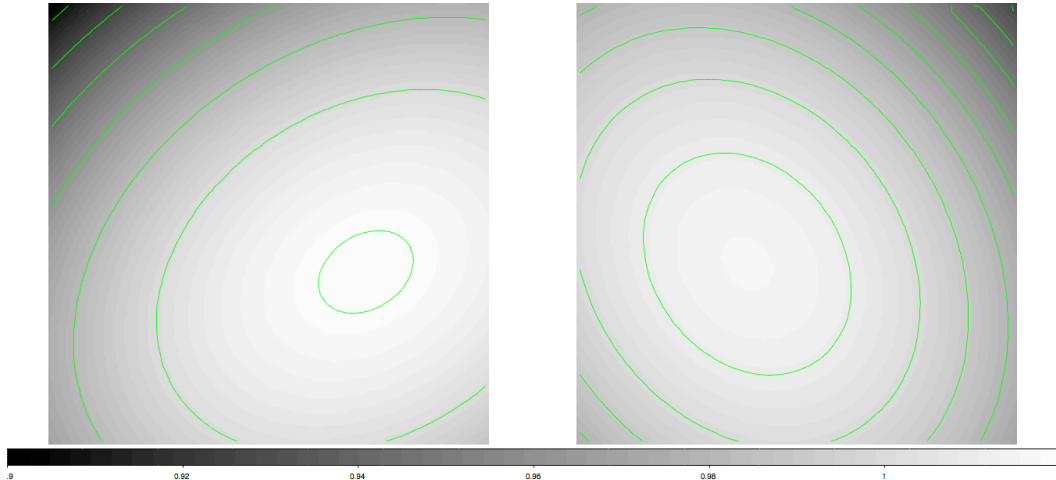
Figure 6.13: Photometric correction images at 3.6 μm (left) and 4.5 μm (right). The contours start at 0.95 for 3.6 μm and 0.94 for 4.5 μm and increment by 0.01. The correction images are normalized to the average response of the array.

6.1.3.2.5   Intra-Pixel Sensitivity Variations

For the InSb detectors, the measured flux of a point source depends on the position of the source centroid with respect to the center of a detector pixel. This effect is due to the efficiency of the InSb pixels not being uniform throughout the entire pixel. The effect is more significant in the warm mission. The variation in measured flux is ~7% at 3.6 μm and ~4% at 4.5 μm for a source as a function of its position on the pixel. Calibration data have been taken to correct this effect to better than 0.1%.

6.1.3.2.6   Pixel Mask

In each array there are pixels that are totally inoperable, or whose characteristics (QE, noise, dark current) fall outside of the allowed range. This is represented by the Operability column in Table 6.4. These pixels are evaluated and masked out during reduction in the pipeline using pixel masks. Interested observers can download the quasi-static bad pixel masks from http://irsa.ipac.caltech.edu/data/SPITZER/docs/irac/calibrationfiles/pmask/. These masks have been updated for post-cryogenic operations. The number of bad pixels has increased by a factor of 5 at 3.6 μm and a factor of 4 at 4.5 μm but is still a small fraction of the array. When the applied biases were tuned for each array, one constraint was to keep the number of bad pixels comparable to the number of pixels affected by radiation hits in the longest frametime used (100 seconds ~ 500 pixels).

6.1.3.2.7 Darks

The detector dark currents at 28.7 K are insignificant compared to the sky background. Ground tests at 30 K measured dark currents of < 0.1 e/s for sister arrays of the IRAC flight InSb arrays. However, there is a significant offset or bias (which can be positive or negative) in a dark frame, and which therefore must be subtracted from the observations. For reference, Figure 6.14 shows dark frames obtained during the warm calibration using 100 seconds frames. In general, the dark offsets have a larger magnitude and more structure than the cryogenic offsets, but are as reliably subtracted by the IRAC pipeline. Especially for shorter frames, the "dark" images are mostly due to electronic bias differences, rather than true dark current; therefore, the number of electrons in a dark image does not scale linearly with exposure time. Note that without the shutter, isolated dark/bias data (as shown in Figure 6.14) cannot be taken in flight. In addition, no lab dark data exist for 30 K operations. Instead, skydarks (Figure 6.14) are subtracted. The skydark subtraction is done using calibration observations taken <1 week from a given science observation. As no lab darks exist at 30 K, a dedicated calibration program is being used to develop an in-orbit calibration of the bias and first frame effect (see 6.1.3.2.11). Observers are reminded that absolute sky brightness measurements are not feasible with IRAC due to the shutterless calibration and lack of lab bias measurements.
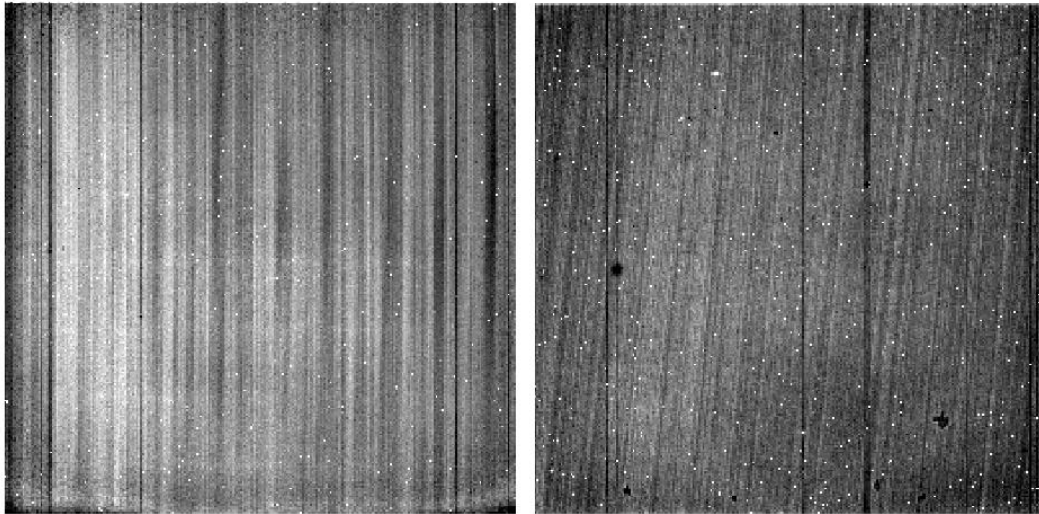
Figure 6.14: IRAC skydark images for the 100 second frametime. The 3.6 μm dark is to the left and the 4.5 μm dark is to the right. The mean dark levels are 190 and 555 DN. Pixel (1,1), in the lower left corner, is the first pixel read out by the electronics. These images are flipped about the y-axis compared to the BCDs.

6.1.3.2.8 Flats

Flats are obtained from observations of the sky during normal operations. Observations through the entire telescope and instrument are necessary to measure the total system response. The responsivity at 30 K is as stable as it is at

15 K in part due to the active temperature control and thermal stability of the arrays. The gain maps vary by only a few percent per pixel compared to the cryogenic flats. Flat-field observations are part of both the initial warm calibration and the routine calibrations for each two week campaign. The data are combined to generate a superflat (Figure 6.15) as was done in the cryogenic mission and the current superflat has approximately the same precision as the cryogenic version.
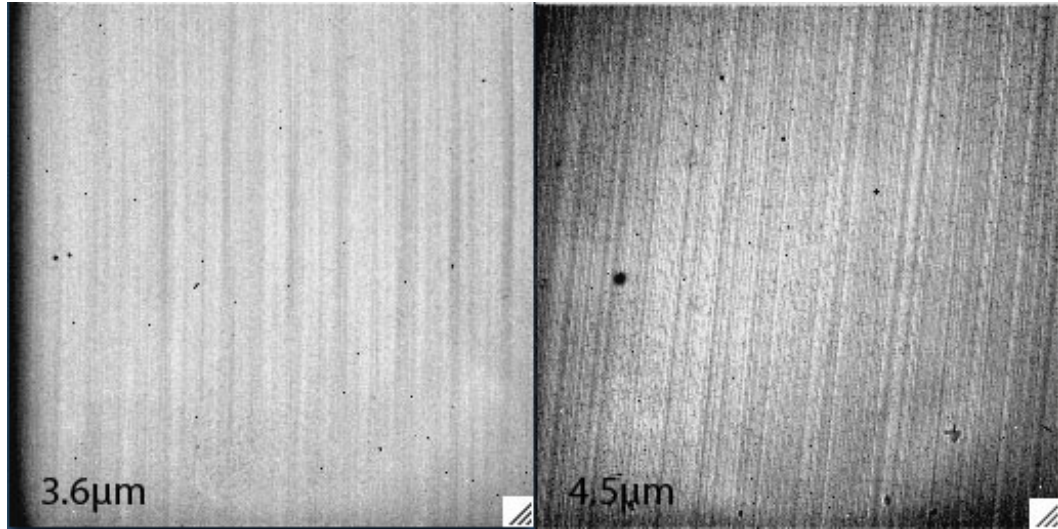
Figure 6.15: IRAC superskyflats for channels 1 and 2 taken during the warm final setpoint calibration. The extended dark spots seen in the channel 2 flat are most likely due to particulate impurities on the pick-off mirror.

6.1.3.2.9   Effect of Cosmic Rays

Cosmic rays will strike the IRAC detectors fairly regularly (about one per array per second, each one affecting on average about 5.5 pixels), so strategies to deal with them in data reduction will have to be implemented. The most common cosmic rays do not affect the pixel performance in subsequent frames, and are confined to a few pixels around the peak. However, other events can cause streaks or other multiple pixel structures in the array, and less common energetic events may cause residual images in subsequent frames. Single cosmic rays should not permanently affect the responsivity of a pixel, but multiple strikes over time, and exposure to strong solar proton events, may lead to an increase in the dark current of certain pixels, and perhaps to a degradation of responsivity. Despite significant solar events during cryogenic operations, no significant degradation of the IRAC arrays has been observed. There is no difference in the effect of cosmic rays on the IRAC arrays between 30 K and 15 K operations.

Figure 6.16 shows portions of a 100-sec IRAC frame at 3.6 μm obtained during IOC/SV. Stars have been subtracted to show only cosmic rays in the images.
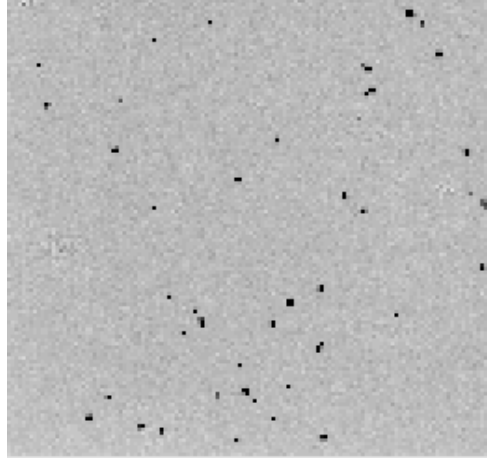
Figure 6.16: Channel 1 IRAC image (100 sec frame time) obtained during IOC/SV. Stars have been subtracted. All the dark pixels are affected by cosmic rays.
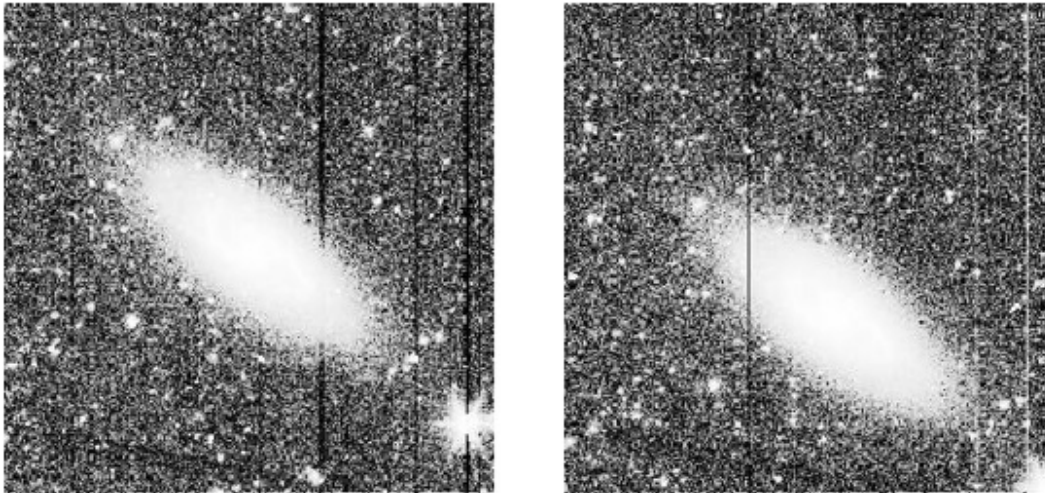
Figure 6.17: Image showing examples of column pulldown and pullup at 4.5 μm. The panels display two sequential 30 second observations of NGC 1353 from the S4G program.

6.1.3.2.10 Thresholds for Triggering Image Artifacts

During cryogenic operations, a variety of image artifacts were produced by observations of bright sources. During warm operations the artifacts are much more benign with only the column pulldown effect persisting. Column pulldown is a columnwise offset produced by a bright pixel. Pulldown is more prevalent and has a more complex behavior than in the cryogenic mission. The effect has a different amplitude above and below the source and decreases in a quadratic fashion with distance along the column from the trigger. In addition, strong cases of pulldown at 4.5 μm can persist long enough that they appear as column pullup in subsequent frames. The switching of polarity is due to a combination of the pulldown decay and the Fowler sampling of the data collection.

Based on examination of 12 sec HDR warm data, it appears that the column

pulldown and pullup (see Figure 6.17) are triggered by pixels above a certain fluence. These levels are likely to be appropriate for all frame times and should be sufficient for planning purposes. Table 6.5 provides estimates of how bright a pixel has to be to trigger various levels of column pulldown. Thresholds are in units of fluence (MJy/sr · sec). To find the threshold for a particular artifact for a given frametime, divide the appropriate value by the frametime. If the surface brightness of a pixel is above a threshold, that pixel will produce a specified artifact. To see if a point source may induce an artifact, convert the estimated flux density to surface brightness (assuming that the source is centered on an IRAC pixel) by scaling the flux density, in µJy, by 0.012. Keep in mind that, if a source is not centered on a pixel, its flux will be distributed more uniformly and be less likely to induce an artifact. The upper limit of the flux falling into the central pixel can be roughly estimated by multiplying the flux by the percent of flux in the central pixel (from Table 6.1) and the projected area of an IRAC pixel ($\sim 3.5 \times 10^{-11}$ sr). The threshold for "strong" column pulldown is that required for the artifact to be noticeable in high background regions such as the Galactic plane.

Table 6.5: Fluence per second (in MJy·sec/sr) of a pixel needed to trigger artifacts.

Ch	Weak pulldown	Pullup	Strong pulldown
1	1200	----	4000
2	1300	2340	4350

The definitions of the columns in Table 6.5 are

Weak pulldown:	Threshold for column pulldown that is noticeable in low background fields.
Pullup:	Threshold for column pulldown that will produce a pullup in one or two subsequent frames.
Strong pulldown:	Threshold above which the column pulldown will be significant in high background fields.

For more information on IRAC instrumental artifacts, please see the IRAC Instrument Handbook.

6.1.3.2.11 First-Frame Effect

Dark frames in all IRAC channels are not constant. A dark image taken with a particular frame time and Fowler number depends on the amount of time elapsed since the previous image, and the frame time and Fowler number of the previous image. In a sequence of images with the same frame time and Fowler number, the variation from one image to the next consists principally of a uniform change over the whole image. To a much smaller extent, there is also a change in the relative offsets on each of the four outputs of an array (pinstriping) and a small spatial gradient across the image. True dark current and multiplexer glow carry with them the usual shot noise in the number of charges collected at the

integrating node, but the rest of the Fowler bias (effective bias due to read strategy) presumably is due to relaxation in the multiplexer and temperature changes. The noise in pixels with low dark current and low glow is the same as the read noise from the multiplexer, so the dark offset variations do not add to the pixel noise. In general, the first frame of any sequence of images tends to have a different offset from the others, because it tends to have an interval, frame time, or Fowler number different from its preceding image. The largest dark offsets occur when a frame is taken with a very short interval from the preceding image, which occurs when multiple frames are commanded at once (using "repeats"). In lab testing, this effect came to be known as the "first frame effect" for this reason. We eliminated commanded repeats from IRAC science observations, so there is always a finite interval between one frame and its predecessor. Most observers will be dithering between frames, meaning that the interval between frames will be in the range 8 to 60 sec. The first frame of every full array AOR with frame time >2 sec is taken with the HDR mode (see Table 6.9) to mitigate the first-frame effect.

The "first frame effect" was calibrated in ground tests with the shutter closed. Figure 6.18 shows the dependence of dark offset on the interval between 30 sec frames. Each symbol is the mean dark signal in one output of each array, averaged over a box near the center of the array. The dashed curves are multiple-exponential fits to the means in the set of 48 images, with the first image excluded. The lower portion of each panel shows the residuals, in electrons, between the data and the fitted curves. The residuals are small compared to the expected sky backgrounds in 30 sec frames (see Table 6.7). During cryogenic operations, channel 1 had very significant variations in offset, compared to the low background in that channel. Channel 2 had very small variations in offset.

In the warm mission, the "first-frame effect" is less pronounced in total offset in both arrays. At 3.6 μm, the average offset is 40 DN compared to 80 DN in the cryogenic mission for delay intervals of 7 to 40 seconds. During the final setpoint calibration, data were collected to create a warm first-frame correction. These data are currently being analyzed and the correction will be incorporated into a future version of the pipeline. It is possible that the residual pinstriping and pixel-to-pixel variations will be more significant than in the cryogenic 3.6 and 4.5 μm data. For both arrays, a gradient in the "first-frame effect" has been noted. These residuals will mainly affect measurements of diffuse low surface brightness sources. To mitigate this potential noise source, observations of low surface brightness objects should not count on using the first integration and would benefit from using a large cycling dither pattern as that is the same pattern used by the skydarks. If data are taken with the same cadence as the skydarks, then the "first-frame effect" is removed entirely by the skydark subtraction.
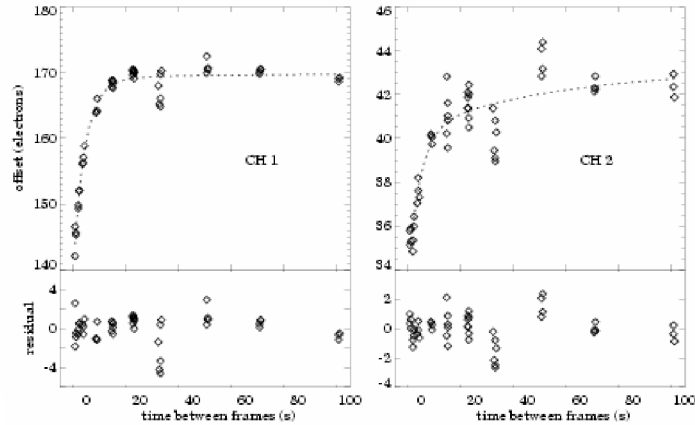
Figure 6.18: Cryogenic first-frame effect – electronic offset as a function of time interval between frames.

6.1.3.2.12 Stability

In-flight data indicate that IRAC is very stable at 28.7 K. The arrays will continue to be thermally controlled to a level of a few milli-Kelvin. As in the cryogenic mission, we monitor the gain, bias and photometric stability using observations of the Ecliptic plane, the North Ecliptic pole and the seven primary calibrators for IRAC every fourteen (seven for the bias) days. As in the cryogenic mission, the gain, bias and flux conversion values are stable in time to within our ability to measure them. The gain is constant to within the precision of our superflat, 0.17% and 0.09% in channels 1 and 2, respectively.

The photometry of IRAC is stable on both short (hours) and long (months) timescales to our ability to measure fluctuations. Figure 6.19 displays the photometry of an IRAC primary calibrator after the final setpoint assertion. To within the measurement error, there is no discernible variation in IRAC photometry.

The absolute offset in the IRAC images also appears stable. Figure 6.20 displays the variation in median value of the routine 12 second skydark measurements taken since the final setpoint assertion. The variation in sky brightness at the North Ecliptic Pole due to the variations in Zodical light has been removed. The remaining variations are extremely small (a few DN) as compared to the photon noise of the lowest backgrounds.
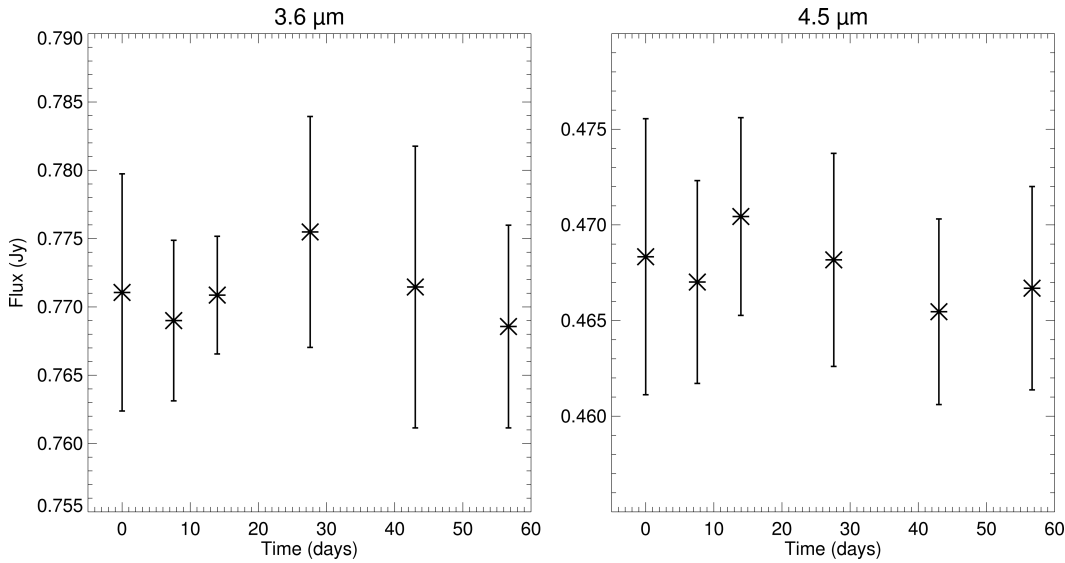
Figure 6.19: Time series of NPM1 +67.0536, one of the IRAC primary calibrators at 3.6 μm (left) and 4.5 μm (right). The asterisks are the stellar photometry averaged over all the data in a single calibration AOR. The error bars are the uncertainty in that mean derived directly from the data.
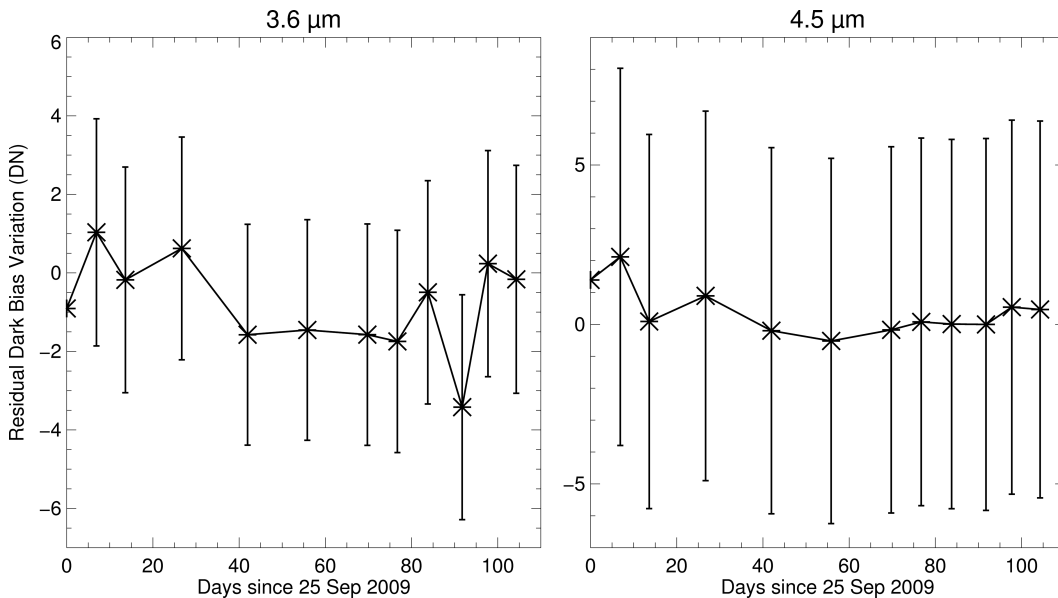
Figure 6.20: Variation with time in the median level of the 12 second warm skydarks at 3.6 μm (left) and 4.5 μm (right). The uncertainty bars plotted are 1 sigma estimates of the photon noise from the North Ecliptic Pole (lowest background region).

6.1.3.3 Hardware

IRAC has no moving parts (other than the shutter, which is not operated in flight). The instrument takes data by staring at the sky and sampling the arrays between resets. IRAC is capable of operating each array independently and/or simultaneously. The standard observing mode is to collect data in both channels simultaneously. The option to collect data in only one channel exists to facilitate

high data rate observations of a point source that would be precluded, due to data volume restrictions, if the off-source field of view data were taken.

6.1.3.3.1   Fowler Sampling

Multiple (Fowler) sampling is used to reduce the effective read noise. This mode of sampling consists of taking *N* non-destructive reads immediately after the reset, and another *N* non-destructive reads near the end of the integration. Differencing is performed in the IRAC electronics to generate one integer value per pixel per exposure to store on the spacecraft and transmit to the ground. The Fowler *N* used for an observation depends on integration time and has been selected to maximize the S/N, based on in-flight performance tests during IWIC.

6.1.3.3.2   Subarray Mode

In subarray mode, only one corner, 32×32 pixels offset by 8 pixels from the edges, is read out from each array. Pixels (9–40, 9–40) of the array are read out (in raw frame coordinates). The subarray pixel size is the same as the full array pixel size (~1.2″). Fowler sampling is performed as in full array mode, but a set of 64 subarray images are generated and tiled into a single 256×256 image before data are sent from IRAC. In subarray mode, Fowler sampling is performed at 0.01 sec intervals. Subarray mode is useful for observing very bright sources and for obtaining high temporal resolution. *Due to data transfer limits images cannot be taken simultaneously in both channels using the 0.02 second frametime*.

6.1.3.3.3   Exposure Time and Frame Time

The relationship between the exposure time (T_{ex}) and frame time is shown in Figure 6.21. The exposure time is defined as the time elapsed between the first pedestal sample and the first signal sample. The Fowler samples are taken consecutively at 0.2-second intervals (0.01 seconds for subarray) in each group (pedestal and signal samples). The frame time (T_f - T_i) is the total time elapsed between resets which could include multiple reads and dead time before and after Fowler sampling. The frames are commanded by specifying the number of Fowler samples for the pedestal (N_F) and the number of "wait ticks" in between the pedestal and signal frames (N_w); then the frame time is $T_F = (2N_F + N_W)\tau$, where τ is the readout time (0.2 sec for full array, 0.01 sec for sub-array mode). The exact number of Fowler samples and wait ticks for each frame time has been optimized during the initial warm checkout. The frame times have remained constant and consistent with their labeling in Spot. The number of Fowler samples has been decreased for the 0.4 and 2.0 second subarray frametimes to maximize the signal-to-noise for photon noise-limited observations. The number of Fowler samples have been increased at 3.6 μm for the 30 and 100 second frametimes to improve signal-to-noise for low background observations.

For very bright sources that saturate the detector during the pedestal reads, the apparent brightness in those pixels will appear to be very small as the pedestal and signal reads difference to near zero. In those cases, the most saturated pixels will

appear as holes in bright sources. The BCD pipeline does not reliably flag these hard saturations, but the cBCD pipeline does attempt to identify them.
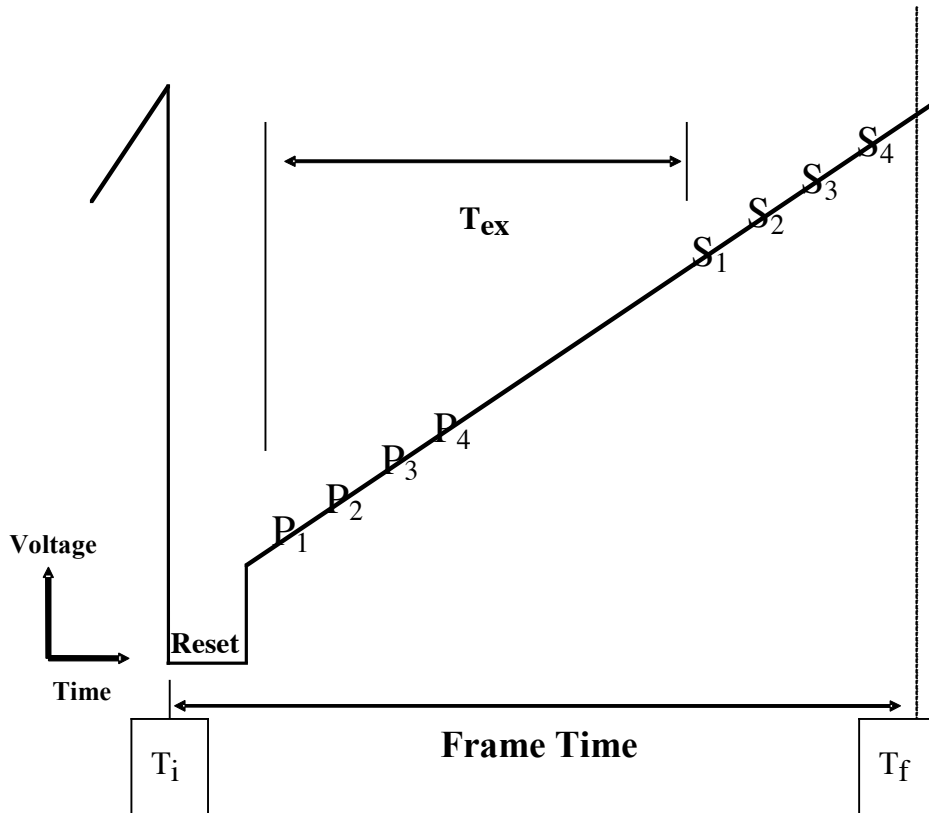
Figure 6.21: Fowler sampling times for one pixel (Fowler *N*=4). The P_n (*n*=1,2,3,4) show the "Pedestal" readouts, and the S_n show the "Signal" readouts. T_{ex} is the effective exposure time, and $T_f - T_i$ is the "frame time," or total time to obtain one IRAC image. The reset part of the sketch is not at the same time and voltage scale as the rest of the figure.

6.1.3.3.4   Calibration Lamps

IRAC contains two types of internal calibration lamps. The transmission calibrator lamps are designed to illuminate all four arrays and provide an internal responsivity measurement. There are two transmission calibrator spheres, each of which contains two lamp elements. To illuminate the arrays, the shutter is closed, a transmission lamp is turned on, and the light from that lamp bounces off a mirror on the back of the shutter. The flood calibrators individually illuminate each detector. The flood calibrators can be controlled individually, and they can be used whether the shutter is open or closed. Neither set of calibration lamps is used on orbit as all calibrations will be performed using observations of the sky.

6.1.3.4 Firmware

The IRAC firmware controls the focal plane assemblies, calibration electronics, and warm electronics boards. Apart from autonomous fault protection, the IRAC firmware responds only to commands sent by the Spitzer Command & Data Handling (C&DH) computer. The C&DH sends setup commands to configure the

electronics, requests for each telemetry packet, and integration commands to generate images. IRAC responds to each command with an acknowledgment. In the case of a command that requests telemetry, the acknowledgment consists of the telemetry packet, which is sent on the low-speed connection between IRAC and the C&DH. There are two types of engineering data: special engineering data, which are collected every 4 sec, and housekeeping data, which are collected every 30 seconds. Special engineering data are used for onboard communication between IRAC and the C&DH, while housekeeping data are used on the ground to monitor instrument performance. A command that generates images from the arrays is acknowledged on the low-speed line, and when the frame is complete, the "data-ready" signal is sent on the high-speed line. The frames (together with their ancillary data) are then transferred one at a time to the C&DH. The rate of transfer is 2 seconds per frame, which limits the data collection rate to a maximum of two frames every 4 seconds for IRAC observations with both arrays.

Autonomous fault protection ensures that none of the monitored voltages or currents enters into a red limit. Fault protection is performed by a "watchdog" daemon that is always running when the instrument is on. The red limits are stored in IRAC memory. If a voltage in the focal plane assembly goes into a red limit, IRAC will turn off the affected focal plane array. (The individual pixel values are not monitored, so a bright astronomical source will not trigger a red limit.) The command sequences will continue to execute; therefore, it is possible for normal completion of an IRAC observing campaign to occur with only one of the two arrays returning data. If the second focal plane assembly has a telemetry datum go into a red limit for 90 seconds, then IRAC will send the C&DH (via the special engineering data on the low-speed line) a request to be turned off. If a telemetry point other than one affecting a single focal plane goes into a red limit, IRAC will also send the C&DH a request to be turned off.

6.2 How to Use IRAC

6.2.1 Performance of the Instrument

6.2.1.1 IRAC Sensitivity

To estimate the sensitivity of IRAC for warm operations, we have used warm calibration data taken after the final setpoint assertion to measure the change in effective throughput from cryogenic operations. For quantities, such as QE and readnoise, which cannot be directly measured in-orbit, we use the required performance based on the design specifications and the results of the 30 K ground tests performed at the University of Rochester (McMurtry et al. 2006) as adjusted to better match in-flight reality. The online tool, SENS-PET (at http://ssc.spitzer.caltech.edu/warmmission/propkit/pet/senspet/), makes this estimation for you and should be used for planning observations. The sensitivity to point sources (expressed as 1-sigma noise in flux density units) is based on the following formula:

$$\sigma = \frac{\sqrt{N_{pix}}}{ST_{ex}f_p}\sqrt{BT_{ex} + (BT_{ex}f_F)^2 + R^2 + DT_{ex}} \,, \qquad (6.1)$$

where the scale factor is

$$S = \frac{Q\eta_T\eta_I A\Delta\lambda}{h\lambda} \,, \qquad (6.2)$$

the background current is

$$B = SI_{bg}f_S\Omega_{pix}f_{ex} \,, \qquad (6.3)$$

and the effective exposure time is

$$T_{ex} = T_F - 0.2N_F \,. \qquad (6.4)$$

In these equations,

the spectral resolving power $\lambda/\Delta\lambda$ is from Table 6.3;
the detector quantum efficiency Q (electrons per photon) is from Table 6.4;
the instrumental throughput η_I is from Table 6.3;
the telescope throughput $\eta_T =[0.889, 0.902]$ for channels 1 and 2, respectively (with Be primary, Al-coated secondary, and 50 nm ice contamination);
the telescope area (including obstruction) A=4636 cm²;
the equivalent number of noise pixels N_{pix} is from Table 6.1 (and defined in section 6.1.2.2);
h is the Planck constant;
I_{bg} is the background surface brightness in MJy/sr;
$f_s = 1.2$ is the stray light contribution to the background;
f_F is the flat-field pixel-to-pixel variance
the dark current D is given in section 6.1.3.2.7;
the read noise R is from Table 6.4;
Ω_{pix} is the pixel solid angle (see Table 6.1);

f_p is the in-flight estimated throughput correction for point sources (Table 6.6);

f_{ex} is the in-flight estimated throughput correction for the background (Table 6.6).

For simplicity as of v12.1 of the SOM, we have updated the scale factor for the warm mission and set the throughput corrections to unity. The value in Table 6.6 will not agree with equation (6.2). The extended source throughput for the InSb arrays was always unity relative to the point source throughput as there is no internal scattering in these arrays. The optical properties of IRAC and the telescope should be almost identical to those in the cryogenic mission. The 30 K lab tests suggest that the read noise will remain close to the cryogenic values; however, the actual read noise (and its variation with temperature) is a property of each individual array. We have increased the read noise slightly (by 5% at 3.6 µm) to account for the slightly poorer performance measured for deep imaging at 3.6 µm. At 4.5 µm, the deep observation sensitivity is unchanged and we use the

cryogenic read noise values. *For both channels, we add the contribution from 1/f noise to the estimated read noise in the following discussion as it is significant at ~30 K operations.*

Table 6.6 lists some useful combinations of IRAC instrument parameters.

Table 6.6: Useful quantities for IRAC sensitivity calculations

Wavelength	3.6 μm	4.5 μm
Conversion factor (electrons/sec)/(MJy/sr)	*29.5*	*25.3*
S (electrons/sec)/(μJy)	*0.84*	*0.73*
Gain (electrons/DN)	3.7	3.7
f_p (throughput correction for point sources)	*1*	*1*
f_{ex} (throughput correction for background)	1	1
Zero magnitude flux densities (Jy)	280.9	179.7

Table 6.7: Background brightness in IRAC wavebands

	3.6 μm	4.5 μm
"low" background model		
$I_\nu f_s$ (MJy/sr)	0.093	0.32
$F_{\nu^{BG}}$ (μJy)	3.2	11
B (elec/sec)	2.7	8.9
"medium" background model		
$I_\nu f_s$ (MJy/sr)	0.15	0.44
$F_{\nu^{BG}}$ (μJy)	5.1	15
B (elec/sec)	*4.4*	*11*
"high" background model		
$I_\nu f_s$ (MJy/sr)	0.52	1.0
$F_{\nu^{BG}}$ (μJy)	18	35
B (elec/sec)	*15*	*26*

Table 6.7 gives the background brightnesses, in useful units, for three nominal observing directions. The low-background model applies near the ecliptic pole; the high-background case is in the ecliptic plane; and the medium-background case is intermediate. The background model includes contributions from emission and scattering from zodiacal dust and emission from Galactic dust. The near-infrared cosmic infrared background radiation is not included because it will be partially resolved by Spitzer.

The quantity f_F is the flat field pixel-to-pixel variance, which depends on the observing strategy. In what follows, we will set f_F =0, which would apply strictly in the case of stable detectors with perfect flat field measurements, and should apply practically for highly-dithered observations. An observation with no dithering will be limited by the correlated noise. The accuracy of a flat field

derived from a single warm observation is measured to be 3.4% and 1.6% in channels 1 and 2, respectively, by comparing flats in several campaigns. Using combined flats ("superskyflat") from the initial warm characterization, the estimated f_r is 0.17% and 0.09% in channels 1 and 2, respectively. Using these values for f_r in equation 6.1, single frames are dominated by background and read noise. When combining multiple frames to generate a mosaic, the background and read noises will average down (as square root of the number of frames), while the flat-field noise will only average down for dithered observations. For N undithered observations on the "medium" background, flat-field noise dominates when the total exposure time, $N \times T_{ex}$, exceeds approximately 210 sec (using individual campaign flats) or 0.8 hrs (using the superskyflat). For dithered observations, the flat-field noise will also average down, and will only be important for the very deep observations of high background fields.

Table 6.8: Fowler numbers for IRAC frames

Frame Time (sec)	Readout Mode	Fowler Number	Wait Ticks
100	Full	32/16	436/468
30	Full	32/16	86/118
12	Full	8	44
6	Full	8	14
2	Full	4	2
2	Subarray	8	184
1.2	HDR	2	2
0.6	HDR	1	1
0.4	Full	1	0
0.4	Subarray	4	32
0.1	Subarray	2	6
0.02	Subarray	1	0

For the frame times used in IRAC operations in flight, Table 6.8 gives the readout mode and Fowler number. For full array readout mode, only the 0.4, 2, 6, 12, 30 and 100 second frame times can be chosen in the IRAC AOT; the 0.6 and 1.2 sec frame times come as part of the "high dynamic range" (HDR) sequences. The frame sets that are taken for each pointing in HDR mode are shown in Table 6.9. The last column, T_h, gives the extra time spent taking the HDR frames. 200 and 400 second frametimes were tested during IWIC but determined to provide no improvement in sensitivity over the 100 second frames and were dropped as they significantly increase the standard calibration time.

Table 6.10 to Table 6.12 and Figure 6.22 to Figure 6.24 present the predicted sensitivities for the two IRAC channels for each of the three background models. The sensitivities in the tables are for point sources extracted from single images (but perfectly flat-fielded). In the figures, the sensitivities are for point sources extracted from coadded images (perfectly registered). We do not include "confusion noise" (due to overlapping images of distant galaxies or other sources

of background structure) in the sensitivity estimates. The detectors are assumed to perform according to the IRAC detector measurements of read noise, dark current, and quantum efficiency in cryogenic observations with a slight (5%) increase in read noise at 3.6 μm, 1/f noise for both channels, and the in-flight measured throughput for warm operations. The first 7 rows in each table show the sensitivity for full-array readouts, and the last four rows show the sensitivity for subarray readouts.

Table 6.9: IRAC High-Dynamic-Range (HDR) framesets

Long Frame Time	List of frames taken	T_h (sec)
100	0.6, 12, 100	15
30	1.2, 30	3
12	0.6, 12	2
6	0.6, 6	2
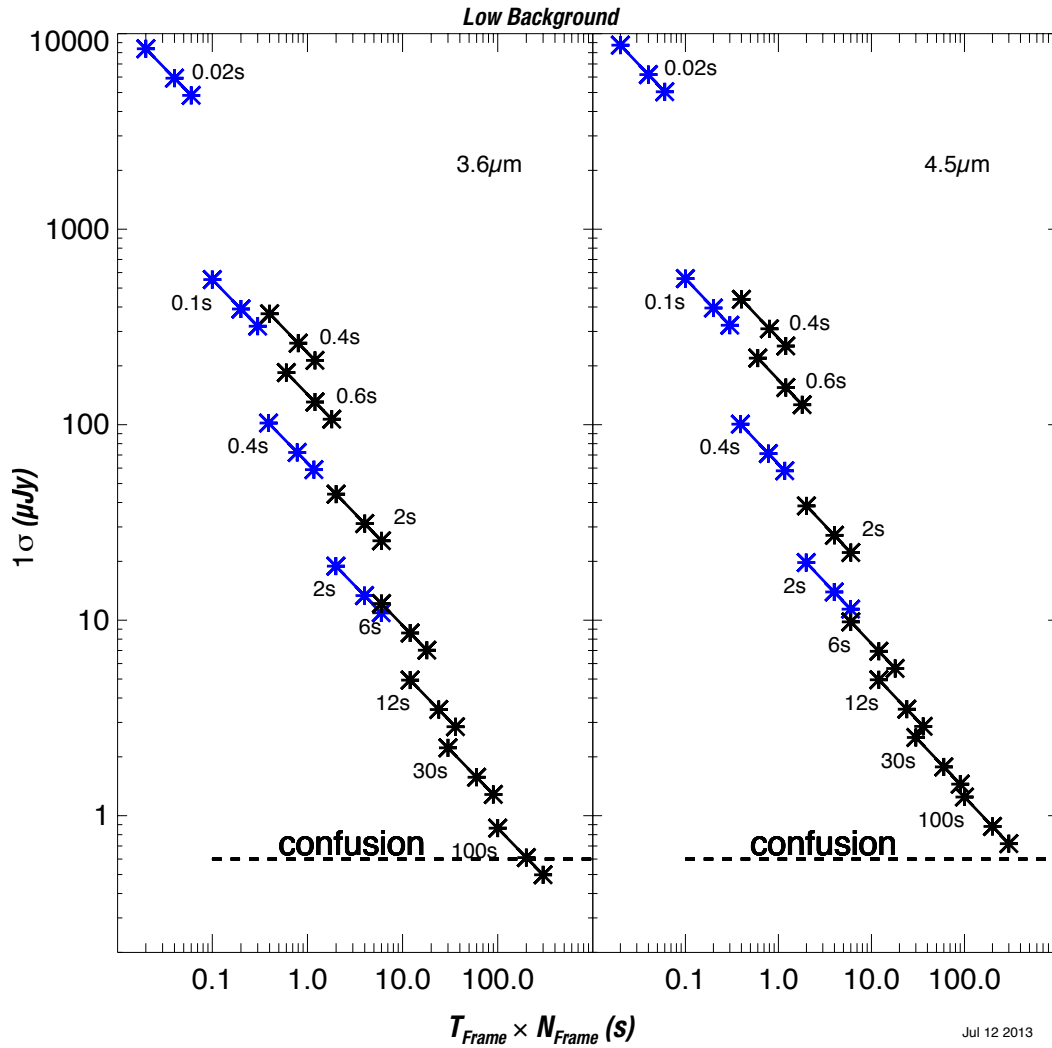
Figure 6.22: IRAC point source sensitivity as a function of frame time, for low background. Full array frametimes are in black, subarray frametimes are in blue. To convert to MJy/sr, see equation 6.8. The three asterisks for a given frame are for 1, 2 and 3 repeats (or dithers)

of that frame time.

Figure 6.22, Figure 6.23 and Figure 6.24 show the point source sensitivity as a function of integration time for each background model. The "time" axes in the plots represent the frame time for the images, which does not include time for moving the telescope. The IRAC full array frame times shown are 0.4, 0.6, 2, 6, 12, 30 and 100 seconds. The IRAC subarray frame times shown are 0.02, 0.1, 0.4 and 2 seconds. The subarray frame times are more sensitive than their full array counterparts as they have both higher Fowler sampling to reduce read noise and longer exposure times due to the higher rate at which the subarray frames are sampled (0.01 seconds compared to 0.2 second for the full array). Other times plotted in Figure 6.22 are multiple exposures (2× and 3×) of those fixed times.

Table 6.10: IRAC point-source sensitivity, low background (1σ, μJy).

Frame Time (sec)	3.6 μm	4.5 μm
100	0.86	1.25
30	2.2	2.5
12	4.9	5.0
6	12.2	9.8
2	44	39
0.6[a]	185	222
0.4	369	443
2[b]	19	21
0.4[b]	102	102
0.1[b]	552	566
0.02[b]	8374	8447

Table 6.11: IRAC point-source sensitivity, medium background (1σ, μJy).

Frame Time (sec)	3.6 μm	4.5 μm
100	1.0	1.44
30	2.5	2.9
12	5.2	5.5
6	12.4	10.4
2	4	40
0.6[a]	185	222
0.4	370	443
2[b]	19	21
0.4[b]	102	103
0.1[b]	553	567
0.02[b]	8374	8447

Table 6.12: IRAC point-source sensitivity, high background (1σ, μJy)

Frame Time (sec)	3.6 μm	4.5 μm
100	1.48	2.16
30	3.3	4.2

12	*6.1*	7.4
6	*13.4*	12.8
2	*45*	42
0.6[a]	*186*	224
0.4	*370*	445
2[b]	21	24
0.4[b]	*104*	106
0.1[b]	555	569
0.02[b]	*8375*	8848

[a] available only in high-dynamic-range mode.

[b] subarray mode (set of 64 32×32 images). Sensitivity is per frame, not per 64-frame coadd.

For bright sources, shot noise due to counting statistics in electrons from the source itself becomes the dominant source of noise. We can estimate the total noise by adding the shot noise in quadrature, so that

$$\sigma_{tot} = \sigma\sqrt{(1+(F/F_b))} \qquad (6.5)$$

where σ is the noise from equation 6.1 and

$$F_b = f_p ST_{ex}\sigma^2. \qquad (6.6)$$

In the bright source limit, $F \gg F_b$, the signal-to-noise ratio becomes

$$S/N = \sqrt{f_p ST_{ex}F}. \qquad (6.7)$$

If the exposure time is in seconds and the source flux density is in μJy, then for IRAC channels 1 and 2, respectively, S/N is 0.86 and 0.85 times $\sqrt{T_{ex}F}$. Thus, for example, to design an experiment that requires a $S/N=1000$, for a star with a brightness of 1 mJy at 3.6 μm, we require an exposure time of 1352 sec. This could be achieved, for example, using 14 frames of 100 sec, because the star is below the saturation limit for 100 sec frames. Note however the systematics discussed in Sections 6.1.3.2.4-5.

In Figures 6.22-6.24 0.6 μJy is the confusion limit predicted by Franceschini et al. (1991, A&AS, 89, 285). This does not represent a hard sensitivity limit, but rather indicates where source confusion affects reliability of source extractions for low background regions. Data from IOC/SV show noise decreasing as $\sqrt{N}$ to 0.25 μJy (channels 1 and 2). A corresponding deep observation has not been done in the warm mission characterization, but ample warm deep data exists from the Exploration Science programs. Moderately deep source counts indicate that a source density equivalent to 36 beams/source is reached at 20.5 mag, or 1.8 and 1.1 microJy at 3.6 and 4.5 μm, respectively (Fazio et al. 2004, ApJS, 154, 10). The confusion estimates by Franceschini et al. and Fazio et al. are for low

background, extragalactic observations only. For observations of higher background or more "cluttered" regions (such as the Galactic Plane) the confusion noise will be much more significant. We recommend that observers examine the archive for available public data from regions similar to their targets to determine appropriate measures of confusion noise.
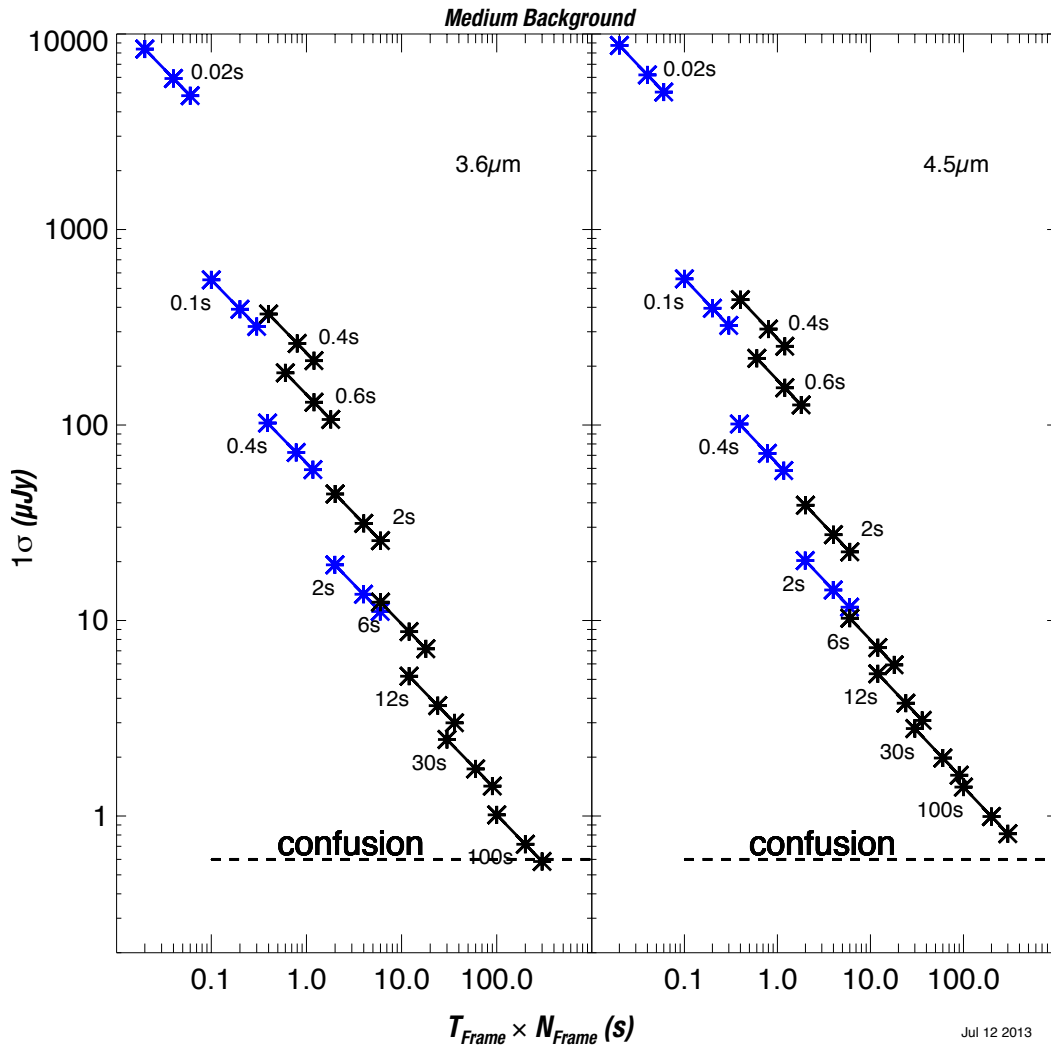
Figure 6.23: IRAC point source sensitivity as a function of frame time, for medium background. Full array frametimes are in black, subarray frametimes are in blue. To convert to MJy/sr, see equation 6.8. The three asterisks for a given frame are for 1, 2 and 3 repeats (or dithers) of that frame time.

For diffuse emission, the surface brightness sensitivity per pixel (in MJy/sr) is

$$\frac{0.03 f_p}{f_{ex}\sqrt{N_{pix}}} \times \text{ the point source sensitivity [in } \mu\text{Jy].} \tag{6.8}$$

(The noise pixels, N_{pix}, are defined in section 6.1.2.2.)

6.2.1.2 IRAC Saturation Limits

The saturation limit for IRAC is calculated as follows. Using the same notation as earlier in this section,
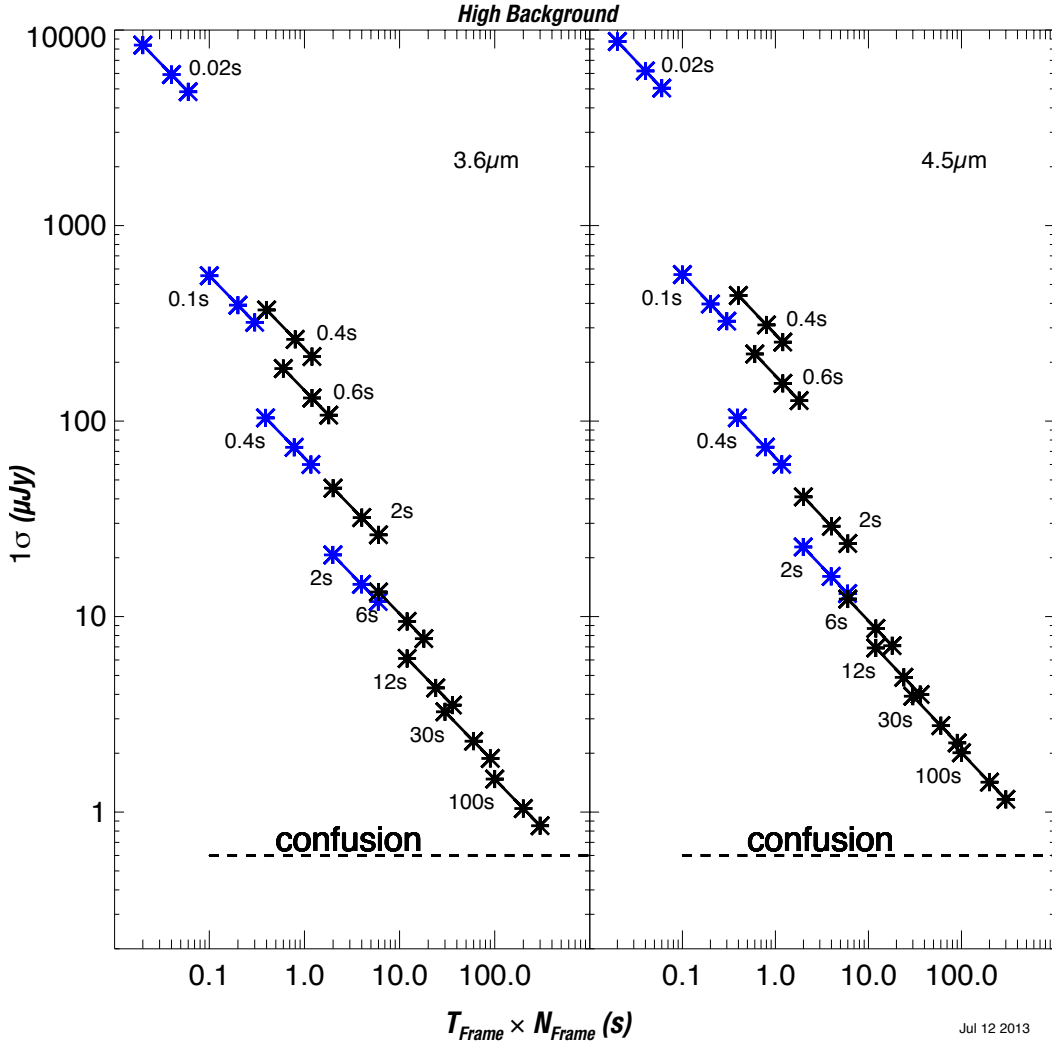
Figure 6.24: IRAC point source sensitivity as a function of frame time, for high background. Full array frametimes are in black, subarray frametimes are in blue. To convert to MJy/sr, see equation 6.8. The three asterisks for a given frame are for 1, 2 and 3 repeats (or dithers) of that frame time.

$$F_{sat} = \frac{Wf_w - BT_F f_{ex}}{ST_F f_{cen} f_p} \quad (6.9)$$

where W is the well depth (Table 6.4), f_w =0.9 is the fraction of the well depth to which we can linearize the intensities, and f_{cen} is the fraction of the source flux falling onto the central pixel (Table 6.1). For warm data, Wf_w = 30,000 DN as discussed in Section 6.1.3.2.1. Table 6.13 shows the point source saturation limits of IRAC at each frame time. If you are observing an extremely bright piece of

sky, such as an H II region, then the saturation limit is lower; you should include your sky brightness in the background B; for the saturation table, we used the "medium" diffuse sky background from Table 6.7. Note that the saturation value is conservatively computed from the worst-case in which the PSF is directly centered on a pixel. While users may find that in their actual data the saturation value of point sources is higher, the values given in Table 6.13 should be used for planning purposes.

To apply Table 6.13 for extended sources,

$$I_{sat}^{ext} = 28.6 \times f_{cen} F_{sat} \quad \text{for compact (diameter} < 30'') \text{ sources} \qquad (6.10)$$

$$I_{sat}^{ext} = 28.6 \times \frac{f_{cen} f_p}{f_{ex}} F_{sat} \quad \text{for more extended sources,}$$

where I_{sat}^{ext} is the total surface brightness (in MJy/sr) at which a pixel saturates; f_p, f_{cen}, and f_{ex} are as defined above, and F_{sat} is the saturating point source flux density for (in mJy) from Table 6.13, appropriate for the channel and integration time.

Table 6.13: Maximum brightness of an unsaturated point source (in mJy), as a function of IRAC frame time.

Frame Time (sec)	3.6 um	4.5 μm
100	2.8	3.5
30	10	12
12	25	30
6	50	60
2	160	200
0.6	500-700	600-900
0.4	900-1400	1000-1700
2*	150	180
0.4*	700	900
0.1*	3000	3700
0.02*	20000-26000	28000-35000

*subarray mode

If the bright extended source extends well beyond the 5´×5´ FOV, then the saturation brightness is *lower* by the factor f_s due to the stray light contribution.

Use Table 6.13, in conjunction with Table 6.10 through Table 6.12, to determine the dynamic range of an individual IRAC frame. If bright point sources (e.g., IRAS sources) are in your field of view, and you want to measure their fluxes as well as those of fainter sources, then you can use the "high dynamic range" (HDR) option. With this option, shorter frames will be taken in addition to your specified frame time.

6.2.2 Observing Time Estimation

The Spot tool provides fast and accurate estimates of observing time for IRAC. To optimize AORs, however, it may be useful to bear the following information in mind.

Each AOR duration includes a flat 180 sec slew overhead to the initial position (an additional 300 sec overhead is charged for moving targets). Check the current Call for Proposals for any updates to the AOR overheads. Command overheads between exposure repeats are very short (1-2 seconds), except for the 2-sec full array and 0.02-sec subarray frame times, in which a delay is put in to ensure that the data can be transferred from the IRAC buffer to the spacecraft (for which the maximum rate is 4 sec per 2 full array frames). For staring mode observations with 2-second frame time, the 2-second subarray mode can be used to reduce overheads at the cost of limiting the field of view.

Slew durations and allowed settle times are a function of slew length. Slews between points in dither patterns, maps or cluster targets (apart from those between cluster targets specified by celestial coordinates) are carried out under gyro control in low-rate mode. Each slew and settle has a command overhead of approximately 2 sec. Slews of 100" or less have a settle time of 4 sec; slews between 100" and 300", 5 sec; and, slews of more than 300", 6 sec. The slew times themselves are a function of the slew length. Slews from 0" to 100" take 0-4.2 seconds (excluding overhead), and those from 100" to 300" take 4.2-8.4 seconds. Slews of a degree take 54 sec. For cluster targets specified by celestial coordinates, a different slew mode is used, with larger command overheads, but with the ability to switch to high-rate mode for longer slews. Overall, slews of >0.5 deg are faster using this mode. AORs with widely spaced cluster targets will therefore be more efficient if RA, Dec positions are given for the cluster points.

Observing strategy is a series of compromises between sensitivity, redundant coverage, and wall-clock time. We recommend a given sky position be visited a minimum of three times (and preferably, five), in order to mitigate the effects of radiation hits and bad pixels. We also recommend that dithering be performed to mitigate the effects of pixel-to-pixel gain variations. Repeat observations at a given sky position should sample different parts of the array, either by using a medium or large dither scale, and/or by making approximately half-array offsets between map positions or between AORs covering the same part of the sky. This technique also ensures good straylight removal. For more details on recommended observing strategies, see section 6.2.4.

6.2.3 Astronomical Observation Template (AOT) Description

The IRAC AOT consists of a (optional) dither pattern superposed on a (optional) rectangular-grid raster. In this section, we describe the manner in which an IRAC AOR is specified by an observer, and the activities that the spacecraft will perform when the specified AOR is executed. Figure 6.25 shows an example of

an IRAC Post-Cryo Mapping AOT dialog box in Spot. For more information, please see the Spot User's Guide.
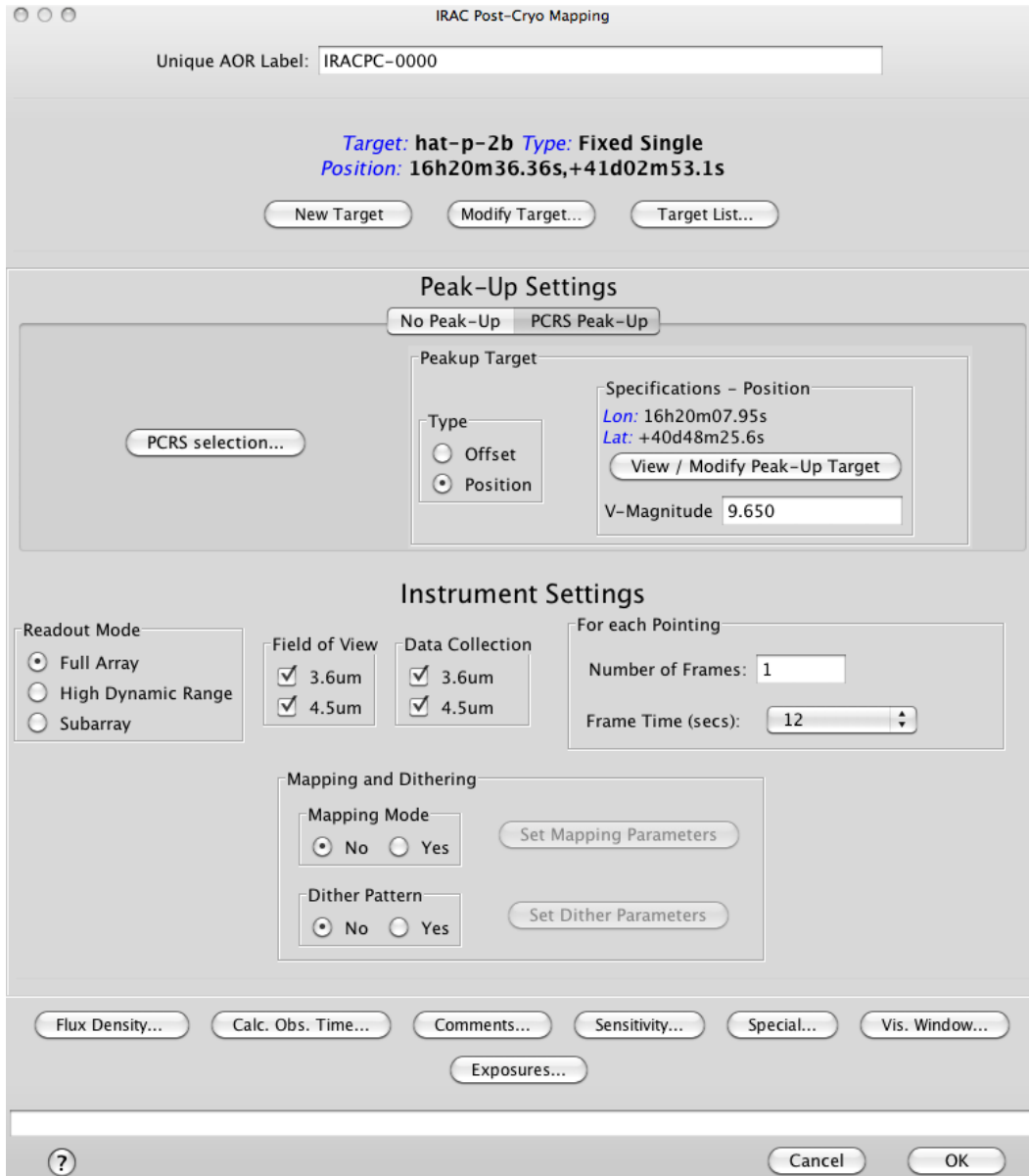
Figure 6.25: IRAC Post-Cryo Mapping AOT dialog in Spot.

6.2.3.1 Readout Modes and Frame Times

In full-array readout mode, there are eight selectable frame times: 0.4, 2, 6, 12, 30, 100, 200, and 400 seconds [Note: 200 and 400 seconds are not supported in the warm mission.]. You should select the frame time that will allow you to reach your target sensitivity while allowing for rejection of cosmic rays, after accumulating all repeat observations of the same piece of sky (by dithers, frame repeats, map overlaps, and map cycles). The cosmic ray rate is about one hit per array per second (see Section 6.1.3.2.9).

It is possible that bright sources will saturate the array at the frame time you choose to meet your sensitivity goal. To allow sensitive observations without losing dynamic range, we provide a "high dynamic range" (HDR) option. When this option is selected, the IRAC AOT will take extra frames, with frame times shorter than your selected frame time. The HDR frame times are given in Table 6.9. You can use the shorter frames to measure the brightness of the brighter sources and the longer frames to reach your sensitivity goal. No spacecraft repositioning is done between frames, and the frames always go from shortest to longest. If you elect to perform repeats using the "Number of Frames" entry box on the AOT form, then only the longest frame time is repeated. However, if you elect to perform dithers, then the entire frame set is repeated at each dither position. Independent of the HDR option, taking frame repeats is recommended only in the case of time series measurements. This is because the first frame effect is worse with repeats, and image artifact rejection is best accomplished with dithers. The repeated frames will need additional processing to remove residual bias patterns.

For very bright sources, which would saturate the array in full-array readout mode, you can select subarray mode. In this mode, only a small 32×32 pixel portion of the array is read out, so the field of view is only 38″×38″. Mapping is not allowed in subarray mode. However, small maps can be made using a cluster target. Therefore, use subarray mode only for observations of single, very bright targets. Advantages of the subarray mode, in addition to the ability to observe sources that would saturate full-array readouts, are that sets of 64 frames are taken back-to-back, enabling better temporal resolution and decreasing the data volume (which means that rapid sampling can continue for longer periods). Also, because of the more rapid (0.01 sec) sampling, more Fowler samples are taken, resulting in lower readout noise per frame compared to full array mode for the same frame time. In subarray readout mode, there are 4 selectable frame times: 0.02, 0.1, 0.4 and 2 sec. For one commanded image in subarray mode, a set of 64 Fowler-sampled frames are taken in succession, so that each time an image is commanded in subarray mode, a "cube" of 64×32×32 pixel images is generated. This means that the durations of a single repeat at each of the four subarray frame times are 1.28, 6.4, 25.6 or 128 sec, respectively. The IRAC AOT moves the telescope to point to the subarray region of each requested channel at the target in turn. For the 0.02 sec frame time, data rate limitations allow only data in the channel actually pointing at the target to be taken. For the 0.1 sec, 0.4 sec and 2 sec frame times, data are taken in both channels at each pointing position, although only one channel at a time will point at the target.

6.2.3.2 PCRS Peak-Up Option

The PCRS peak-up option is designed to facilitate high precision (<1000 parts per million) relative photometry and will not generally benefit other observations. If you are not making observations that require very high precision photometry, we recommend ignoring this option as it introduces an overhead of 2-5 minutes into the observation.

The PCRS peak-up option uses the spacecraft's optical pointing system for peak-up. This option, used frequently in the cryogenic mission with IRS, provides enhanced accuracy (down to about 0.1 pixels) in positioning a target on a science instrument FOV default pixel (full array or subarray), and can improve greatly the photometric precision in staring mode observations (e.g., exoplanet observations) by reducing the range of the pixel phase effect (see Section 6.1.3.2.5). The pixel phase effect is very well known and minimal in a sweet spot region approximately ¼ pixels on a side near the center of the subarray in channels 1 and 2.

The PCRS can measure the centroids of stars to an accuracy of better than 0.14" (1 sigma radial). For PCRS peak-up to succeed, the peak-up target must be in the magnitude range 7.0 mag < V < 12.5 mag, and there should be no stars brighter than 13.0 V mag within 40 arcseconds of the peak-up target. You have the choice of peaking up on either the science target itself or an offset star. If the visual magnitude of your target is between 7 and 12.5, then we recommend using the target itself. Otherwise you can either use the "PCRS selection" button in Spot to choose a nearby star from the PCRS Guide Star Catalog, which contains a carefully selected subset of stars from the Tycho catalog, or specify your own offset star. If you are using an offset target, we recommend that you choose the closest possible star to your science
target (but no further than 30 arcminutes away), to optimize the slew from the offset star on PCRS to the science target on IRAC. Make sure that the relative astrometric positions of your peak-up star and your science target are as precisely known as possible, as the efficacy of the peak-up using the guide star method depends directly on the knowledge of the angular offset between the guide star and the target. See the IRAC PCRS Peak-UP web page at http://irsa.ipac.caltech.edu/data/SPITZER/docs/irac/pcrs_obs.shtml for how to set the target type for a peak-up AOR and how to set the offsets to use the sweet spots. Remember especially to select Offset Coordinates "Array" (Row/Perp, Col/Para) when specifying the cluster target, and to check "Observe the offsets only" when specifying the cluster target. Offsets both for subarray and full array observations are available. Remember to use the staring mode ("Mapping Mode" = No and "Dither Pattern" = No) and use only one FOV per AOR.

In order to mitigate against a drift caused by a thermal-mechanical response to changes in the pitch angle of the spacecraft with respect to the Sun from the previous spacecraft attitude to the target pointing, observers should add a 30 minute duration staring mode AOR at the position of their target before their long staring mode AOR with PCRS peak-up. This "leading" 30 minute AOR should also have PCRS peak-up configured and it should use the same frame time as the long staring mode AOR(s) following it. If multiple AORs are to be used, for example, to observe a target for 40 hours, just one leading 30 minute AOR is needed, placed first in the chain constraint with all the other AORs that span 40 hours.

One important scientific benefit of the PCRS peak-up is the ability to reposition a target onto the same spot on a pixel during a long stare, thus enhancing the precision of time-domain measurements. Typically, the Spitzer pointing system drifts systematically by approximately 0.35" per day (this is in addition to any potential short-term drift due to change in pitch angle). This means that in about 12 hours a target placed halfway between the center and the edge of the well-characterized 0.25-pixel "sweet spot" of the Channel 1 or Channel 2 subarray has a good chance of drifting out of the region of minimal response variation. To mitigate this problem, we recommend breaking up all staring observations that are longer than 12 hrs into separate AORs lasting 12 hrs or less, all of which should have PCRS peak-up. The AORs should be identical copies of each other, with the exception being that the Number of Frames should be changed to make each AOR shorter than 12 hrs and obtain the total duration as desired. They should also be linked together using Chain constraints, to ensure that they are scheduled as a single unit. We do not recommend peak-ups more often than about 10 hours, however, as the reacquisition error using peak-up is of order 0.1 arcseconds, which is comparable to or in excess of the expected pointing drift for observations shorter than about 10 hours.

6.2.3.3 Map Grid Definition

If you select "No mapping," then your map grid will consist of a single position at the coordinates specified in the Target section of the AOT. (Dithering can still be applied even if the "No mapping" option is selected.) With "No mapping" selected, if you select both fields of view, first the 4.5 μm field of view will be pointed at your target, then the telescope will be repositioned so that the 3.6 μm field of view is pointed at your target. In both cases, data from both arrays are collected, whether they are pointed at your target or not unless you choose to take data in only one channel (see section 6.2.3.5).

Figure 6.26: Map grid dialog box in Spot.

If you select "Yes" under "mapping mode," then you will be presented with a dialog box, shown in Figure 6.26, wherein you specify the rectangular map grid. The map grid may be specified in either "array" or "celestial" coordinates. If you

choose array coordinates, then the map grid will be aligned with the edges of the array, such that the map rows and columns will correspond to rows and columns of the array. Specifically, a "column" will be along a line of constant solar elongation, and a "row" will be along an ecliptic parallel [line of constant ecliptic latitude]. In the reference frame of a BCD, columns are in the negative y-direction and rows are in the positive x-direction. It is worth noting that the two IRAC fields of view are at approximately constant solar elongation, so that a map with 1 column and several rows will make a strip along the direction of the separation between the two fields of view and will yield 2-array coverage along part of the strip (if it is long enough). If you select celestial coordinates, then the rows and columns will correspond to J2000 Right Ascension and Declination. You may specify a position angle, degrees E of N, to orient the raster in Equatorial coordinates. Specifically, if the position angle is zero, a "column" will be along a line of constant Right Ascension, and a "row" will be along a parallel (line of constant Declination). This option allows two separate AORs, both in celestial coordinates, to have a fully specified location of map grids such that they can be made adjacent to one another independent of observing date (but see below, regarding gaps).

The most important advantage of mapping in array coordinates is that the sky coverage can be custom-tailored and the coverage precisely defined, independent of the date when the observation is scheduled. In general, we do not recommend using celestial map grids. A celestial map grid can yield highly non-uniform coverage (including gaps), unless the individual pointings are spaced closely together. There are cases in which a celestial grid is preferred, specifically for mapping a highly elongated region. We recommend that all observers considering a celestial grid inspect their survey coverage for a range of possible spacecraft roll angles. Overlaying your AORs on a sky image in Spot can do this. The roll angle itself can be obtained in the Target Entry/Visibility section of Spot, by choosing an observing date when the target is visible. The roll angle is essentially fixed if the source has an absolute ecliptic latitude smaller than 10° (when the total roll angle freedom as a function of observing date is less than 8°). Figure 6.27 shows two examples of 3×3 map grids, one in array coordinates and the other in celestial coordinates. For the celestial grid, the spacecraft roll at the time of observation had a position angle of 30° east of north. Not only are there large gaps in the celestial grid, but the coverage is non-uniform in the observed region as well. To eliminate the gaps, you could tighten the spacing of the map grid positions (sacrificing some area covered or some dithering), or you could fix the date of the observation such that the roll angle will be equal to your desired celestial position angle. But be aware that away from the ecliptic poles, not all position angles are available over all positions on the sky.
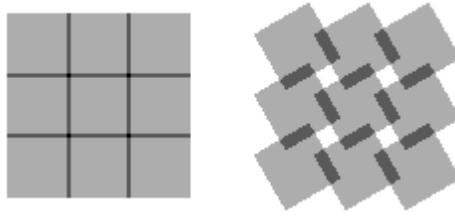
Figure 6.27: Simulated IRAC coverage for a map in array coordinates (left) and celestial coordinates (right).

For large maps, which take more than the 24-hour maximum AOR duration, you will have to break the observation into multiple AORs. For most large maps, multiple AORs will have to be used even if a single AOR would be below the maximum duration, as there is also a limit to the number of commands in a single observation request. This is a hard limit imposed by the spacecraft C+DH system. Spot will display an error message if you create a request with more instructions than the limit and your observation will have to be done with multiple AORs. If your map grid is oriented in array coordinates, then you will not know the boundaries of each AOR precisely, unless you specify the observing date. Therefore, care must be taken in planning and managing large observations. If the large observation can be broken into separate rectangular map grids, they can be specified in individual AORs using the same central target position, by specifying a "Map center offset" (see Figure 6.26). An example of how to use the map center offsets is given in the Examples section below. In general, to calculate observing times for a large map, generate an AOR that covers a fundamental "tile" for your project, and multiply the observing time of that tile by the number of tiles needed to cover your desired area. Allow for some overlap between tiles, both for calibration and for inefficiencies in the way tiles mesh together.

6.2.3.4 Selecting the IRAC Field of View

As described above (see also Figure 2.1 and Figure 4.5), the two IRAC arrays are fed by two entrance apertures, which are located one above the other in the focal plane with a gap of about 1.5′. For subarray mode, there are two separate fields of view, corresponding to the subarray section of each of the two arrays. In subarray mode, you select one or both of the two subarray fields of view, and the dither pattern will be performed with each of the selected fields of view pointed at the target.

When making an IRAC map (not allowed in subarray readout mode; note however, that you can make small maps of bright sources in subarray mode using a cluster target), you can use the field of view checkboxes to control the way the IRAC AOT performs the map. Regardless of your selection, data will be collected with both arrays unless you deselect data collection in an array (which is generally not recommended). If you select the 3.6 μm field of view as primary, then your specified map will be performed with the 3.6 μm field of view. A nearby portion of sky (significantly overlapping for large maps) will be covered

with the other, 4.5 μm field of view. This is illustrated in Figure Figure 6.28, for which the sky coverage of a 3 column × 5 row map is shown. If you select the 3.6 micron field of view, the target position will be centered in the left-hand panel. The serendipitous sky coverage by the 4.5 micron field of view is shown in the center panel, and the sky covered by both fields of view is shown in the right-hand panel.
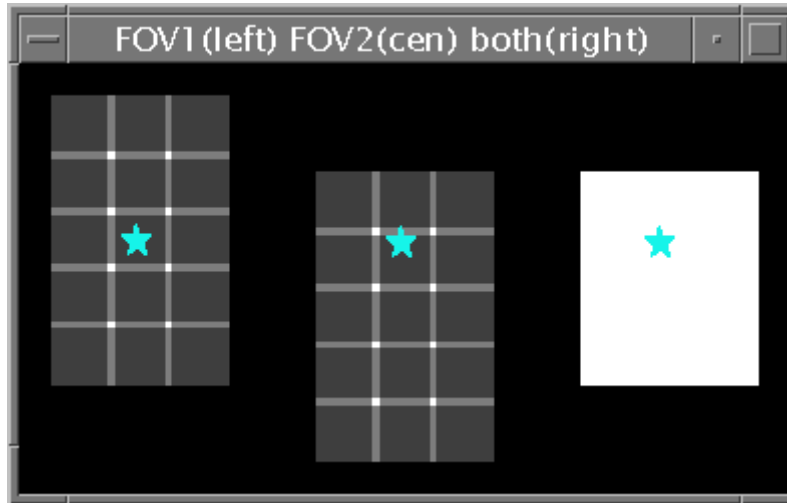
Figure 6.28: Schematic diagram of sky covered by the two IRAC fields of view during a 3×5 map. On the left is the sky covered by the 3.6 μm field of view; in the middle is the sky covered by the 4.5 μm field of view; and on the right is the sky covered by both fields of view. In the left and center panels, lighter shades indicate a higher depth of coverage, while darker shades indicate less coverage. The right-hand panel is white when both fields of view cover the sky.

Selecting both fields of view changes the way the pointing is commanded. If you have selected a "celestial coordinates" map, the AOT performs your map grid, once with the 4.5 μm field of view centered on each map grid position, then again with the 3.6 μm field of view centered on each map grid position. This may lead to significant redundancy (and cost in observing time) for large maps. You may prefer to choose a single field of view as your primary field of view, and make your celestial map grid large enough that both fields of view will cover your desired area, regardless of the scheduled date of observation. High-precision photometric monitoring measurements using PCRS peakup (section 6.2.3.2) should always observe only a single field of view per AOR. This is because offsetting between arrays adds significant errors to the pointing, eliminating the benefits of the PCRS peakup.

As of Spot version 19.0, the mapping field of view (the FOV centered between the two arrays) can be selected when using all target types and mapping modes except the subarray mode. Previously, the mapping field of view was used only for a single target and mapping in array coordinates. The intent of this change is to provide observers with the additional flexibility of using the mapping field of view in designing customized map patterns. To use the mapping FOV, deselect both arrays in the field of view dialog. In previous versions of Spot, at least one

field of view needed to be selected. The mapping FOV is still used when mapping in array coordinates with both fields of view selected. See examples at http://ssc.spitzer.caltech.edu/warmmission/propkit/spot/s19/ and remember to always view an animation of your observation in Spot after you have specified it to make sure it does what you intended to do.

If you have selected "array coordinates" and "both" fields of view, then the map is centered on the point directly between the two IRAC fields of view. If your map is 1 row by 1 column, the map center will not be imaged by either of the IRAC arrays. Therefore, if you want the same desired area to be covered by both arrays, you will have to increase the number of rows in the map. For example, suppose that you want to cover an area with a diameter of D, and you want the spacing between map grid positions to be δ. The number of columns in your map is just $1+[(D\text{-}A)/\delta]$. One IRAC field of view size is $A=5.2'$ and the gap between the two fields of view is $G=1.5'$. The number of rows required to cover this area with both fields of view is therefore $1+(D+G)/\delta$. (You should round the number of rows and columns up for any fraction, or else some area at the top and bottom of the desired region will not be covered by both arrays.) For example, if your region has diameter $14'$ and you are using a $280''$ map grid spacing, then your map should have 3 columns and 5 rows.

There are special cases for which observers should be careful with their choice of field of view. For example, if you want to make a sparse map, with spacing greater than the array size ($\delta > A$), then each of the 3 choices of field-of-view (3.6 μm, 4.5 μm, or both) will yield a significantly different map. To make a sparse map with both fields of view, ensuring that both arrays cover the exact same sky, you should split the observation into two AORs, one per field of view. Also, for a very small map ($\delta \times M \sim A$, where M is the number of rows), be sure to make the map large enough that both fields of view will cover the target. If the number of extra rows required using the equations above is excessive, you may prefer to create two AORs, one per field of view.

6.2.3.5 Selecting Arrays to Take Data With

A new feature of the warm IRAC AOT is the ability to turn off data taking in one of the channels. By default, observations take data in both channels. This new mode is intended for staring observations of a target in a single field of view (such as exoplanet transits), where the off-field does not contain useful data and when the data volume of the observation is high. This option should only be selected when instructed by the SSC to reduce the data volume of a given observation.

6.2.3.6 Dither Patterns

Dithering performs a number of functions. It allows the identification and removal of small-scale detector defects such as bad pixels, it reduces noise from the effects of pixel-to-pixel errors in the flat field (in fact for large numbers of dithers a flat field can be constructed from the data themselves), and sub-pixel

dithering can be used to recover some level of information which would otherwise be lost through undersampling of the array. These considerations drive the optimization of the dither patterns in different ways; there is thus no "ideal" dither pattern. For the standard IRAC dither patterns, we have chosen designs that we think should satisfy most requirements. However, the option always remains for observers to define their own dither patterns using array offsets in cluster mode.

For the full-array mode there are two types of dither patterns available. Five such patterns are fixed patterns, which are performed identically at each mapping position. Conversely, the cycling pattern is a set of dither positions (also referred to as "points"), a different subset of which is performed at each map grid position.

Different patterns are available in subarray mode, as the angular scales covered by the arrays are quite different. Two fixed patterns are available for this mode.

Table 6.14: Characteristics of the full array dither patterns

Dither Pattern	Scale	Max dither (pixels from (0,0))	Median dither separation (pixels)	Sub-pixel dither pattern
Cycling	Small	11	10.5	½ pixel
	Medium	119	53	½ pixel
	Large	161	97	½ pixel
5-point Gaussian	Small	26	23	½ pixel
	Medium	52	46	½ pixel
	Large	105	92	½ pixel
9-point random	Small	16	14	1/3 pixel
	Medium	34	28	1/3 pixel
	Large	69	59	1/3 pixel
12-point Reuleaux	Small	13	15	½ pixel
	Medium	27	30	½ pixel
	Large	55	59	½ pixel
16-point spiral	Small	16	12	¼ pixel
	Medium	32	23	¼ pixel
	Large	64	45	¼ pixel
36-point Reuleaux	Small	17	19	¼ pixel
	Medium	34	39	¼ pixel
	Large	67	78	¼ pixel

6.2.3.6.1   Dithering Strategies

The dithering strategy adopted for a particular observation will depend on the type of object and the required depth and resolution of the final image. The characteristics of the available dither patterns are given in Table 6.14. The Reuleaux Triangle patterns were designed with the idea of optimizing the Figure of Merit of Arendt, Fixsen, & Moseley (2000, Astrophysical Journal, 536, 500).

They thus sample a wide range of spatial frequencies in a fairly uniform manner, and are well suited to the Fixsen least-squares flat fielding technique. The 9-point and 16-point patterns were designed to be the optimum size for 1/3 and ¼ sub-pixel dithering, respectively. The "random 9" pattern is based on a spatially uniform random distribution. The "spiral 16" pattern was designed by R. Arendt to provide a pattern which is both compact and has a good figure of merit for self-calibration.
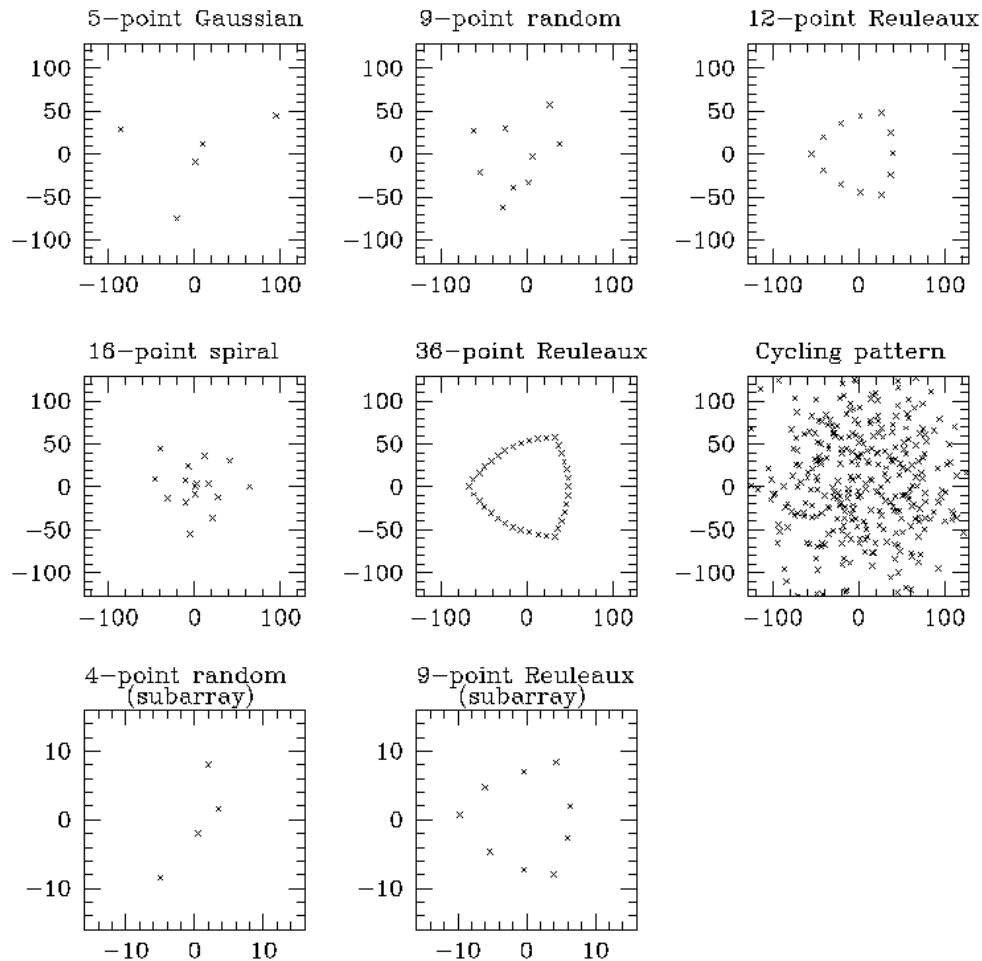
Figure 6.29: IRAC dither patterns for the "large" scale factor.

The cycling patterns are designed for AORs having many mapping/dithering observations, but may also be of more general use. The large and medium patterns are Gaussian distributions (with dithers >128 pixels removed). The small pattern is specifically designed for mapping, where only a few dithers are taken at each map position. It is also based on a Gaussian distribution, but the center is downweighted to decrease the fraction of very small dithers in the pattern, and it is truncated at a maximum dither of 11 pixels to ensure that maps with up to 280″ spacing have no holes, even if there is only one dither per map point. All the patterns are constrained to have no pair of dithers closer than three pixels in any

run of four consecutive points. To use these patterns, you specify the number of dithers to perform at each map grid position and the starting point in the cycling dither table. You may specify a single dither at each map grid position. This will result in a single observation at each map grid position, but the location of that observation will be slightly shifted from the rectangular grid. Such a "fuzzy" grid should allow a better flat field determination and reduce jail-bar and other pattern noise in the resulting mosaic. The cycling dither table will wrap around once the final (311th) element is reached. For example, selecting a starting point of 310 and three dithers per map, the first grid position will use points 310, 311 and 1 from the table, the second 2, 3 and 4 and so on. This pattern has a ½ sub-pixel sampling pattern superposed on it, starting with point 1 and repeating continuously every four points (at point 311, the final cycle is simply truncated early, thus patterns which wrap around the table will miss a sub-pixel dither point).

The five-point Gaussian pattern is a general use pattern suitable for shallow observations where the exact sub-pixel sampling is unimportant. It has a ½ sub-pixel pattern, with the 5th point at sub-pixel (¼,¼).

Figure 6.29 shows the dither patterns at the default (large) scale. Figure 6.30 shows the cycling dither patterns and the distribution of both the dithers and of the separation between dithers for each scale.

Cosmic ray and residual image rejection is greatly facilitated by taking highly-dithered observations. The SSC mosaicking software provides good outlier rejection in cases in which each position on the sky is observed with several dithered frames. The SSC mosaicker works well with five or more dithered observations per position on the sky, though will manage some rejection with fewer. It has not been found necessary or more useful to take repeated, non-dithered observations at each position in a map or dither pattern to obtain good cosmic ray rejection if dithering is being carried out with sufficient redundancy.

6.2.3.6.2   Scales and Pattern Selection in Spot

Each of the IRAC dither patterns is available in three sizes, large (default), medium, and small. For most of the patterns, the scaling of the large, medium, and small patterns is approximately in the ratio 4:2:1. Exceptions are the small cycling pattern, which is about 1/5th the size of the large cycling pattern and has a lower-weighted inner region to reduce the numbers of small separation dithers, and the 4-point subarray pattern for which the scaling is 4:3:1.5. For all the patterns, the sub-pixel dithering is maintained, independent of scale.
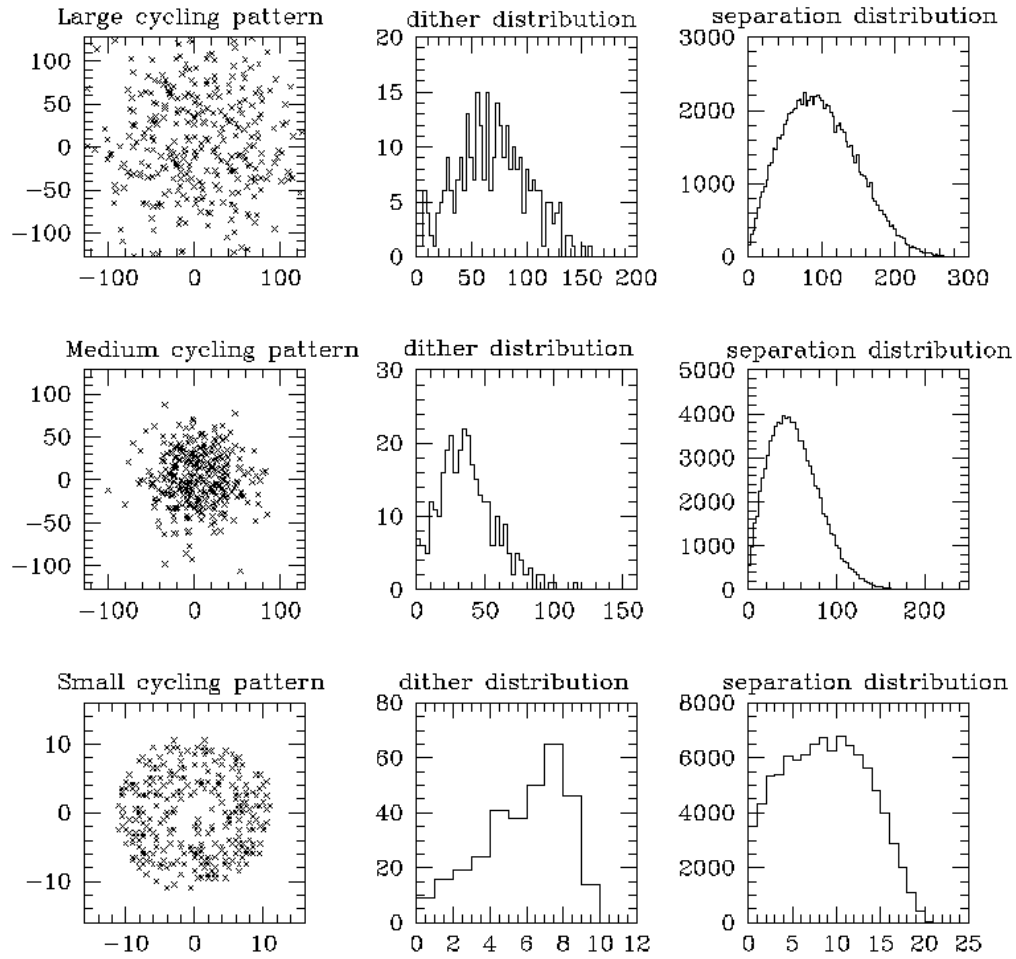
Figure 6.30: Characteristics of the cycling dither patterns, in pixels.
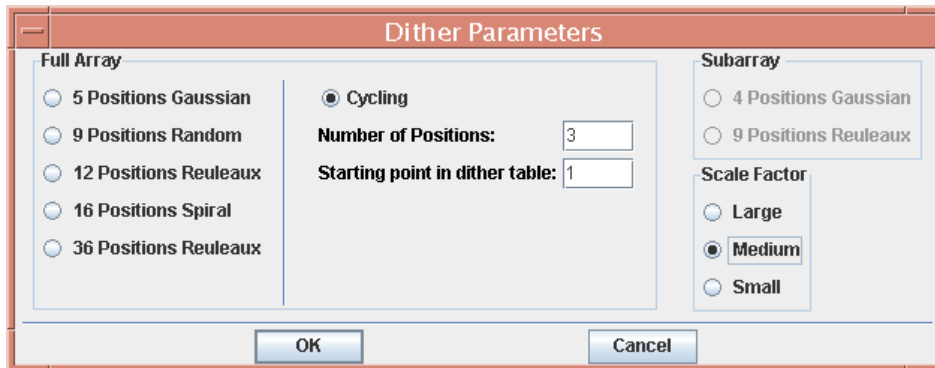

Figure 6.31: Dither pattern dialog box in Spot.

The dialog box in Spot for the dither patterns is shown in Figure 6.31, which illustrates how the pattern and scale are selected.

6.2.3.6.3   Sub-Pixel Dithering

Sub-pixel dithering, combined with the drizzle technique (Fruchter & Hook 2002, PASP, 114, 144) to reconstruct the images, can improve the sampling of the mosaics that are obtained from IRAC (or any other) observations. Such strategies have been used for the WFPC2 and NICMOS instruments on the HST for some time (for details see the HST Drizzle Handbook). Dithering is also needed to calibrate intra-pixel sensitivity variations, and needed for programs requiring accurate photometry and astrometry (Anderson & King 2000, PASP, 112, 1360). To be effective, however, accurate pointing and low image distortion are required. The offsetting accuracy of Spitzer is in the range 0.1″–0.4″. This, combined with the image distortion in the IRAC arrays, places a limit of about ¼ pixel on the sub-sampling that is likely to prove useful in practice. For example, the distortion of the IRAC camera is <1% (see Figure 6.5). Thus for the largest dither patterns, which typically offset up to ±64 pixels from the starting point, the offsets will be up to ±0.6 pixels from the nominal values. Thus only in the small-scale patterns, where the offsets are less than ±16 pixels, will the sub-pixel sampling work well, though even on the larger scales some improvement of the images will probably be noticeable.

6.2.4 IRAC AOT Recommendations and Examples

In this section, we present some advice and some completely worked examples of IRAC observations. Further detailed examples are found in the Spitzer Observation Planning Cookbook.

6.2.4.1 Best Observing Practices with IRAC

We recommend the following guidelines when planning IRAC observations. More information on these items can be found below and elsewhere in this Chapter.

1. Always check your planned observation by overlaying it on an appropriate astronomical survey image such as one from the 2MASS/DSS/WISE surveys. Check for the range of allowed observing dates (visibility windows). Verify that bright objects, e.g., from the 2MASS or IRAS catalogs, will not ruin the planned observations in terms of scattered light (section 6.1.2.2.3), persistent images (section 6.1.3.2.3), image artifacts (section 6.1.3.2.10), or saturation (section 6.2.1).
2. Use dithering instead of in-place repeats (see section 6.2.4.1.1 below) unless the goal is high-precision photometric monitoring (see section 6.2.4.1.8).
3. Use medium- or large-scale dither patterns unless performing a map with very tight requirements for uniform coverage or maps with 1/3-1/2 array mapping offsets (see section 6.2.4.1.1 below).
4. If the field you are planning to observe includes very bright sources, consider using the HDR mode to allow for flux measurements of bright sources and identification of saturating sources (section 6.2.4.1.2 below). If you plan to

observe a single very bright point source, consider the subarray mode (section 6.2.4.1.3 below).

5. Inspect the field being observed, including the "serendipitous" field covered by one detector while the other is observing the target of interest. Residual images can persist for some time and ruin your observation (section 6.2.4.1.5 below).

6. If rejecting asteroids is important, plan at least two observations of your target, separated by a few hours (section 6.2.4.1.7 below).

7. For the most sensitive observation, plan observations using the 100-sec frame time and dithering as much as possible.

8. For highest quality images, put your source in the inner 1/3rd of the array.

Depending on the number of bright sources in your planned field, and the placement of your observation in the schedule relative to other observations that may have bright sources, there may be persistent images in the arrays during your observations. The calibration data (flats and darks) are carefully planned to avoid such artifacts. If your observation is contaminated by persistent images, the effect on the final data quality is reduced in a dithered observation by at least a factor of 1/N, where N is the number of dithers. Greater reduction occurs when robust averaging (outlier rejection) is used.

6.2.4.1.1 Dithering vs. In-Place Repeats

Dithering is used to eliminate array-dependent or transient artifacts from a true celestial map. A well-dithered map will mitigate the effect of pixel-to-pixel gain differences, which will average down when a celestial-coordinate mosaic is generated. Radiation hit and residual image rejection is greatly facilitated by taking highly redundant observations. The SSC mosaicking software provides good radiation hit rejection in cases where each position on the sky is observed with several dithered frames. The medium- and large-scale dither patterns with five or more dithers per position are adequate for this. It is also possible to achieve sufficient redundancy, and accurate maps of large-scale structures, by making a raster map with spacing between rows and columns that is ½ array or less, together with a superposed small-scale cycling dither pattern.

Scattered light from bright sources near the edge of the field of view sometimes cannot be avoided, but it can be prevented from contaminating multiple frames by using a dither pattern larger than the characteristic size of the regions that produce stray light. Scattered light is well-rejected by the post-BCD pipeline if dithering and mapping offsets are large enough, for example, with the medium and large dither patterns (but not small), to ensure that stars in subsequent images are moved out of the scattering zones, and the redundancy is high enough to allow for effective outlier rejection (five dithers is sufficient).

We discourage using in-place repeats (successive frames taken at the same position), especially in observations that have less than ten different dither positions, both for the reasons mentioned above and also because the residual

first-frame effect will lead to a bias pattern difference between the "repeats" and the "first frames" of a repeat set. Taking in-place repeats is recommended only in the case of time series measurements with stringent requirements for stability, such as observations of planet transits. In general, the better handling of pixel-to-pixel variations using dithers will more than compensate for the reduced amount of integration time; that is, the realized signal-to-noise level will be higher using *N*-1 dithered observations than *N* observations with repeats. (In-place repeats are specified in the AOT window under "For Each Pointing/ Number of Frames;" dithers are specified lower in the AOT window under "Dither Pattern.").

Taking into account possible residuals of the first frame effect and image artifacts due to bright sources, we recommend that sensitive, background-limited maps be made using either as many dithers as possible, or a fine map grid combined with the cycling dither pattern. Shallow, read-noise-limited observations, or raster maps specially designed to identify phenomena with a certain time-dependence (such as asteroid motion), may be best done with combinations of medium or large dither patterns and small map steps. The small-scale dither patterns should only be used in conjunction with mapping using 1/3–2/3 array offsets. The small-scale dither patterns do not provide sufficient redundancy under other circumstances.

The only case in which we recommend in-place repeats ("staring mode") is that of high-precision photometric monitoring. See section 6.2.4.1.8 for more information.

6.2.4.1.2   HDR Mode
It is possible that bright sources will saturate the array at the frame time you choose to meet your sensitivity goal. To allow sensitive observations without losing dynamic range, we provide a high dynamic range (HDR) option. When this option is selected, IRAC will take extra frames with frame times shorter than your selected frame time. HDR mode is recommended if the target or nearby sources will saturate in the desired frametime. The short frame data are very useful in recovering the photometry of saturated sources, fitting PRFs to saturated sources, and in removing artifacts due to bright saturated sources. HDR mode is only slightly more expensive in observing time than the full frame counterpart.

6.2.4.1.3   Subarray
Subarray mode is useful for observing single, very bright sources, and for obtaining high temporal resolution, since sets of 64 frames are taken back-to-back, with no gap between frames. The saturation limit is much higher in the subarray mode (see Table 6.13).

6.2.4.1.4   Mapping
In most cases, we recommend mapping in array coordinates since the sky coverage can be custom-tailored, independent of the date when the observation is scheduled. A celestial map grid can yield highly non-uniform coverage

(including gaps), unless the individual pointings are spaced closely together. There are cases for which a celestial grid is preferred, specifically for mapping a highly elongated region (see the example in section 6.2.4.4). We recommend that all observers considering a celestial grid inspect their survey coverage for a range of possible spacecraft roll angles using Spot visualizations. Be aware that away from the ecliptic poles, not all position angles are available over all positions on the sky. If a large observation can be broken into separate rectangular map grids, as is necessary when the total map duration is more than 24 hours, then individual AORs for each map "tile" can use the same central target position and a "map center offset." Allow for some overlap between tiles of a larger map, both for offset correction and for inefficiencies in the way tiles mesh together.

In general making large maps with half array (or smaller) offsets and fewer dithers will produce better quality mosaics than using almost full array offsets and more dithers to provide the same coverage. Large diversity of sampling the focal plane will reduce edge effects between map positions and smaller steps should provide more uniform coverage.

6.2.4.1.5 Observing Near Bright Targets

If you observe a target next to a very bright target and want to image it with both arrays, and it will be impossible to avoid having the bright target in one of the arrays (e.g., due to the small roll angle range), it may be better to make the observation in two separate AORs, imaging one channel at a time, or to take more frames (with dithers) than would be strictly needed for sensitivity purposes, to beat down persistent images. Remember to justify this in your proposal.

A challenging type of observation is to search for a faint source near a much brighter one. The choice of observing strategy and assessment of the technical feasibility for such a search requires great care. First, it is important to determine the brightness of the point source function (PSF) of the main source at the distance where the putative companion is being sought. The distinction between PSF and PRF is not relevant outside the core of the PSF and when fitting/subtracting the wings of the PSF/PRF (see Section 6.1.2.2).

Table **6.15** gives the intensity of the PSF, normalized to the peak for a source centered in a pixel, at several distances from the center. Figure 6.32 shows the relative surface brightness of a point source in each channel both along and off a diffraction spike.

A well-designed experiment will be able to "cancel" the PRF down to a certain level. For example, if the PRF is down by a factor of one thousand from the peak at the distance being searched, it is plausible to search for features at a level of 1×10^{4} if some type of PRF removal is done. And, furthermore, having knowledge of the potential shape of the companion (e.g., a point source or disk) will obviously discriminate it from the remaining PRF of the bright source. Remember that the Poisson noise of the bright source at the location of the faint target will always limit the accuracy of the PRF removal.

Here is a recommended strategy for this type of observation based on the work of Marengo et al. (2009, ApJ, 700, 1647) and Janson et al. (2012, ApJ, 747, 116) to enable photon-limited identification of faint companions. Center the bright source on the array, and observe it with a dither pattern with small scale factor. Use one of the Reuleaux patterns as they are regular patterns with good subpixel sampling that emable construction of an extended PSF. Use a frame time that maximizes your sensitivity at the anticipated separation of the source to the bright star. The selected frame time will usually saturate the center of the field of view; therefore, your observation will be more difficult to schedule.
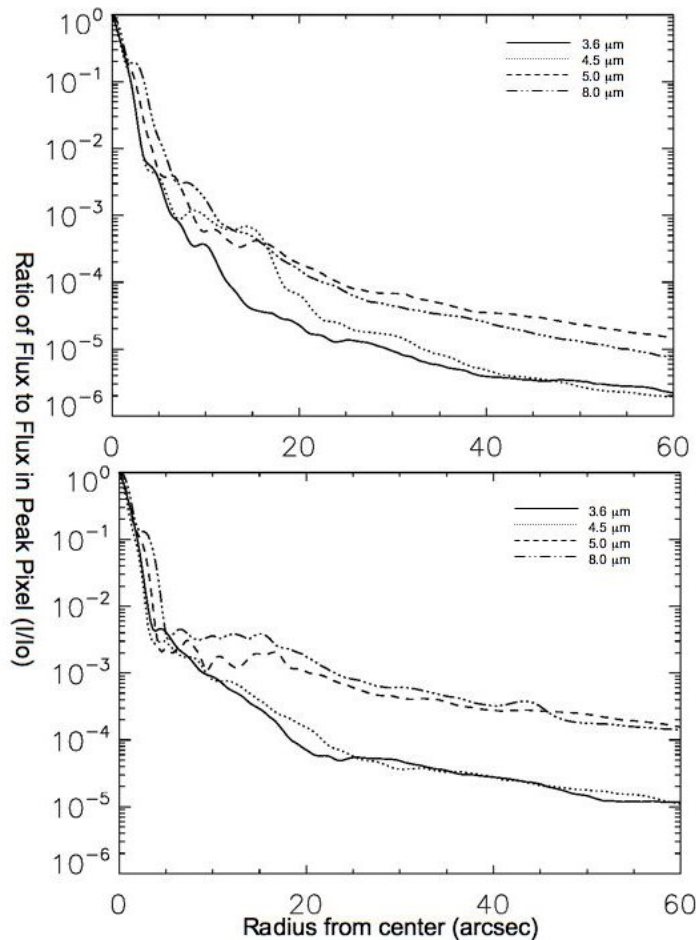
Figure 6.32: Relative surface brightness of a point source for each channel as a function of radius out to 60″ along a diffraction spike (bottom panel) and off a diffraction spike (top panel) as measured using the extended PSFs available on the SSC website.

Finally, and probably most importantly, design the experiment as multiple AORs, with timing constraints such that the source will be seen at a variety of different roll angles. The range of possible roll angles depends on the ecliptic latitude of the source and must be verified using Spot visualizations near the beginning and end of the visibility windows for a given source. Typically the available range of roll angles is about 20 degrees. The PSF will remain fixed in array coordinates, so

the basic calibrated images at the two epochs can be subtracted. While any detector artifacts and most of the light from the bright source should subtract out, two images of any real faint object(s) should remain. The extended PSF for IRAC can also be used to remove bright point sources and improve contrast for the detection of faint companions.

Table 6.15: PSF intensities*

	Radius (″)	2.44	4.88	7.32	9.76	12.20
Ch 1	I/I_0	1.272e-02	6.799e-04	1.390e-04	3.899e-05	1.231e-05
	Enc. Energy	0.855	0.942	0.974	0.991	1.000
Ch 2	I/I_0	1.628e-02	7.040e-04	9.919e-05	6.316e-05	1.928e-05
	Enc. Energy	0.836	0.930	0.968	0.987	0.998

·Values are derived from 5× (0.24″/pixel) oversampled PRFs created from observations of calibration stars. I/I_0 is calculated as the flux density/pixel in a 1-pixel annulus at the respective radii, divided by the flux density measured in the central pixel. Enc. Energy is the ratio of the flux density enclosed within the representative apertures to the flux density in a 12.2″–radius aperture.

6.2.4.1.6   Observing Single Faint Sources

Despite residual image mitigation procedures, observations of a faint source may be affected by long-term residual images at 3.6 μm from prior observations of bright sources. For observations of single faint sources, we suggest offsetting the target position by 5″-10″, to reduce the chance of placing a residual image from a preceding observation of a bright star that may have used the same dither pattern as your science observation. This offset is most easily accomplished by using a cluster target with array coordinate offsets, entering the offset as the first (and only) cluster position, and then selecting the option to observe offsets only.

6.2.4.1.7   Confusion and Other Background Issues

If you know the positions of your sources to better than 0.6″ and you are only interested in measuring their fluxes, then the classical confusion limit is not really relevant. It is generally straightforward to align an IRAC image in celestial coordinates to <0.6″, and often 0.2″ accuracy can be achieved when there are multiple 2MASS sources in the field.

To separate faint asteroids from more distant targets, it is a good idea to observe your target field at least twice, separated by a few hours at least, if your source lies at a low ecliptic latitude (within 15° of the Ecliptic).

6.2.4.1.8   High Precision Relative Photometric Monitoring

For observations of exoplanet transits and other sources requiring high precision relative photometry, it is important to minimize systematic effects in the data. In this special case, we recommend observing with repeats and not dithering. By staring for the entire observation, variations in photometry, caused by moving the source to other pixels on the array or other positions on a pixel, are minimized. A

PCRS peakup should be added for these staring observations, as discussed in Section 6.2.3.2 and at http://irsa.ipac.caltech.edu/data/SPITZER/docs/irac/pcrs_obs.shtml. The longest possible frametime that does not saturate the source should be used to maximize the signal compared to the read noise. The field should be inspected to make sure that stray light will not contaminate the observation and that artifacts (column pulldown) from bright sources will not overlap the target. If the total duration of the observation is greater than 12 hours, multiple staring AORs, each with a PCRS peak-up, should be supplied, with appropriate chain constraint to indicate the AORs should be scheduled together. These observations necessarily produce high data volumes. In most cases, the SSC will recommend that data collection be selected only for the field of view imaging the target. For more information about high precision photometric observations please consult https://irachpp.spitzer.caltech.edu/.

6.2.4.2 Shallow Survey Example

The goal of a shallow survey is to cover sky rapidly, while maintaining some redundancy in order to reject cosmic rays and reduce effects of pixel-to-pixel gain variations. For this survey, we request coverage of our target region with both IRAC channels. The survey will be conducted with a rectangular grid, with the grid steps aligned with the focal plane array in order to make coverage uniform. *We will step by about 50% of the array width for each grid step in the column direction and 95% of the width in the row direction; specifically, we will use a step size of 292.8″=244 pixels. At each map grid point, we will observe 2 dither positions using the small cycling dither table to achieve a coverage of four pointings at each sky position. Combined with the half-array offsets, the small scale cycling dither provides adequate diversity against stray light and prevents the accumulation of residual images in the resulting mosaic through the random placement of detector pixels on the sky.* The frame time at each position is 30 sec.

We can make an 18×11 map grid, covering 0.6 deg², with both arrays, in 4.5 hours as determined using Spot. Except for the small overlap regions between map grid positions and a crust at the edge of the map, the observing time per sky pixel is 4×30 seconds. Using the sensitivity tables above, assuming medium background and a perfect flat field, the 5-σ point source sensitivity is 6.2 μJy at 3.6 μm.

The observation described here could be used as a "tile" for a survey of a larger area. Suppose you want approximately 9 times the area, so that your survey region could be broken into a 3×3 set of these "tiles." The entire observation could not be done in a single AOR, because it would exceed the number of allowed instructions in a single observing request. To implement this large survey, you would generate 9 identical AORs and constrain them to occur within a reasonably short period of time (in order to keep the relative roll angle between the AORs small). Further, you would specify offsets for the center of each AOR. You will need to specify, in addition to the AOR parameters already described, the array coordinate offsets for each AOR that would place them onto the desired

grid. Thus if the two array coordinate axes are called (Y, Z) and the desired spacing between map grids is G, then the map center offsets would be $(G, G), (G, 0), (G, -G), (0, G), (0, 0), (0, -G), (-G, G), (-G, 0), (-G, -G)$ for the nine AORs, respectively. Using the constraints editor, you would constrain that the observations all occur within a reasonable time (typically <1 week) of each other, but you should not specify the exact date. The dither pattern for each map tile should be slightly different if possible. This is most easily achieved for the cycling dither pattern by choosing a different starting dither for each map.

6.2.4.3 Deep Image Considerations and Example

When obtaining deep imaging there are several important factors to consider. The first consideration is artifact mitigation. Persistence from previous observations can create both large-scale background structure and small-scale artifacts that can make it difficult to extract faint sources. Subtracting a median "delta-dark" frame generated from your data best mitigates the persistence and requires taking very well dithered data. A medium or large scale random dither pattern is best for this. We recommend against using the Reuleaux or other regular dither patterns because artifacts accumulated in prior observations using these dither patterns will constructively add in your data. A small scale random dither pattern should be used with great caution because extended and bright sources may not be well dithered enough to be removed from the "delta-dark" frame. If you are covering an area larger than one IRAC FOV it is good practice to offset by half an array between mapping points to mitigate artifacts.

A second consideration is that the background typically varies by a factor of 2-3 over the observing window. To obtain the deepest possible images the observations should be constrained to the darkest part of the observing window, which will always be at the start or end of the observing window, or use the part of the observing window where the background is <1.5 times the minimum background. To determine the dark period for your objects ask Spot to estimate the background on the first and last day of each observing window for each target. Note the dark period alternates from start to end in alternating observing windows.

The third consideration is that most deep images are well below the Spitzer confusion limit and so source fitting is generally used to measure faint source photometry. The IRAC PRF is non-Gaussian, very asymmetric, and rotates with the instrument PA. So, taking data over a short period will generally result in a better-defined PRF.

Finally, many programs have taken advantage of the fact that the instrument PA rotates by 180 degrees between observing windows to obtain both 3.6 and 4.5um data in a single IRAC FOV. While this may seem efficient it has a number of drawbacks: 1) Because the dark period alternates, you can not take both sets of data during the darkest part of the observing window if you match the FOV. This can cause a loss in sensitivity nearly as great as the gain in observing time per

pixel. 2) The 180 degree flip will exactly match row-correlated artifacts such as column droop making artifact mitigation more difficult. 3) The 180 degree rotation means the PSF will be very inhomogeneous in the overlapping area making PRF fitting photometry more difficult.

Suppose we want to make a sensitive image at 3.6 μm of an object that is less than 4′ in size. In this case, we will not map, but instead will perform many dither steps in order to minimize the effect of pixel-to-pixel gain variations. For this example, we will use the 16-position spiral dither pattern, medium size, and 100 sec frames. We repeat the pattern nine times using a cluster target with nine small array offsets (+n, -n), where n=1.8, 3.6, 4.8 to reach the desired depth. Using Spot we determine that the observation takes 8.8 hours. The 5σ point source sensitivity (low background) is 0.35 μJy at 3.6 μm, which is below the confusion limit (0.6 μJy) and the per-pixel surface brightness sensitivity is 0.004 MJy/sr at 3.6 μm. A neighboring field (not overlapping with the target field) will be observed at 4.5 μm. If the observation is to be repeated, we suggest using slightly different offsets (or starting dither positions for the cycling dither) for each AOR.

6.2.4.4 Elongated Object Example

We wish to make an image of an elongated galaxy oriented 60º E of N. The galaxy has an optical size of 13.5′ by 2.5′, and we want to cover about 17′ with both fields of view. The galaxy is very bright, so we need to use a short frame time (12 sec will work) to avoid saturating or operating exclusively at the high end of the linearity curve. To get the desired sensitivity and source confirmation, we take 5 frames using the small scale cycling dither pattern. In this example, we will perform the observation two different ways, to compare the results.

6.2.4.4.1   Array Coordinates

In order to cover the desired area regardless of schedule date, we will need to make the map much larger than the galaxy size. Using the equations in Section 6.2.3.4, to cover 17′, we need 5 columns and 4 rows. We select both fields of view to center the image on the nucleus. The duration of the observation is approximately 2320 sec. The map grid size is equal to the array size. It is possible to make a smaller map, tailored to the size of the target, if we fix the observing date. For a very large observation, fixing the date may be the best solution. But for a small observation such as this one, a better solution is given in the next subsection.

6.2.4.4.2   Celestial Coordinates

Another way to observe the elongated galaxy that is both efficient and independent of scheduling constraints is to observe a map grid in celestial coordinates. To get the desired depth of coverage at each position, we could use many different options, but there is one method that will optimize the sky coverage and provide the desired redundancy with minimal overhead. We make a

finely spaced map grid that avoids holes due to the (unknown *a priori*) roll angle on the scheduled date and yields the desired 5 observations of each sky position. To do this, we use a map grid spacing of *A*/5=61.4″. The number of rows is 13. The position angle is 60º E of N. We select the cycling dither pattern (small scale) with a depth of one. Making a 13×1 map in celestial coordinates covers the desired long axis of the galaxy, but the perpendicular coverage with the desired depth is only for a relatively narrow strip about the same size as the optical disk.

Therefore, we add 1 extra column to the map and make a 13 by 2 celestial-coordinate map. Figure 6.33 shows the sky coverage by one field of view for this observation. Since both fields of view were selected, the map will be performed twice, with the galaxy centered first in the 4.5 μm field of view and then in the 3.6 μm field of view. In Figure 6.33, there are two bands of sky coverage: the upper band is the sky covered in the first map pass by the 4.5 μm field of view; the lower band is the "serendipitous" sky covered by the 4.5 μm field of view during the second map pass. Using Spot, the duration of the observation is approximately 1500 sec, even with both fields of view selected. This is significantly less than in the array-coordinate map. The savings are entirely due to the celestial coordinate map covering a smaller area, custom-tailored to the desired object size.
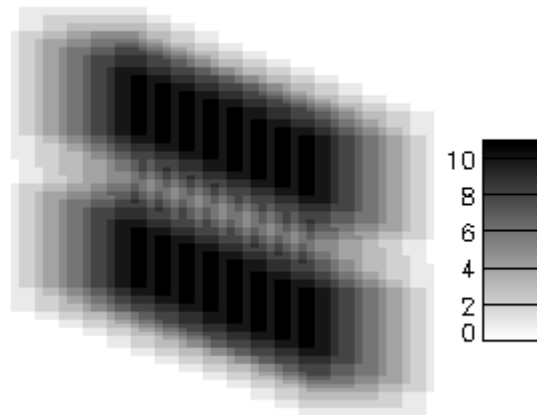

Figure 6.33: Sky coverage for an oversampled, celestial-coordinate map of an edge-on galaxy. The map was made with a position angle 60º E of N. The scale bar gives the number of times each sky position is observed.

6.3 Data

6.3.1 Instrument Calibration

The SSC performs routine calibration of IRAC using observations of standard stars, a low background region near the North Ecliptic Pole and high background regions along the Ecliptic Plane. Additional diagnostic data may also be taken at various times to perform certain calibration operations. The data obtained in these observations are used to construct the necessary calibration inputs to the

pipeline for the IRAC data processing of science observations. The calibration data files, as well as the pipeline inputs, are available to the general user in the Spitzer archive maintained by the SSC. For more information, consult the IRAC Instrument Handbook and the absolute calibration paper by Reach et al. (2005, PASP, 117, 978) and the warm calibration summary by Carey et al. (2010, SPIE, 8442). In the remainder of this section, we refer to instrument campaigns which are two week segments of the schedule. Unlike the cryogenic mission where the instruments were cycled through and IRAC was power-cycled at the beginning and end of each campaign, IRAC is powered on for the entire warm mission and the campaign nomenclature is a convenience for scheduling, processing and calibration.

6.3.1.1 Astronomical Flux Standards

A number of astronomical standard stars are observed in each instrument campaign to obtain a valid absolute flux calibration. Stars with a range of fluxes are observed at a number of positions across the array and many times throughout the mission to monitor any changes that may occur. Calibration stars with known spectral types and accurate absolutely calibrated fluxes in the IRAC bands have been determined. These absolute calibration stars are in the continuous viewing zone (CVZ) so that they can be observed at any time and are being monitored throughout the mission.

Nine stars are observed in the CVZ every 14 days. These standards remain the same throughout the warm mission, and provide the absolute flux reference for IRAC. Additionally, secondary calibrators near the Ecliptic plane are observed once per data downlink, typically every 24 hours with a given secondary monitored for 14 consecutive days. The secondaries used are chosen to minimize telescope slews. These calibrators are used to monitor any short-term variations in the photometric stability.

Analysis of the flux calibrator data during the cryogenic mission indicates that absolute flux calibration is accurate to better than 2%. Repeatability of measurements of individual stars is good to better than 1%, and can be as good as 0.01% with very careful observation design (e.g., Charbonneau et al. 2005, ApJ, 626, 523). The absolute calibration is derived taking several systematic effects into account. The steps are described in detail by Reach et al. (2005, PASP, 117, 978). If this methodology is not applied, then point source photometry from the BCDs can be in error by up to 10%. The absolute calibration factor for the Warm Mission has been determined in an analogous fashion from the final setpoint calibration campaign and confirmed with the per-campaign observations. The initial absolute calibration accuracy is currently on the order of 3%, but we expect it to improve to better than <2% after we commence the reprocessing of the data.

6.3.1.2 Sky Flats

To get the most accurate measure of the full system gain, including the effects of the telescope and the IRAC pickoff mirrors, one must use observations of the sky.

This is done using many dithered observations of a network of 22 high zodiacal background regions of the sky in the ecliptic plane, which ensures a relatively uniform illumination with a reasonable amount of flux. One such region is observed every 14 days. The data are combined with object identification and outlier rejection, producing a product analogous to a "median sky flat," as is commonly constructed during ground-based observing, and which will be an image of the presumably smooth celestial background, further smoothed by the dither pattern. The resulting flat field is divided into the science data. Using data taken throughout the post-cryogenic mission phase, the current flats have a median 1-sigma accuracy of 0.17% and 0.09% in channels 1 and 2, respectively. The flats are significantly different from those derived during the cryogenic mission, and the two cannot be interchanged. Users should note that the flat field data are generated from the zodiacal background, and are appropriate for objects with that color. There is a significant color term, of order $5\% - 10\%$, for objects with a Rayleigh-Jeans spectrum in the mid-infrared (such as stars); see the IRAC Instrument Handbook for more information. This color term has changed from the cryogenic version as discussed in the IRAC Warm Image Features and Caveats on our IRAC web pages:
http://irsa.ipac.caltech.edu/data/SPITZER/docs/irac/warmfeatures/.

Note that for deep survey observations and other data sets with a large number of frames and a good dithering strategy, the system gain could in principle be determined by the actual survey frames themselves, rather than using the standard set of dedicated observations of some other part of the sky. The dither and mapping pattern need to be specified to optimally relate each pixel in the array to all the others, as well as mapping out the region at the required sensitivity. Tests of self-calibration with suitable datasets have shown that the SSC pipeline results are comparable. The SSC will not, as a matter of course, undertake such special processing (self-calibration) as part of the automated pipeline. The SSC-generated data products will always use the dedicated calibration data.

6.3.1.3 Skydarks

Dark current and bias offsets are calibrated via the standard ground-based technique of dark subtraction. As part of routine operations, the SSC observes a dark region of the sky ("skydark") near the north ecliptic pole every seven days. These data are reduced and combined in such a way as to reject stars and other astronomical objects with size-scales smaller than the IRAC array. The resulting image of the minimal uniform sky background contains both the bias and dark current. When subtracted from the routine science data, this eliminates both of these instrumental signatures. Naturally, this also subtracts a component of the true celestial background. The SSC includes a COBE-based model estimate of the true celestial background, which is the same as that returned by Spot. *Note that our lack of an isolated measurement of the dark current and bias offset during shutterless operations limits the ability of IRAC to measure the true celestial background*. Our understanding of the history-dependent bias variations

(section 6.1.3.2.11) is currently incomplete and will improve as our temporal sampling improves.

6.3.1.4 Distortion and PSF Map

The PSF over the field of view of each of the two channels has been characterized, and the optical distortion has been measured. This has been done by observing an open star cluster for which we have good ground-based astrometry. The distortion is included in the WCS header keywords. The positions of both IRAC fields of view have also been determined relative to the PCRS. To our ability to measure, the distortion map and optical PSF have not varied from the cryogenic measurement.

6.3.1.5 Linearization

During cryogenic observations, non-linearities in the IRAC detectors were extensively calibrated during ground-testing using special ground support equipment and also in flight using extended astronomical objects. These calibration data allow the detectors to be linearized to better than 1% for 90% of their full-well capacity. A similar set of calibrations was performed as part of the final warm setpoint calibration; however, the warm linearity solution was best derived from science observations of extragalactic fields that had also been observed in the cryogenic mission (see Section 6.1.3.2.1). Final improvements were made from an analysis of the instrument optical performance, under the assumption that the observed PSF should remain invariant as a function of observed flux.

6.3.2 Data Products

This section describes the basic data products the observer will receive from the SSC. More details are contained in the IRAC Instrument Handbook, which describes the algorithms implemented in the IRAC pipeline and provides a detailed guide to the data products and how to use them. The data delivery consists of a directory hierarchy with a name unique to that AOR. In this hierarchy are the BCD data, as well as a number of subdirectories containing the raw data, the calibration files, log files, and the post-BCD data. The exact contents of the data delivery vary according to what the observer has requested from the Spitzer Heritage Archive. IRAC data are supplied as standard FITS files.

Each file consists of a single data collection event (i.e., a single exposure), and contains one image corresponding to one of the two IRAC arrays (the exception being post-BCD products, described below). The FITS headers are populated with keywords including (but not limited to) physical sky coordinates and dimensions, a photometric solution, details of the instrument and spacecraft, including telemetry when the data were taken, and the steps taken during pipeline processing. There are three primary image data types that are supplied for each AOR (raw, BCD, mosaic).

6.3.2.1 Raw Data

Raw data are wholly unprocessed except for those steps necessary to render them into a readable FITS format, i.e., depacketization and decompression. This is the form in which data enters the IRAC pipeline. Most observers are unlikely to use these data beyond sanity checking of the pipeline data products. They are, however, supplied in the event that observers wish to reprocess their IRAC data in a different manner from the SSC pipeline. By comparison to ground-based astronomy, these are the raw data one gets from a camera and writes to disk while observing at the telescope. The raw data consist of 16-bit integer FITS files. The data are unsigned integers and the files do not strictly follow the FITS convention; however, this is the format of the data as delivered. The headers are populated with all of the ancillary science telemetry keywords.

6.3.2.2 Basic Calibrated Data, or BCD

BCDs are exposure-level data after having passed through the IRAC pipeline. There is one BCD for each integration taken by IRAC. Instrumental signatures have been removed (as described in section 6.3.3.2), and the BCDs are absolutely calibrated into physical units (i.e., $MJy/sr = 10^{17}$ erg s^{-1} cm^{-2} Hz^{-1} sr^{-1}). In addition, the pointing refinement (see section 6.3.2.4) based upon 2MASS astrometry will be supplied in the BCD header. Continuing the analogy with ground-based observing, the BCDs are data that have been reduced, but not yet combined into a final image. This is the primary science data product produced by the SSC.

Ancillary files are supplied with each BCD (see Table 6.16). These ancillary files contain several types of information regarding each pixel in each image. A version of the BCD with correction of bright source artifacts is produced (cBCD). In general, it should be better than the BCD; however, the corrections are not always robust. An image containing an estimate of the uncertainty for each pixel is supplied. A mask image contains status bits indicating the probability that any given pixel has been affected by a radiation hit; whether or not the linearity solution could be applied; if a pixel is saturated, dead, hot (always on), or abnormally noisy. Pixels with strong residual images are flagged in the mask file, as are those with artifacts induced by bright sources. Log files are also supplied, and from these and the header keywords the entire pedigree of every data product can be derived.

Table 6.16: IRAC Basic Calibrated Data (BCD) pipeline products

Data	Contents
BCD	Basic Calibrated Data - dark-subtracted, linearized, flat fielded, and flux-calibrated among other things (see section 6.3.3.2)
cBCD	Artifact-corrected BCD; BCD with empirical corrections for artifacts due to bright sources
Uncertainty Image	Array of calculated uncertainties for the BCD

Imask
  Residual Image pixels
  Radiation hit pixels
	Data quality flag image for the given science DCE
	Bit that is set to indicate residual image prediction
	Bit that is set to indicate the probability of radiation hit event for a given pixel

All of the data and ancillary files are in FITS format, containing a header with keywords and their values followed by a binary image, except certain log files that are in simple ASCII format. The standard FITS header keywords are all present, so that essentially any FITS file reader is able to read the files, and all images have 256×256 pixels. Subarray data are in a cube (32×32×64 pixels). Observers should expect to receive a data volume of approximately 3.5 Mbytes per frame of BCD data, including ancillary files as described in Table 6.16. Information about the data that observers receive is included in the IRAC Instrument Handbook.

6.3.2.3 Calibration Files

For each BCD, the pipeline calibration server generates several estimates of the current detector characteristics. These include a map of the pixel-to-pixel response variation (flat field) and an estimate of the dark bias consisting of a sky dark and an estimate of the first-frame effect. These calibration files are supplied to the observer. Observers are also able to request from the Archive the files that were used to generate the sky darks, sky flats, and absolute calibration. The photometric calibrators are not included with each science observation, but they are available via a separate request to the Archive.

6.3.2.4 Extended Pipeline Products (Post-BCD Pipeline)

Pipeline processing of IRAC data by the SSC also includes more advanced processing of many individual IRAC frames together to form more "reduced" data products. Known by the generic title of "post-BCD" processing, this extended pipeline refines the telescope pointing, attempts to correct for residual offset variations and produces mosaicked images. We do not attempt to improve (relative to the BCD) the point source or extended emission flux calibration by automatically comparing to a reference source catalog. The mosaic only includes data from a single AOR, so that observers who break their map into multiple AORs (for example those whose maps cannot be completed within the 24 hour time limit of an IRAC AOR, or those who are making multiple-epoch observations) need to recombine them to obtain their ultimate images.

All IRAC BCD images contain a pointing estimate based on the output of the Spitzer pointing control system (startracker and gyros), i.e., the boresight pointing history file. This initial pointing estimate is accurate to about 0.5″. The post-BCD pipeline performs additional pointing refinement for all IRAC frames. This is achieved by running the SSC point source detector on the channel 1 and 2 frames and comparing the resultant list of point sources to the 2MASS catalog. The results are then averaged, and the known focal plane offsets between the two channels are applied to produce a "superboresight" pointing history file, which is then applied to the data during end-of-campaign reprocessing. This improves the pointing accuracy of the frame to better than about 0.3″. The refined RA, Dec appears in the header as the CRVAL1, CRVAL2 keyword values.

The SSC pipeline mosaicker produces a single image (1 per band) from many input images. First, the BCDs are corrected for overlap consistency. The parts of the images that overlap are forced to have the same background value via addition of an offset. Then a "fiducial frame" is derived. This is the definition for the output frame in terms of its physical size, projection, and orientation. Because projection and distortion effects are non-negligible, the mosaicking and coadding process must reproject the data. The fiducial frame finder seeks to minimize the amount of "blank" area in the output mosaic by rotating the output projection such that it is aligned with the map axes. This is useful for long thin maps, where potentially the output mosaic could be very large, but with a great deal of empty space. The mosaicker then reprojects all of the input data onto the output projection. It reads the SSC WCS, which contains the field pointing center, rotation, scale, and instrument distortion, and reprojects this onto a standard TAN FITS projection. In the process, the data are undistorted. The reprojected images are interpolated onto the fiducial image frame with outlier rejection, rejecting radiation hits that happen in overlapping observations. The outlier rejection scheme is specifically designed to work well in the case of intermediate coverage and may not be adequate for all observations and science programs. In addition to a sky map (in units of surface brightness), a noise image and coverage map are also produced.

The post-BCD pipeline has been made available for general public use by the SSC. It consists of a number of C-modules connected via PERL wrapper scripts and a graphical user interface. Namelists are used for input. In most cases, their operation simply consists of supplying the software with a list of input image files; by default they read and understand the IRAC image headers.

6.3.3 Data Processing

6.3.3.1 Overview

The main processing of the IRAC science data takes place in the "BCD pipeline," which is a set of modules that work in tandem with calibration and pointing servers. The BCD pipeline takes as input the raw data files, and generates the Basic Calibrated Data (BCD) as its final output. The pipeline is run automatically

upon receipt of individual raw files. The BCD pipeline is triggered for all science frames generated as part of an AOR. Calibration data are sent to other pipelines for processing, and their output is made available for the calibration server. When the BCD pipeline is running and requires a calibration file (such as a dark current image), a query is sent to the calibration server, which returns the appropriate file. The calibrated images (BCDs) from an AOR are combined by the post-BCD pipeline to create a mosaic. The extended pipeline (mosaicker, source extractor, overlap corrector and pointing refinement modules) is exported to observers, so that they can combine data from multiple AORs. The BCD pipeline is not exported, because of its inextricable link to the Spitzer Science Operations DataBase (SODB) which is needed to identify the appropriate calibration files for a given observation. A copy of the BCD pipeline code is available at the SSC website for reference purposes, but no support is available for running the code outside the SSC.

6.3.3.2 Science DCE Processing

The following is an explanation of the steps taken by the IRAC BCD pipeline (Figure 6.34). Further guidance to IRAC data reduction is provided in the IRAC Instrument Handbook.

1. The header of the raw data file is validated to ensure that it is an uncorrupted IRAC image with the shutter open and lamps off.
2. Several computed keywords (such as exposure time, commanded instrument and telescope parameters, and the pointing information) are added to the image from the telemetry and the SODB. Many of the detailed IRAC telemetry channels (mostly instrument parameters such as voltages and various temperature measurements) are removed from the header; they are still present in the raw header.
3. The 16-bit integer FITS images are received and then rectified so that increasing flux produces increasing DN (which is not the case initially for the IRAC InSb arrays).
4. The 16-bit integer FITS images are converted to 32-bit floating-point FITS images.
5. Detector wraparound is detected and corrected. IRAC can generate negative flux numbers as a result of Fowler sampling. Although IRAC uses a signed 24-bit internal data representation, it only sends unsigned 16-bit integer data and in the process of doing so discards the sign bit. The wrap detection module uses the knowledge that very high DN values exceed the full-well capacity of the detector, and hence they are actually wrapped negatives. Fowler number, barrel-shift (number of bits shifted to map 24-bit raw pixel value to the 16-bit value returned to the ground without losing dynamic range), and gain have been chosen such that the entire full-well capacity of the detectors can be represented by 16 bits.
6. The raw data units are renormalized to account for IRAC Fowler sampling and bit-shifting. Observers need not take Fowler sampling into account when reducing their data.

7. Due to the design of the IRAC electronics, there is a maximum rate at which the four readout outputs can react to changes in pixel intensity during readout. Thus, it is not possible to go from full to zero pixel intensity between two adjacent pixels in a single readout channel (equivalent to "pixel latency"). This artifact appears as a decaying ghost following a bright pixel, along the fast readout channel, which is horizontal in the IRAC images. This bandwidth limitation is corrected, based on measurements of the detector bandwidth in each readout channel taken during IOC/SV. The correction is assumed to be the same in warm operations.

8. The dark current and bias offset are subtracted using a laboratory dark, which should be a good first-order approximation of the dark current. Currently, the laboratory dark is zero for the warm data.

9. First-frame effect (timing-dependent bias offset) is subtracted. These offsets are being determined as a function of array timing and will be implemented in a future version of the pipeline. These offsets are a constant level per readout column, and thus they can be subtracted from the images.

10. Multiplexer-bleeding correction was applied to cryogenic data, but is not in the warm mission as the artifact no longer exists.

11. Data are corrected for non-linearity. A function (quadratic) is fit individually to the response function of every pixel based on warm operations calibration. This function is then used to linearize the response of the individual pixels. Saturated pixels are identified and marked in an image mask file. The processed pixels should be linear to better than 1%.

12. Scattered light patterns are removed from data. A "butterfly" pattern in channels 1 and 2 caused by internal scattered light is scaled using the estimated zodiacal background level and subtracted from each image. They are subtracted from all calibration data as well.

13. The "skydark" is subtracted from the image; the bias is monitored throughout the mission every 7 days by observing fields near the North Ecliptic Pole. The applied skydark is the nearest in time clean calibration.

14. Radiation hits (cosmic rays) are detected at the single frame level using a median filter. Radiation hits are not removed from the BCD. Instead, a probability that a given pixel is affected by a radiation hit is noted in the data quality file (imask). The primary method for removing radiation hits is in the post-BCD pipeline, which uses robust averaging of observations of the same piece of sky.

15. The data are flat fielded. The flat field image is generated from observations of low ecliptic latitude fields with high zodiacal emission.

16. The channel 1 and 2 images are flipped. This transposition is a result of the dichroic beamsplitters. As a part of this operation, associated mask files are flipped as well. The orientation of the BCDs for the cryogenic and warm missions is identical.

17. The photometric calibration, appropriate for point sources, is applied. The pixels are then in units of surface brightness (MJy/sr).

18. All of the DCEs from the present AOR are used to determine where there are potential residual images. The data pipeline does not correct the BCD for residual images, since this correction may be quite complex and dependent on a number of different factors, and hence cannot be easily executed in an automated fashion. However, we determine which pixels are likely to produce residual images above the local noise level, and we flag those pixels in subsequent DCEs based on the residual image decay curve.

19. The 2MASS data are used to refine the pointing. The refined pointing keywords are added to the header of the final BCD product at this stage.

20. The BCDs are copied and further processed to remove instrumental signatures caused by bright sources. The corrections are empirical and fit directly to the data. Artifact-corrected BCDs and uncertainty images are created and the mask file is updated. In general, the corrected BCDs (cBCDs) should be better and used in place of the BCDs. The current version of the warm cBCDs only corrects in part the column pulldown. However, as the corrections are not always robust, the BCDs can be used when the corrections are suspect. The online post-BCD pipeline uses the corrected BCDs (cBCDs).

At this stage, the BCD has been produced and consists of a single image corresponding to each exposure made by IRAC. The header of the image contains the standard FITS keywords and the image distortion coefficients, as well as sufficient information to trace the calibration and pipeline pedigree. This image is calibrated in physical units and has a pointing solution attached.

Further processing to generate the extended pipeline products mentioned above will use the cBCD files as input. Post-BCD pipeline modules are available on the SSC website to match the background brightnesses of overlapping images, take care of column pulldown (see the IRAC Instrument Handbook for more information), register images (relative to each other) using sources in the overlapping region, and generate mosaics from all the images in an AOR. Another set of pipeline modules has been developed to extract point sources from the images and measure their flux densities (performing photometry using PRF-fitting), place the flux densities into source lists for each wavelength, and merge the wavelength-dependent source lists. The algorithms have been designed to be robust and strive for completeness at the 10σ level, thus they do not reach the ultimate sensitivity of the data. Yet another pipeline module has been developed to create supermosaics from observations of the same area of the sky. The supermosaic and source list data have been made available at the NASA/IPAC Infrared Science Archive's (IRSA) Spitzer Enhanced Imaging section.

6.3.3.3 Data Reduction Software

6.3.3.3.1   Data Reduction

The actual BCD pipeline will not be released, due in large part to the degree to which it is tied to SSC-specific infrastructure. However, detailed documentation on the algorithms used by these modules is in the IRAC Instrument Handbook, and the source code for the pipeline is available at the SSC website.

The software modules that make the post-BCD products (mosaicker/coadder, point source extractor, and bandmerger) have been released to the general community and are available from the SSC website. This software consists of modules written in C with PERL wrapper scripts to control them. The primary advantage they offer over existing astronomical software packages is the ability to read the IRAC ancillary data (mask files, etc.) during processing, and a robust handling of image distortion and reprojection. The latter is important due both to the non-negligible distortion in the IRAC detectors and their large areal coverage. The SSC has encoded image distortion using the TAN-SIP projection type, which is now supported by several software packages. It is anticipated that the community will also find this software useful in processing multiple related AORs, which the SSC does not do automatically.

6.3.3.3.2   Data Analysis

Most scientific analysis, such as optimal mosaicking and source extraction, require additional processing beyond the Basic Calibrated Data. Since data products are delivered in standard FITS format, observers may use any of the large variety of data processing packages available to the general community (e.g., IRAF, IDL, etc). The SSC pipeline provides mosaicked images of entire AORs, and the part of the pipeline that takes the cBCDs and combines them into the mosaic is provided to observers. Users should be able to use the post-BCD software themselves for additional, multi-AOR data reduction, or to improve the quality of mosaics as necessary for the desired science goals. The software is designed without arbitrary limits to the size of datasets that it can process.
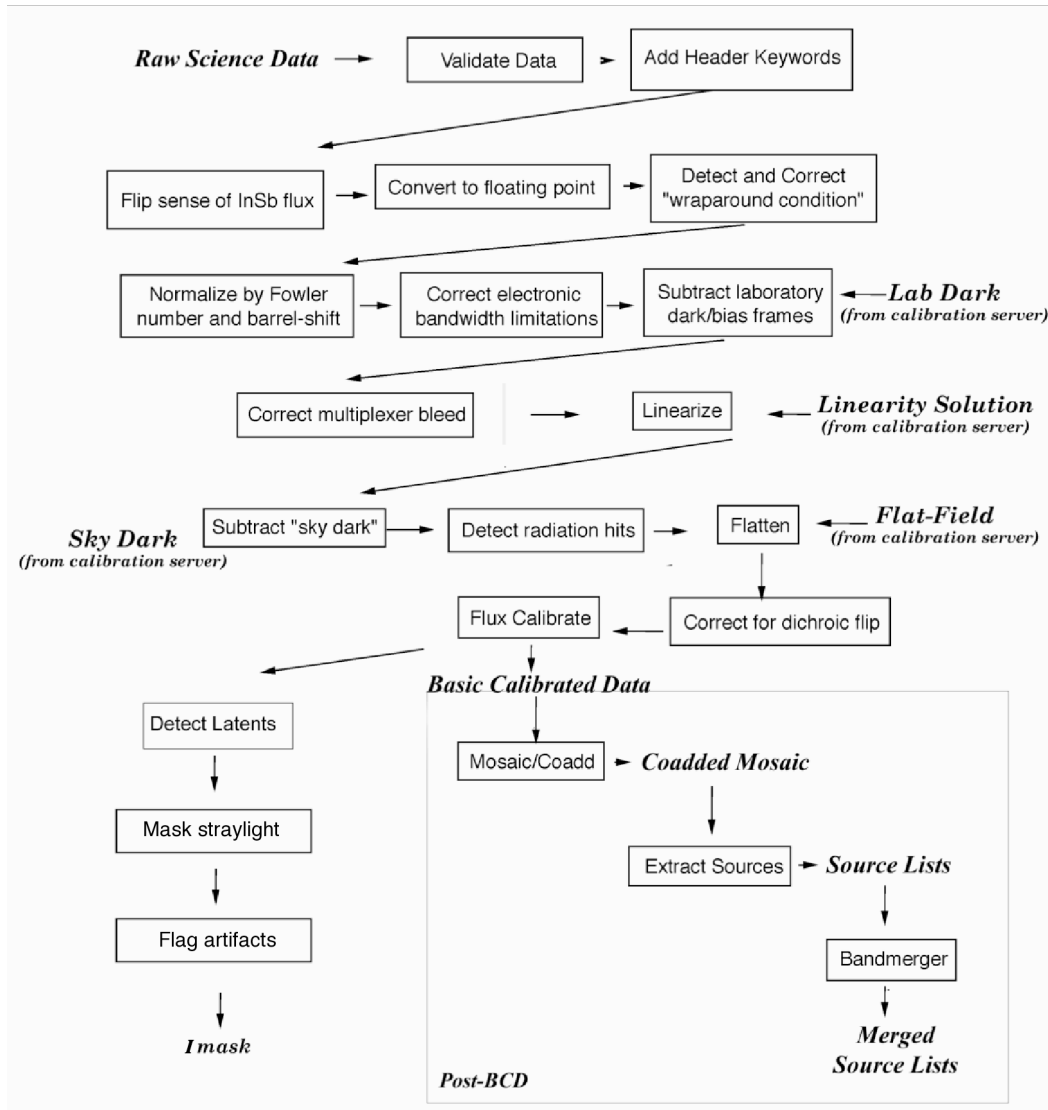
Figure 6.34: IRAC pipeline

7 Appendices

7.1 Infrared Flux Units

The infrared flux density from a point source is most commonly given in units of Jansky (Jy) where:

$$1 \text{ Jy} = 10^{-23} \text{ erg s}^{-1} \text{ cm}^{-2} \text{ Hz}^{-1} = 10^{-26} \text{ Watts m}^{-2} \text{ Hz}^{-1} = F_\nu \qquad (10.1)$$

The conversion between Janskys and flux density in W m^{-2} per unit wavelength is given by:

$$F_\nu \times 10^{-26} \times c / \lambda^2 = F_\lambda \qquad (10.2)$$

The infrared flux density from an area on the sky, such as the surface brightness of an extended object, or the background emission, is commonly given in 10^6 Jy steradian^{-1} = 1 MJy sr^{-1}. Another common unit is Jy per square arcsecond; 1 MJy sr^{-1} = 2.350443×10^{-5} Jy arcsec^{-2}.

Table 7.1– Table 7.3 list the zero magnitude fluxes for various common optical and infrared filters. Note that the photometric system of filter sets can vary, depending on the manufacturer. The magnitude of a source can be converted to a flux density using:

$$F_\nu = F_0 \times 10^{(-m/2.5)}. \qquad (10.3)$$

There is an on-line Javascript tool available from the SSC website that interactively converts Janskys to magnitudes (or any of a variety of flux units) and vice versa.

Table 7.1: 2MASS system zero points

Passband	Effective wavelength (μm)	Zero point (Jy)
J	1.235	1594
H	1.662	1024
Ks	2.159	666.7

References: Table 2 from Cohen, Wheaton, & Megeath 2003, AJ, 126, 1090; see also 2MASS All-Sky data release web document, http://www.ipac.caltech.edu/2mass/releases/allsky/doc/explsup.html.

Table 7.2: Johnson system zero points

Passband	Effective wavelength (μm)	Zero point (Jy)
U	0.36	1823
B	0.44	4130
V	0.55	3781
R	0.71	2941
I	0.97	2635
J	1.25	1603
H	1.60	1075
K	2.22	667
L	3.54	288
M	4.80	170
N	10.6	36
O	21.0	9.4

References: Allen's Astrophysical Quantities, Fourth edition, 2001, Arthur N. Cox (ed.), Springer-Verlag; Campins, Rieke, & Lebofsky 1985, AJ, 90, 896; Rieke, Lebofsky, & Low 1985, AJ, 90, 900.

Table 7.3: UKIRT system zero points

Passband	Effective wavelength (μm)	Zeropoint (Jy)
V	0.5556	3540
I	0.9	2250
J	1.25	1600
H	1.65	1020
K	2.20	657
L	3.45	2.90
L'	3.80	2.52
M	4.8	163
N	10.1	39.8
Q	20.0	10.4

References: UKIRT web page:
http://www.jach.hawaii.edu/UKIRT/astronomy/calib/phot_cal/conver.html

7.2 Infrared Backgrounds

Various astronomical sources emit radiation in the infrared part of the spectrum. Cool stars (M class) have their peak emission just short of the near infrared.

However, stars with dusty envelopes or shells and circumstellar disks can be quite bright in the infrared. Regions of star formation, HII regions, and planetary nebulae are strong infrared sources. The (relatively) cool interstellar medium in galaxies has an infrared component. There are also ultra-luminous infrared bright galaxies that are very strong sources of infrared radiation.

As in the optical, the infrared zody is concentrated toward the ecliptic with weaker emission, by approximately a factor of 4, toward the ecliptic poles. The infrared zody is strongest from about 5 μm to about 30 μm with peak emission at about 10 μm. The infrared zody has structure on most scales and, as observed from Earth, varies from season to season. The intensity of the infrared zody will also vary with solar elongation, or how close to the Sun one is pointed. The infrared zody is difficult to model.

As one moves to longer wavelengths (≥100 μm), diffuse Galactic emission from dust clouds in the interstellar medium becomes the dominant contribution to the infrared background. This infrared cirrus is patchy, with higher concentrations found in the Galactic disk and toward the Galactic center. However, it is important to realize that the cirrus is ubiquitous, and it is critical to examine the IRAS maps or radio maps of cirrus tracers when planning longer-wavelength observing. Far-infrared emission from external galaxies in the field of view will add to the overall background flux.

For more information on infrared backgrounds, see the "Backgrounds" section of the Infrared Compendium, available on the SSC web pages.

7.3 Solar System Objects Included in Bright Object Avoidance

Also see the list of bright inertial objects on the SSC website.

- Earth
- Moon
- Mars
- Jupiter
- Saturn
- Uranus
- Neptune
- 4 Vesta
- 6 Hebe
- 1 Ceres
- 7 Iris
- 15 Eunomia

8 Acronyms/Glossary

Note: The following lists the acronyms used in this manual.

Table 8.1: Acronyms used in this manual

AOR	Astronomical Observation Request(s)
AOT	Astronomical Observation Template(s)
BCD	Basic Calibrated Data
C&DH	Command and Data Handling
CA	Cryogenic Assembly
cBCD	Corrected BCD
CE	Combined Electronics
CMOS	Complementary Metal-Oxide Semiconductor
CTA	Cryogenic Telescope Assembly
DCE	Data Collection Event
Dec	Declination
DN	Data Number
DSN	Deep Space Network
FAQ	Frequently Asked Question
FITS	Flexible Image Transport System
FLS	First Look Survey
FOV	Field-of-View
FPA	Focal Plane Array
FWHM	Full Width at Half Maximum
GSFC	Goddard Space Flight Center
GO	General Observer(s)
GTO	Guaranteed Time Observer(s)
HGA	High Gain Antenna
HST	Hubble Space Telescope
ICRS	International Celestial Reference System
IER	Instrument Engineering Request – like an AOR, but for specific engineering tasks not able to be accomplished using an AOR.
IOC	In-Orbit Check out
IPAC	Infrared Processing and Analysis Center
IR	Infrared
IRAC	InfraRed Array Camera
IRAS	InfraRed Astronomical Satellite
IRS	InfraRed Spectrograph
IRU	Inertial Reference Unit
Jy	Jansky
LGA	Low Gain Antennae
MIC	Multi-Instrument Chamber
MIPS	Multiband Imaging Photometer for Spitzer
mJy	milliJansky
MJy	megaJansky
MPC	Minor Planet Center

OPZ	Operational Pointing Zone
PAO	Period of Autonomous Operations
PCRS	Pointing Control Reference Sensor
PCS	Pointing & Control System
PIN	Positive Intrinsic Negative (Diode)
PM	Primary Mirror
PRF	Point Response Function (like a PSF, but having been transmitted through the telescope+instrument optics)
PSF	Point Spread Function
PST	Point Source Transmission
RA	Right Ascension
RCS	Reaction Control System
rms	Root Mean Square
SAO	Smithsonian Astrophysical Observatory
SBRC	Santa Barbara Research Center
S/C	SpaceCraft
SED	Spectral Energy Distribution
SIRTF	Space InfraRed Telescope Facility, Spitzer's old name
SLO	Second-Look Observation
SM	Secondary Mirror
SODB	Science Operations Database
SOM	Spitzer Observer's Manual
S/N	Signal to Noise
Spot	Previously listed here as an acronym meaning "Spitzer Planning Observations Tool" but now it is simply a proper noun
sr	Steradians
SHA	Spitzer Heritage Archive
SSC	Spitzer Science Center
SSC website	http://ssc.spitzer.caltech.edu/
SSO	Solar System Objects/Observations
ST	Star Tracker
ST/IRU	Star Tracker/Inertial Reference Unit
TAC	Time Allocation Committee
ToO	Target of Opportunity
TPG	Time Pattern Generator
TP, TPM	Total Power Mode
QE	Quantum Efficiency
WASS	Wide Angle Sun Sensor
WEA	Warm Electronics Assembly

9 Index